Doctor of Philosophy

A Numerical Study on Residual Gas Effects on Combustion, Performance and Emission of a Small Spark Ignition Engine

The Graduate School

of the University of Ulsan

Department of Mechanical Engineering

Nguyen Xuan Khoa

A Numerical Study on Residual Gas Effects on Combustion, Performance and Emission of a Small Spark Ignition Engine

Supervisor: Prof. Lim, Ocktaeck

A Dissertation

Submitted to

the Graduate School of the University of Ulsan

In partial Fulfillment of the Requirements

for the Degree of

Doctor of Philosophy

by

Nguyen Xuan Khoa

Department of Mechanical Engineering

University of Ulsan, Republic of Korea

December 2020

A Numerical Study on Residual Gas Effects on Combustion, Performance and Emission of a Small Spark Ignition Engine

This certifies that the dissertation of Nguyen Xuan Khoa is approved.

Committee Chair	**Prof. Park, Kyu Yeol**
Committee Member	**Prof. Lee, Sang Wook**
Committee Member	**Prof. Lee, Yoon Ho**
Committee Member	**Dr. Lee, Young Jae**
Committee Member	**Prof. Lim, Ock Taeck**

Department of Mechanical Engineering

University of Ulsan, Republic of Korea

December 2020

ABSTRACT

A Numerical Study on Residual Gas Effects on Combustion, Performance and Emission of a Small Spark Ignition Engine

Department of Mechanical Engineering
Nguyen Xuan Khoa

There are a large number of motorcycles in operation today, with that number constantly increasing, the goal of improving motorcycle engine power, while satisfying emission standards, is worth investigating. Two essential factors in the study of engines are engine efficiency and the reduction of pollutant emissions. Past researchers are attempting to optimize engine combustion systems by used experimental optimization method. However when the optimization tasks focus on hardware components such as changing the geometry of the combustion chamber, bore, stroke or injection nozzle, the experimental optimization method is limited because of its high cost, manufacturing time and resource consumption. It is complicated to determine the residual gas ratio, the effective release energy and control combustion duration under the various testing conditions from the experiments. As a result, experimental investigations in detail of residual gas and effective release energy with various combustion duration, bore-stroke ratios, valve port diameter and exhaust valve closing timing is limited till date.

The residual gas fraction is known as effective factors, which influence energy efficiency and pollution engine exhaust gas. The trapped residual gases in the combustion chamber will premix with the fresh air-fuel and take part in the next combustion stroke. This trapped exhaust residual gases also effect on the NO_x , HC and CO emission of the engine. The peak pressure rise shows the increasing pressure value per crankshaft angle, this peak pressure rise is expected higher value to reduce heat loss and improve engine efficiency. An effective method for determining the residual gases, effective energy, and peak pressure is necessary. To obtain this target, the experimental system is installed with a dynamo system and a simulation model base on AVL-boost software was setup. Through combined experimental and simulation methods, author eliminated certain above drawbacks. From results of the research, we thoroughly investigated the effects of combustion duration, bore-stroke ratio, intake port diameter-bore ratio, exhaust valve closing timing and internal exhaust residual gases to improve engine performance and emission characteristics.

Keywords: combustion duration, bore-stroke ratio, valve port diameter-bore, exhaust valve closing timing, exhaust residual gas, engine performance.

ACKNOWLEDGEMENT

The first words, I would like to express my deep and sincere gratitude to my advisor Professor Ocktaeck Lim, for giving me the opportunity to come and study at The Smart Powertrain Laboratory. I have studied so much from his vision, dynamism, sincerity and motivation. It was a great honor to work and study under his guidance. I am extremely thankful for what he has supported me in the research works and thesis preparation.

I am extremely grateful to my parents for their love, caring and sacrifices for educating me. I am very much thankful to my brother, my sisters and my future wife for their love, understanding, and encouragement to complete this thesis successfully.

I would also like to thank to all members of the Smart Powertrain Laboratory for many nice memories we have together spent and their valuable support during my research work.

I would also like to express my thanks to the Graduate School of Mechanical and Automotive Engineering, University of Ulsan and Hanoi University of Industry for providing me the opportunity, approval, and support to pursue my PhD program.

I am extending my thanks to the KR Company and K-Tech Center Daejeon Republic of Korea for cooperating, sharing experiment, knowledge of the automotive engine during my research work.

Finally, I am thankful to my supervisory committee members for spending their time and for giving me their advice and comments to improve the quality of the PhD thesis.

This PhD thesis is written during the spring semester of 2020, and has completed in my quarantine time by following the Corona-virus situation policy. This PhD thesis contains total research work conducted during the doctor's study period. All the contents of this thesis are written for partially fulfilling the degree requirement of the PhD of Science in Mechanical and Automotive Engineering at the University of Ulsan.

Nguyen Xuan Khoa

TABLE OF CONTENTS

LIST OF FIGURES

LIST OF TABLES

NOMENCLATURES

SI-engine : Spark ignition engine

CI-engine : Combustion ignition engine

TDC : Top dead center

BTDC : Before top dead center

ATDC : After top dead center

BSFC : Brake specific fuel consumption, (g/KWh)

BMEP : Brake mean effective pressure, (Bar)

HC : Hydrocarbon

PM : Particulate matter

THC : Total hydrocarbon emissions

CA : Crank angle, deg

ERG : Exhaust gas recirculation

BTR : Bore-stroke ratio

VPD/B : Valve port diameter-bore ratio

EVCT : Exhaust valve closing timing

Q_h : Total fuel heat input ,(W)

α : Crank angle, (deg)

α_0 : Start of combustion, (deg)

$\Delta\alpha_c$: Combustion duration, (deg)

m : Shape parameter, (-)

a : Vibe parameter

Q_T : Heat lost to the wall, (W/m^2)

A : Total surface area of cylinder head, piston and cylinder , (m^2)

q_{coeff} : Heat transfer coefficient , (W/m^2 K)

T_c : Combustion gas temperature, (K)

T_w : Wall temperature of cylinder (K)

$\frac{dm}{dt}$: Air mass flow rate (-)

A_{eff} : Effective flow area (-)

P_1 : Upstream stagnation pressure, (Pa)

T_1 : Upstream stagnation temperature, (K)

P_2 : Downstream static pressure, (Pa)

K : Ratio of specific heats (-)

x_{SOC}^{cp} : Residual gas at start of combustion (SOC)

ρ : Local cylinder density (kg/m^3)

x^{cp} : Local cylinder combustion product mass fraction at SOC

V : Local cylinder volume (m^3);

$Q_{released,\ eff}$: Effective release energy (kJ)

$Q_{released}$: Release energy (kJ)

Q_{cp} : Amount of fuel energy was not effectively released in the cylinder but went into combustion products (kJ)

V_D : Displacement volume, (m^3)

r : Compression ratio (-)

r_i : Demotes reaction rates of table 2 and 3 (mole/cm^3s)

C_p : Denotes post processing multiplier, (-)

C_k : Denotes kinetic multiplier, (-)

m_{HC} : Mass of unburned charge in the crevices (kg)

P_c : Cylinder pressure (Pa)

$V_{crevice}$: Total crevice volume (m3)

M : Unburned molecular weight (kg/kmol)

R : Gas constant (J/(kmol.K))

T_{piston} : Piston temperature (K)

m_{air} : Air mass flow [kg/s]

AFR : Air-fuel ratio (-)

n : Engine speed (rpm)

T_{eff} : Engine effective torque, (Nm)

K_{cycle} : Simulation cycle parameter, (cycle)

1. INTRODUCTION

1.1 Background

There are a large number of motorcycles in operation today, with that number constantly increasing. The vehicles' pollution has significant impact on human health and environment.

The researchers and producers have trying to control and reduce the harmful gases and greenhouse gases emissions from vehicles by applying the exhaust gas treated systems and using alternative fuels or new energy sources. However, the air quality is still a serious problem and challenge until nowadays, so the goal of improving the engine power, and satisfying emission standards is worth investigating.

In the scope of research on engine hardware optimization, past researchers attempting to optimize engine combustion systems by used experimental optimization method, it is continuing until present. This confirmed that the important and necessary to improve the engine performance and engine emission characteristics. Recently, various approaches have been taken to deliver improved engine power and reduce pollution emissions, (bore-stroke ratio) including re-designing the intake pipe [1], recovering heat lost from the cooling system [2], optimal combustion phasing [3], using fuel injection instead of a carburetor to improve engine performance and resist knock [4], the use of multiple sparks to improve the thermal efficiency of lean spark-ignition (SI) engine operation [5] and improving SI engine performance with a turbocharger [6]. However, when the optimization tasks focus on hardware components such as changing the geometry of the combustion chamber, bore, stroke or injection nozzle, the experimental optimization method is limited because of its high cost, manufacturing time and resource consumption. As a result, experimental investigations in detail of residual gas, peak pressure rise and effective release energy and optimal parameters such as: bore-stroke ratio, valve port diameter – bore ratio, exhaust valve closing timing is limited till date.

In the scope of research on engine software optimization, some effective methods to improve engine power and engine emission are reported in the published articles such as: investigation the optimal ignition timing [7], optimal injection timing [8], optimal air-fuel ratio [9], optimal compression ratio [10].

From the historical trend of research on engine software parameters optimization, we know that almost software parameters could be optimized through experimental methods. However,

it was complicated to optimize combustion duration or determine the exhaust residual gas in the combustion chamber through experiments with the various testing conditions. In the previous studies are due to the lack of control and lack of ability to determine the precise combustion duration and exhaust residual gas inside the combustion chamber. These were the main reasons for the loss of time, researching cost and less confident in the results. This is a drawback of the experimental method in the scope of research on engine software optimization.

The drawback in the scope of research on engine hardware and software optimization, which was above discussed is a significant vacuum in the open literature which evaluates so the author seek to fill this important gap through the work presented in this thesis. To achieve this goal, an experimental system was installed within a dynamo testing system, and a simulation model was established using AVL-Boost software. Through combined experimental and simulative methods, the effects of combustion duration, bore-stroke ratio, valve port diameter-bore ratio, exhaust valve closing timing and exhaust residual gas on the engine efficiency and emission characteristics are completely investigated. This method also provides good accuracy in control combustion duration and prediction of exhaust residual gas.

1.2 Objectives of the study

This study focuses on the combination experimental and simulation methods to determine exhaust residual gas, combustion duration, optimal hardware and software parameters to improve engine efficiency and engine emission.

The objectives of this study are given below:

(i) Setup an experimental system to provide the basic data for validation the simulation model. The basic data are ignition timing, air-mass flow, peak pressure, peak temperature, engine torque.

(ii) Setup a simulation model base on AVL-boost software to estimate the engine performance and engine emission characteristic with the various testing conditions.

(iii) To control and investigate the effects of combustion duration on the exhaust residual gas and engine performance and emission characteristics.

(iv) To investigate the effects of bore-stroke ratio on the exhaust residual gas and engine performance and emission characteristics.

(v) To investigate the effects of valve port diameter - bore ratio on the exhaust residual gas and engine performance and emission characteristics.

(vi) To investigate the effects of exhaust valve closing timing on exhaust residual gas and engine performance and emission characteristics.

(vii) To investigate the influence of the hardware and software parameters on exhausts residual gas.

(viii) To investigate the effects of exhaust residual gas on the engine performance and emission characteristics.

To obtain above targets, the brief explanation in the effect flowchart as seen in the Fig 1.1.

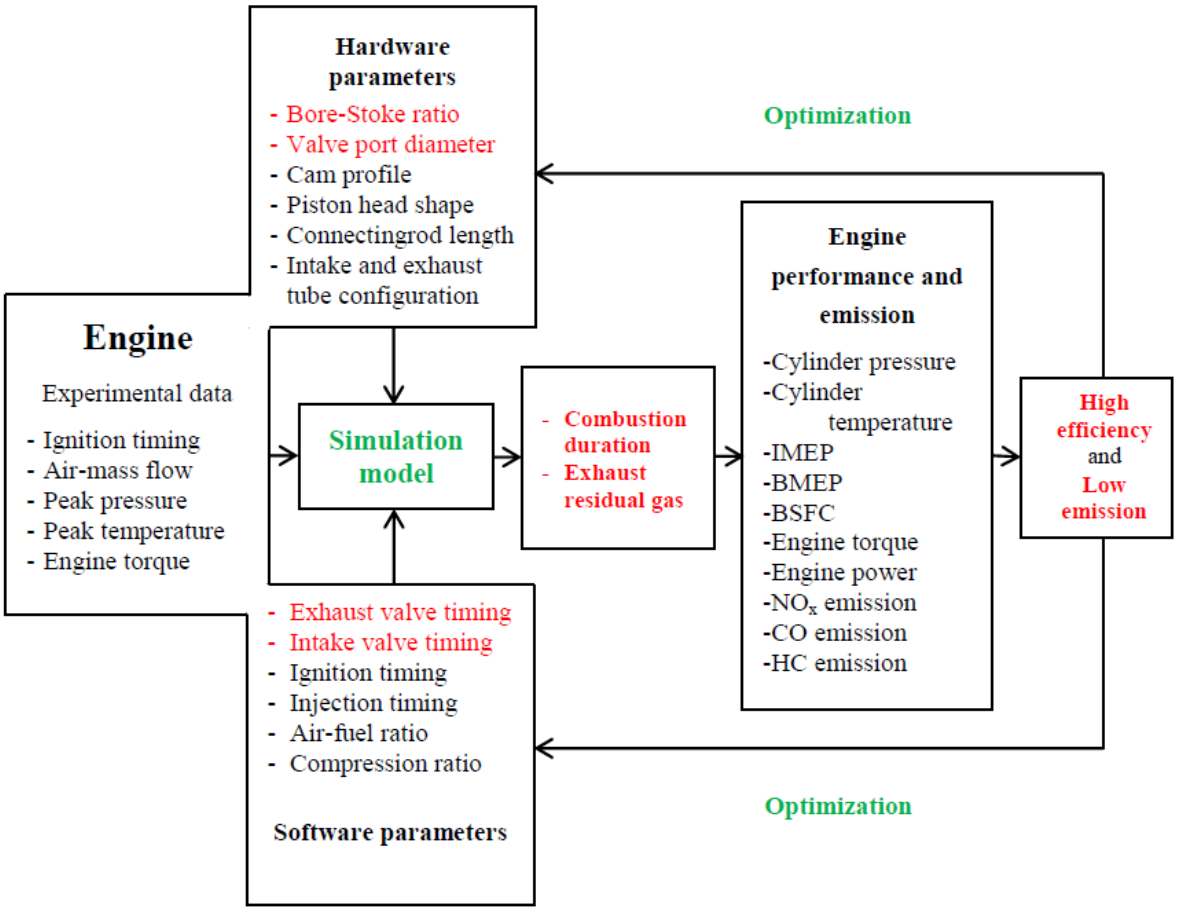

Fig. 1.1 Effect flowcharts of the potential strategies to obtain high efficiency and low emission through experimental and simulation approach

1.3 Scope of the study

In the efforts of provides a good accuracy method to control combustion duration, prediction of exhaust residual gas and to determine optimal parameters to improve engine efficiency and engine emission. This method also helps to eliminate the drawback of the experimental method in the scope of research on engine hardware and software optimization.

The scopes of the study include:

(i) The basic experimental results for the simulation validation are from the experiments were conducted at steady state and full load condition.

(ii) The multi-functions of the simulation model are used base on using Version 2018 of AVL-boos software

(iii) The engine performance and emission characteristics is estimated with a band of combustion duration is from 40 to 110 deg CA

(iv) The reference bore-stroke ratio value is the engine's original bore-stroke ratio value

(v) The reference valve port diameter-stroke ratio value is the engine's original valve port diameter-stroke ratio value valve

(vi) Estimation the effect of exhaust valve closing timing on the exhaust residual gas with the maximum intake valve and exhaust valve lift is 6.5 mm.

(vii) The NO_x, CO and HC emission is used to estimate the engine emission characteristics.

(viii) The obtained results may only valid for the engine used in this study.

1.4 Thesis outline

- **Chapter 1**: this chapter gives a briefly introduction of thesis general topic area of small SI-engine, explanation how important in improvement engine efficiency and engine emission, brief introduction the effective solution which research specific aims and scope of the research.

- **Chapter 2**: this chapter gives a briefly literature review of the research object most closely related to the work such as: small SI-engine, engine efficiency, engine emission and exhaust residual gas. A briefly review of familiar previous research that has been done in this area. Highlight the gap of the research on engine hardware and software optimization that has not been well researched or solved. This gap will be filling up by this thesis work.

- **Chapter 3:** this chapter briefly describes the research engine specification, experimental system and experimental condition.

- **Chapter 4:** this chapter briefly introduces the AVL-software, numerical modeling and governing equations for the analysis.

- **Chapter 5:** this chapter presents the simulation results and discussion in detail, here the optimization of combustion duration, bore-stroke ratio, valve port diameter – bore ratio, exhaust valve closing timing and the effect of exhaust residual gas on engine performance and emission characteristics will be completely studied.

- **Chapter 6**: this chapter shows a summary through all of this thesis and suggestions to further work.

2. LITERATURE REVIEW

2.1 Introduction

This chapter presents a review of the research objects most closely related to the research work: small SI-engine, engine efficiency, engine emission and exhaust residual gas. From a review of the previous research which has been done in this area such as the research on engine hardware, software optimization method and determination of exhaust residual gas. Author will find out the drawbacks that have not been well researched or solved. This gap will be filling up by this thesis work.

2.2 Small SI-engine

The Spark ignition (SI) engines are the most popular reciprocating engine. This engine is equipped on the various vehicles such as cars, motorcycles or equipping for agriculture machine as lawn mowers and chain saws. The spark ignition engines are four stroke or two-stroke engines. In the scope of this thesis, the four stroke small SI engine will be focused. The small SI engine may have single or two cylinders, the engine capacities typically ranged from about 50 cc to 350 cc normally.

This type of SI engine is most popular in motor cycles nowadays. The motorcycle has some advantages when compare to automobile such as:

- Lower cost price
- Generally better fuel economy
- Better performance per dollar
- More parking options
- Advantages in slow or stopped traffic
- Retains value
- Customization

These advantages explain why the motorcycle is very popular and the number of this vehicle is increasing day by day, especial in the Asian countries.

This table 1 shows the registered motorcycles in thousand in the year from 2008 to 2017 of Asian countries:

Table 2.1: the registered motorcycles in thousands of the Asian countries through years [11]

Country	2008	2009	2010	2011	2012	2013	2014	2015	2016	2017
Brunei Darussalam	3.47	1.70	2.59	3.28	4.00	4.00	6.00	3.00	10.27	10.31
Cambodia	188	275	236	218	233	244	303	342	464	381
Indonesia	47,683	52,767	61,078	68,839	76,381	86,253	94,243	100,457	106,538	108,594
Lao PDR	623	711	804	818	1,005	1,111	1,218	1,318	1,413	1,504
Malaysia	8,487	8,940	9,442	9,985	10,590	11,087	11,629	12,094	12,677	13,173
Myanmar	1,609	1,674	1,881	1,934	3,153	3,419	4,162	4,505	5,122	
Philippines	2,983	3,201	3,482	3,881	4,117	4,251	4,489	4,623	5,330	6,174
Singapore	146	147	148	147	144	144	144	143	143	142
Thailand	16,448	16,729	17,322	18,174	19,169	19,987	20,327	20,519	20,276	20,501
Viet Nam	25,273	28,195	31,155	33,774	36,894	38,643	41,197	44,128	47,131	54,063

Due to the rising number of motorcycles in operation and the motorcycles exhaust gas has harmful impact on human health and environment, the need to improve motorcycle engine power and to reduce emission pollution is worth pursuing. To achieve this goal the researcher have to understand the engine thermal efficiency theory and emission characteristics formation which will be introduced in the next parts.

2.2.1 Engine efficiency

In the internal combustion engine, the compression ratio (CR) is known as a sensitive parameter influence on the thermal efficiency. CR is the ratio of the maximum in-cylinder volume before compression stroke to the minimum in-cylinder volume after compression stroke. The SI engine efficiency obeys on the Otto cycle efficiency:

$$\eta_{th} = 1 - \frac{1}{r^{\gamma-1}} \tag{1}$$

$$\gamma = \frac{C_p}{C_v}$$

where

η_{th} is theoretical engine efficiency,

r is compression ratio,

γ is specific heat ratio (depend on monatomic gas or diatomic gas),

C_p is specific heat capacity with constant pressure (J/(kg.K),

C_v is specific heat capacity with constant volume (J/kg.K).

Equation (1) shows two methods to improve engine efficiency: by increasing engine compression ratio or specific heat ratio.

The increasing of CR in an SI engine is limited by a phenomenon that is known as engine knock. Because CR is influenced by the geometry of engine hardware parameters: bore, stroke, connecting rod, piston head so optimal engine hardware parameters as a way to improve engine efficiency.

On the other hand, the exhaust residual gas and engine emission characteristic was a factor that influenced the specific heat ratio because it causes N_2 gas to increase in the cylinder. Meanwhile, the specific heat ratio of N_2 gas (1.47) was greater than that of mixed gas in the cylinder (1.2 – 1.4). A method to determine and control exhaust residual gas is necessary to improve engine efficiency.

In the next parts, the engine emission characteristics formation and exhaust residual gas formation will be introduced.

2.2.2 Engine emission formation and emission standards

The main pollutants of the internal combustion engine considered are NO_x, CO, unburned hydro carbon (HC) and particulate matter (PM). The high combustion temperature was known as the most sensitive effect of NO formation. In the power stroke, the fuel chemical energy was converted to thermal energy when burned fuel. The dominant reactions in NO formation are show in equation (2), (3) and (4):

$$N_2 + O = NO + N \quad (2)$$

$$N + O_2 = NO + O \quad (3)$$

$$N + OH = NO + H \quad (4)$$

Though the formation of NO_x depends on combustion characteristics, the major source of NO_x is NO. Due to the high combustion temperature in the power stroke, a high NO_x emission in the SI engine emission is recognized. CO is generally formed when the mixture is rich in fuel and HC emissions are produced from unburned air-fuel mixture trapped in cold crevice regions between the piston and piston rings. The HC and CO emission is strong depended on the homogeneous air-fuel mixture, because a less homogeneous of air-fuel mixture in the cylinder to increase the rich fuel with lack of Oxygen area. The dilution of the air-fuel mixture and the lack of oxygen led to reduce chemical reaction between HC, CO with Oxygen (as equation 5 and 6). This is reason for increasing the unburned HC and CO emissions:

$$4HC + 5O_2 = 2H_2O + 4CO_2 \quad (5)$$

$$2CO + O_2 = 2CO_2 \quad (6)$$

A suitable an amount of high temperature exhaust residual gas trapped in the cylinder to raise the evaporation and homogeneity in the air-fuel mixture. The homogeneous air-fuel mixture helped the thermal energy can be released in a shorter time to improve peak temperature and pressure rise and reduce heat loss. However, when too much exhaust gas gets trapped in the combustion chamber it may restrict the fresh air-fuel mixture into the combustion chamber and due to poor combustion. From above discussion, we know that the exhaust residual gas is not only influence on engine efficiency, it also influences on the engine NO_x, CO and HC formation. A more understand and discussion of exhaust residual gas will be given in section 2.2.3.

As the most types of vehicle along with passenger as cars, bus, trucks, trains. The motorcycle emission has to meet the existing standards because the harmful emission effects on health and environment. Nowadays, Euro-V standard for motorcycle emission is applying in almost countries. This standard limits the emission in NO_x, CO and HC of the vehicle. Table 2.1 shows a detail the limited emission of NO_x, CO and HC.

	EURO 1	EURO 2	EURO 3	EURO 4	EURO 5
CO (g/km)	13.0	5.5	2.0	1.14	1.00
HC (g/km)	3.0	1.0	0.3	0.17	0.10
NOx (g/km)	0.3	0.3	0.15	0.09	0.06
PM (g/km)	–	–	–	–	0.0045
SHED* test	–	–	–	Yes	Yes
On-board diagnostics	–	–	–	Yes (OBD1)	Yes (OBD2)
Durability	–	–	–	20,000km	Lifetime

*Evaporative emission
Source www.motorcyclenews.com

Fig. 2.1 Motorcycle emission standard

2.2.3 Exhaust residual gas

In internal combustion engines, the exhaust residual gases is known as essential factor, which influence engine performance and emission characteristics. Some exhaust residual gases are trapped inside the combustion chamber after the exhaust stroke. These residual gases will premix with the fresh air-fuel mixture and affect combustion stability, charge mass, flame speed, and emission of toxic products in the next combustion stroke. The engine speed and valve overlap are known as the most sensitive factors that influence the exhaust residual gas of the internal combustion engine.

The increase of engine speed led to increases in the velocity and inertia of the exhaust and intake gas flows. In the exhaust stroke, the increased velocity and inertia of the exhaust gas flow expelled more exhaust gas from inside the cylinder to the outside. In the intake stroke,

the increased velocity and inertia of the intake air flow introduced fresher air-fuel mixture to sweep the exhausted gas out of the cylinder.

The intake valve timing is known as an effective factor which effects on inlet airflow into the cylinder, in the other hand the exhaust valve timing is a factor has strong effect on the exhaust gas flow. The intake and exhaust valve timing are the sensitive factors which has strong effect on valve overlap. An optimal valve overlap allowed for fresh air-fuel mixture into the cylinder and carried more exhaust gas out of the combustion chamber. An early valve overlap may cause the exhaust gas to be expelled into the intake port, and a late valve overlap may result in the reverse flow, which would bring exhaust gas flow back into the cylinder.

From above discussion, for the first step, the effect of exhaust residual gas on engine performance and emission characteristics was introduced. The engine parameters get influence on exhaust residual gas also were mentioned.

In the next part, some previous studies on the exhaust residual gas will be reviewed, and there results has been done and didn't completed yet in this area will be highlighted.

2.3 Review of previous studies on improvement engine efficiency, emission characteristics and determination the effect of exhaust residual gas

This part presents a review of familiar previous research that has been done in this area. The previous results of study the effect of combustion duration, bore-stroke ratio, valve port diameter – bore ratio, exhaust valve closing timing and residual gas on engine performance and emission characteristics will be shown. The drawback of those research also are pointed out and will be solved.

2.3.1 Optimal combustion duration previous studies review

In the four-stroke SI engine, the power stroke is the most important stroke. The combustion process has been the major factor affecting engine performance with pollutant emissions associated to the conversion of the chemical energy gotten from fuel into thermal energy, and the emission of harmful gases such as NO_x, CO, HC, and PM. Because of the combustion

process had a significant effect on the engine performance and emission characteristics so the parameters involve in the combustion duration process also were studied, for example: the effect of flame stretch on fuel performance of spark ignition engine [12]. Lean-burn mixture was used to improve combustion quality and reducing heat transfer losses [13]. The impact of the combustion phasing on the performance of dual-fuel engine [3]. From literatures, higher effective combustion process has been reported through newly applied technologies such as: an improvement of the thermal efficiency and knock resistance of a gasoline engine by applying a Miller cycle with split injection [4]. A multiple spark discharge using multi-coil ignition system was applied to ensure the stable, complete and fast combustion of lean SI engine operation [5]. Using direct injection with low-pressure strategies to improve efficiency and reduce emission of a small SI natural-gas two-stroke engine [14].

In the power stroke, the combustion duration is a crucial parameter that indicates the optimum burning process. Generally, for extremely short combustion duration, an incomplete conversion of fuel from chemical energy to thermal energy seems to exist. Moreover, excessive thermal energy loss tends to occur during long combustion duration due to the increase in the duration for the heat transfer process in and out of the cylinder, piston and flowing exhaust gas. Some recently published papers relating to combustion duration presented the combustion duration effect on engine performance as well as the parameters affecting the combustion duration such as: ignition timing, engine speeds, engine load conditions, and fuels etc. [15] This research reflected on the trend of combustion duration discovered in HICE and affirms that when the equivalence ratio was greater than 0.6, the combustion duration was almost independent of engine speed. However, the low speed and leaner mixtures of the combustion duration were reduced sharply when engine speed increases. [16] An SI-engine was studied, and the effect of air-fuel ratio, engine speed, spark advance, and compression ratio in combustion duration was found based on the comparison between the experimental method and theory to determine the combustion duration, which uses the empirical correlation method. [17] The presented investigation was of the combustion duration of a diesel engine that used a dual fuel and hydrogen engine. The research shows that the combustion duration increases 2.5 degrees CA and the ignition advance decreases 2 degrees CA when the engine operated at a light load. At 80% load and 50% volume of hydrogen in the fuel, the combustion duration increased to a maximum of 9 degrees CA, and the ignition advance decreases to 6 degrees CA. [18] The engine combustion

duration had a large effect on engine performance and NO_x emission of the engine with dual-fuel diesel-LNG. At a light load, the combustion duration increased from 1.7–6.0 degrees. After the top dead center, the engine thermal efficiency increased to 16.7%, and the NO_x declined. However, THC and CO emissions increased. If the advance of combustion duration was before top dead center (TDC) then the NO_x emission will increase. [19] The engine working at light load saw the combustion duration increase to 5.0 degrees CA compared to a hydrogen or diesel engine. However, the combustion duration was reduced by 5.0 degrees CA at the engine load around 80.0 % with a mixing fuel of 50.0 % hydrogen and 30.0 % LPG. [20] This suggests to us that both the main and initial combustion durations were affected by the addition of hydrogen; when the amount of hydrogen was increased, the combustion duration decreased. [21] Haroun A.K, Maher A.R. showed that the addition of hydrogen affected combustion duration and increased flame speed, leading to complete combustion. When the amount of hydrogen increased to 10.0% in volume, the combustion duration decreased to 24.0% and the flame speed increased by 46.0%. Also, the combustion duration decreased the heat transfer rate so that engine efficiency increases. [22] The combustion duration has decreased from the norm and two stages of combustion in the same condition as the coke oven gas. In normal combustion phases, the combustion duration changes from 24.0 – 29.0 degrees of CA, while that of two-stages combustion changes from 11.0 – 14.0 degrees of CA. [23] The optimum engine combustion duration is said to vary from 24.5 to 27.5 degrees of CA upon addition of 20.0% hydrogen and from 28.5 to 32.0 degrees of CA when 13.7% hydrogen was added. However, in two-stages combustion, the combustion duration was reduced at excess amount of hydrogen. [24] Using the diesel engine for research, the effects of engine load and volume hydrogen addition on combustion duration were presented. If a small amount of hydrogen was added, the effects on combustion duration would not be high. At a 70.0% load, the hydrogen volume fraction decreases the combustion duration, by using a zero-dimension, two-zone model to study the effect of the combustion process on thermal efficiency and to determine the best thermal efficiency in each combustion phase. [25] In this research, the best thermal efficiency occurred when the maximum pressure in the cylinder was 9.0 degrees after TDC. The development of combustion duration had a higher heat transfer rate. [26] A compression ignition engine using dual fuel hydrogen-ethanol was set in 1,500 rpm, 100% load, and 0 – 80% hydrogen volume fraction. The appropriate condition in terms of engine performance was a combustion duration range of 35 – 42 degrees. [27] An analytical model was used to study the combustion duration effect on engine

performance, and emission characteristics for the four-stroke, spark ignition engine were analyzed using propane as fuel. The results have shown that the combustion duration has a large effect on engine performance and emission characteristics, so the designer should carefully design the engine to achieve optimal performance characteristics.

All previous studies have focused on the heavy-duty engine with alternative fuel as well as used dual fuel (hydrogen-ethanol) and LPG fuel. However, these results were difficult to apply in a small SI-engine since it failed to shed light on the combustion duration effect on residual gas and effective release energy. Besides that, many previous studies reported the combustion duration effect on engine torque, engine power without elaborating on the effect on engine emission characteristics. Other studies presented the effects of combustion duration on engine emission characteristics but nothing was stressed on its effects on engine torque, BSFC, IMEP, BMEP. In our research, the combustion duration effect on the engine performance and engine emission characteristics are presented.

In the previous studies due to the lack of control and lack of ability to determine the precise combustion duration inside the cylinder. These were the main reasons for the loss of time and researching cost. However, through combined experimental and simulative methods, author has been able to eliminate these drawbacks.

2.3.2 Optimal bore-stroke ratio previous studies review

Two essential factors in the study of engines are engine efficiency and pollutant emissions. Due to the increasing number of motorcycles in operation, the need to improve motorcycle engine power and to reduce emission pollution is worth pursuing. Recently, various approaches have been taken to deliver improved engine power and reduce pollution emissions, including re-designing the intake pipe [28], recovering heat lost from the exhaust gas system [29], optimal combustion phasing [30], using fuel injection instead of a carburetor to improve engine performance and resist knock [31], the Influence of spark discharge characteristics on ignition and combustion process and the lean operation limit spark-ignition (SI) engine [32]and improving SI engine performance with a turbocharger [33]. In the scope of research on engine hardware optimization, the bore-stroke ratio (BTR) is the most significant factor that affects the heat transfer, friction, and air-fuel mixing time [34].

From the historical trend of research on engine efficiency and engine emission, heavy-duty compression ignition (CI) engines with various bore-stroke ratios are known to be characterized with an excellent compression ratio, high NOx and soot emissions. Fasolo et al. [35]evaluated a new 2-liter, 4-cylinder turbocharged diesel engine with a common-rail injection system to study the main characteristics of the CI engine combustion systems and discovered that the bore-stroke ratio had a sensitive effect on engine combustion, friction losses and air filling. The decrease of this ratio leads to decreased air mass flow into the cylinder and decreased brake specific fuel consumption (BSFC). It was also noted that at a bore-stroke ratio of 0.93, the engine power was improved by 7% compared to a reference bore-stroke ratio of 0.81. Kermani et al. [36] also conducted similar study on engine performance, emissions and fuel consumption. According to authors, the piston bowls and cylinder heads were designed to provide the same bowl profile and same top dead-center swirl, respectively. Their results showed that the bore-stroke ratio had a sensitive effect on thermal losses; an increase in bore-stroke ratio led to increased heat losses due to larger wall surfaces. Conversely with a lower bore-stroke ratio, the friction losses were reportedly higher due to the larger piston-swept surface. The engine showed optimal performance at a bore-stroke ratio of 0.9 to 0.95. Generally, the bore-stroke ratio does not only affect the heat transfer loss; but also has a significant impact on friction. According to Payri, F. et al. [37][38] a bout 4%-10% of the injected fuel energy is consumed by mechanical losses. In further research they reported a 50% mechanical loss due to friction between the piston and cylinder, suggesting that the bore-stroke ratio has an effect on the fuel economy. Filipi et al. [39]reported that the stroke-bore ratio affects heat transfer, combustion, and overall efficiency in a homogeneous charge SI engine. Authors assessed three values of bore-stroke ratio, 0.7, 1.0, and 1.3 and found that the ratio had a significant effect on the geometric interaction of the flame front and turbulence levels. Thus, the increased stroke-bore ratio led to an increase in thermal efficiency associated to lower heat loss and faster burning.

Research on engine performance and emission characteristics with various bore-stroke ratios continues to this day. Miles et al. [40] studied the effect of basic geometric architecture on light-duty diesel combustion engine performance. Their results showed that the bore-stroke ratio was a potential factor to improve air-fuel mixing time, heat transfer and friction. By modifying the bore-stroke ratio, engine efficiency could be improved. Benajes et al. [41] used computational analysis to determine the effect of bore-stroke ratio on high-speed direct

injection (HSDI) combustion emission and efficiency. They used a CFD model to assess engine performance with a bore-stroke ratio range of 0.8-1.1. They discovered that the engine efficiency was improved with a lower bore-stroke ratio because of faster combustion and lower heat transfer losses. The lower bore-stroke ratio also led to increased NO_x emissions and decreased soot emission.

As described here, past researchers attempting to optimize engine combustion systems by used experimental optimization method, this confirmed that the important of study the engine performance and engine emission characteristics with various bore-stroke ratio. However when the optimization tasks focus on hardware components such as changing the geometry of the combustion chamber, bore, stroke or injection nozzle, the experimental optimization method is limited because of its high cost, manufacturing time and resource consumption. As a result, experimental investigations in detail of residual gas, peak pressure rise, combustion duration and effective release energy with various bore-stroke ratios is limited till date.

In summary, most of the previous studies have focused reporting on heat transfer losses, friction, fuel consumption, NO_x and soot emission. Few studies have addressed small SI engines such as motorcycle engines without sufficient information on the residual gas, effective release energy and combustion duration. This is a significant vacuum in the open literature which evaluates so the authors seek to fill this important gap through the work presented in this thesis.

2.3.3 Optimal valve port diameter-bore ratio previous studies review

As stated earlier, the estimation of the effect of hardware factors and software factors on engine power and reduce pollution emission were presented such as: changing cam profiles [42], piston head profile [43], optimal intake and exhaust valves [44], using optimal cylinder head to improvement of the diaphragm compressor [45] and effect of intake port diameter [46][47].

Can, et al. [48] have studied the effets of valve lift on the engine performance and emission of a homogeneous charge compression ignition (HCCI) engine. The conditions of the experiment were 800 rpm to 1900 rpm engine speed, 0.5 to 2 air-fuel ratio, and 20^0C to 120^0C air temperature. In this research, the intake valve lift and exhaust valve lift were

reduced from 9.5 mm to 2 mm. The results of the experiments show that the intake and exhaust valve lifts have a substantial effect on the performance and emission of an HCCI gasoline engine. The mixture of air and fuel into the cylinder increases when the intake valve lift increases. The maximum indicated mean effective pressure (IMEP) of the engine was 11 bars, the intake valve lift was 5.5 mm, and the exhaust valve lift was 3.5 mm. When using low cam lifts, the engine operation ranges are extended to include misfiring and knocking conditions. Y, et al. [49] presented a study on the effects of changing valve timing and cam lift in controlled auto-ignition combustion. In their study, a single cylinder engine was used. The valve lift was changed from 0.3 mm to 9.5 mm. The results showed that: the low cam lifts effected the heat release rate and pressure in the cylinder. Ghazal, et al. [50]presented the effect of various inlet valve diameters at different inlet valve opening, inlet valve closing and valve overlap on a spark-ignition engine performance. In their research, a spark-ignition engine was conducted with engine speed band from 500 to 3500 rpm. The original inlet port diameter is 31 mm and exhaust port diameter is 26 mm. The inlet diameters were 29, 30, 31, 32 and 33 mm was presented. The results showed that the decrease of the inlet valve close angle of all inlet port diameters is due to decrease engine power and increase NO and CO emissions. A reduction of valve overlap till 50 deg crank angle could improve engine power. Raghu, et al. [51] presented the effect of intake port parameters on the air motion characteristics of a diesel engine. The intake port parameters were analyzed such as: intake valve diameter, valve seat angle and width, intake port eccentricity and orientation angle. In their research, the results showed that the geometries of the combustion chamber and intake port had a significant effect on the flow into the cylinder. They also found that, when the intake valve diameter increased from 43 to 55 mm, the swirl ratio decreased 27.61% with directed port and decreased 17.65% with helical port. Yasar, et al. [52] also experimented with an internal combustion engine to study the effect of various intake port shapes on the intake air flow motion in the cylinder. In order to analyses the air flow behavior and to measure air flow velocity distribution, a particle image velocimetry technique (PIV) was employed in their research. Their results showed that the intake port geometry had a sensitive effect on the air flow structure into the cylinder. With valve lift was 7mm and intake valve seat angle was 30 degrees, the inlet flow into the cylinder was a jet flow. Most of the air flow direction followed the axial direction; a reversed flow appeared due to the presence of the side wall of the cylinder. QI, et al. [53] used CFD simulation model to study the effects of intake port geometry on the intake air flow characteristics in the cylinder of an SI-engine.

They found that a small change of intake port has a significant effect on in-cylinder flow. A suitable inlet port design helps to increase tumble and reduce recirculation of the intake air flow. A strong tumble leads to increase the homogenous of air-fuel and improve the stability of combustion. Their final design improved by 20% of the fuel vaporization. Latheesh et al. [54]also studied with a compression ignition engine to analyze the designed intake port and exhaust port by using the CFD simulation model. In that research, the exhaust port was increased form 2 valves to 4 valves. They found that by using the simulation software helps to save the number of times in experiments and the swirl motion generated inside the cylinder was sensibly affected by the position of tangential and helical intake port.

All previous studies lacked detail on the investigation the effect of exhaust port diameter-bore ratio on effective release energy, residual gas fraction and engine emission characteristics. These studies focus to present the inlet port configuration effect on intake air flow characteristics such as: swirl ratio, air flow motion, flow velocity distribution or air flow tumble. There are no articles present in detail the residual gas, effective release energy with various intake and exhaust port. A comparison between the two cases is necessary. This is an existing gap in the open literature will be filled up through the work presented in this thesis.

2.3.4 Optimal exhaust valve closing timing previous studies review

Previously, there have been studies on the engine parameters that have an influence on airflow and exhaust mass flow motion in the combustion chamber such as: backpressure at the exhaust manifold, intake and exhaust port shapes [40][54]; and intake and exhaust tube configuration [55][56]The valve timing is known to be a crucial parameter that has a strong influence engine efficiency and emission characteristics [57][58]. Some recently published papers presented the effect of valve timing on engine efficiency and emission characteristics. [59] A 3D code KIVA-3V was used to conduct simulations of the spark-assisted compression ignition combustion. The Coherent Flamelet model was used to simulate the Turbulent Flamelet spread. This simulation model was used to investigate the dependence of heat release rate the spark timing, charge temperature and change negative valve overlap. The testing engine speed was 2000 rpm, and the compression ratio was 12.4:1. The results of the research showed that with advance spark timing and negative valve overlap, the total end-gas mass, the thermal and equivalence ratio distributions lower the peak values. This shift led a

43% reduction in the peak heat release rate. [60] Using a spark ignition (SI) engine with methane fuel, the intake valve timing was changed while the exhaust valve timing was fixed. The engine compression ratio was 10.93:1 and the engine speed in two tests was 1250 and 2000 rpm. The results showed that the variable valve overlap has a large effect on exhaust gas emission (NO_x, THC and CO), combustion phasing, and engine performance. With a positive valve overlap of 55 to 85 deg, emissions of CO and THC increased nearly 75% while NO_x decreased 67%. [61][62] A physical model was defined to satisfy the conservation law and the physical gas exchange model was derived from the high level model description. The simulation's engine speed was 1000 rpm. Those papers presented a method to estimate and control the residual gas fraction based on the cylinder pressure, heat transfer to the cylinder wall, and the CO_2 concentration in the combustion chamber. In addition, dynamic behavior of the effect of residual gas on the air-fuel ratio was presented. C. Guardiola et al. [63] presented a method for simultaneous estimation of the residual mass and the intake in an engine with negative valve overlap. The experimental engine was modified to perform multi-mode combustion such as spark ignition combustion, homogeneous charge compression ignition combustion, and spark assisted compression ignition combustion. The compression ratio was increased from 9.2:1 to 11.25:1. The negative valve overlap was 50 crank angle degrees. The testing engine speed was maintained at 2000 rpm. The results showed that this method could estimate the mass of residual gas and intake mass in SI-engine, the spark-assisted compression ignition combustion engine, and the homogeneous charged compression ignition engine. [64] Their experiments used a direct injection gasoline, which was equipped with a fully flexible valve mechanics system to change the negative valve overlap. Negative valve overlap was used to help retain internal exhaust gas recirculation. The testing engine speed was 2000 rpm, and the compression ratio was 12.5:1. In the case of varying spark advance, the negative valve overlap was from 114 to 136 crank angle degrees. In the case of constant spark timing, the negative valve overlap was from 104 to 130 crank angle degrees. The results showed that with constant combustion phasing at 50 crank angles degrees the peak heat release rate was decreased 40% and the ringing intensity decreased 75% with no influence on thermal efficiency. Over the range of the negative valve overlaps that were tested, the potential variation of thermal and compositional stratification had only a small effect on burn characteristics. The changing of temperature and spark timing were the main effect of the spark-assisted compression ignition burn rate. Hui Xie et al. [65] presented the effect of positive valve overlap on gasoline engine performance at a medium-high load. In

this research, a Ricardo Hydra 140 four-stroke engine was used for experiments. The combustion ratio was 10.66:1 and the testing engine speed was fixed at 1500 rpm. The research was focused on the spark-assisted compression ignition using positive valve overlap to investigate optimal engine performance. The results of the research showed that the positive valve overlap had a large effect on the combustion process and gas exchange. In the case of late exhaust valve closing, inhomogeneous distribution and internal exhaust gas recirculation were higher than that in case of early intake valve opening. The external exhaust gas recirculation and positive valve overlap were the primary controlled factors of the load of the spark-assisted compression ignition combustion. At a constant engine middle load, a small positive valve overlap and high exhaust gas recirculation improved the fuel economy. The optimal positive valve overlap was also determined to improve NO_x emission, pumping loss, and fuel economy. Cheolwoong Park et al. [66] presented the effect of valve timing on emission characteristics of a hydrogen-compressed natural gas engine at the full load. In this research, an 11-L 6-cylinder compressed natural gas (CNG) engine was used for experiments. The combustion ratio was 11.5:1 and the testing engine speed was 1260 rpm. The results of this research showed that with a reduced valve overlap duration, the engine gave a lower torque at the lean burn limit. The reduced valve overlap duration increased residual gas and NO_x emission. By using hydrogen compressed natural gas (HCNG) fuel and opening the exhaust valve early, the THC and CH_4 emissions were reduced by approximately 41%. Jacek Hunicz [67] presented the effect of negative valve timing on combustion in a homogeneously charged gasoline compression ignition engine. In this research, a single cylinder engine with an 11.7:1 compression ratio was used for experiments. The testing engine speed was held at 1500 rpm. The negative valve overlap values ranged from 157 to 182 crank angle degrees. The results of this research showed that negative valve overlap injection had a large effect on the combustion process and emission characteristics. When fuel injection is at the early stage of negative valve overlap, 46% of the fuel carbon was converted into carbon species. One kg of fuel was converted into CO (206 g), acetylene (26.5 g), propene (70.8 g), ethylene (133.7 g), formaldehyde (13.5 g), and methane (78.3 g). When fuel injection was at the late stage of negative valve overlap, 4.6% of the fuel carbon was converted into carbon species.

In summary, most previous studies only focused on reporting the effect of intake valve timing on NO_x emission and engine torque. A few articles mentioned the influence of exhaust valve closing timing (EVCT) on residual gas, but there has been a lack of detailed investigation on

the amount of residual gas in the combustion chamber. Moreover, to the best of our knowledge, no published article has completely mentioned the effective release energy, peak firing pressure rise and engine performance and engine emission with various exhaust valves closing timings. This is a significant gap in the open literature and the authors seek to fill this gap through the work presented in this thesis.

2.3.5 Determination exhaust residual gas previous studies review

In internal combustion engines, the exhaust residual gases and effective release energy are known as essential factors, which influence engine performance and emission characteristics. Some exhaust residual gases are trapped inside the combustion chamber after the exhaust stroke. These residual gases will premix with the fresh air-fuel mixture and affect combustion stability, charge mass, flame speed, and emission of toxic products in the next combustion stroke. In diesel engines, the exhaust gas recirculation (EGR) method is an excellent approach to decrease the NO_x emissions [68] [69] [70][71][72][73].

From the historical trend of research on the factors which affect the mass of exhaust residual gas in the cylinder, the effects of residual gas on engine performance, and engine emission characteristics. Past researchers attempting to control the amount of residual gas trapped in the cylinder and used new techniques to measure exhaust residual gas, such as Variable Valve Timing technologies [57][74][75][76], and an exhaust gas prediction method [77][78]. Because it is complicated to determine the residual gas and the effective release energy in the cylinder through experiments under various testing conditions, computational analysis methods are powerful and effective tools to eliminate this problem.

Thompson et al. [79] built a one-dimensional model in GT-Power to evaluate the effect of valve timing strategies on the exhaust residual gas factors of a Ricardo Hydra camless spark ignition (SI) engine fueled with wet ethanol. The engine was operated at a partial load condition and 1500 rpm of engine speed. They discovered that an increased percentage of water in the wet ethanol led to an increase in the residual gas fraction, which in turn led to an increase in the maximum pressure in the cylinder.

Costa et al. [80] presented a study on the effect of exhaust gas recirculation on engine combustion and engine emissions of a natural gas-hydrous ethanol dual-fuel SI engine. In that

experimental setup a single-cylinder AVL 5495 SCRE engine with a 13.6:1 compression ratio was used. The testing engine speed was 1800 rpm and the stoichiometric air-fuel condition was maintained at 4 bars. A 1-D combustion model was created in the GT Power software to predict the exhaust residual gas fraction with an advanced intake valve opening strategy. Their results showed that an increase in internal exhaust gas recirculation led to increased ignition delay and combustion duration, and decreased NO_x emissions. The effect of internal exhaust recirculation was more sensitive when the dual-fuel mode was applied.

Lei Zhou et al. [81]evaluated a single-cylinder, four-stroke Ricardo E6 to study the influence of exhaust gas recirculation on the engine combustion characteristics under low load conditions. The intake valve timing and exhaust valve timing were used to adjust the exhaust residual gas ratio. They found that under partial load conditions, when the exhaust residual gas ratio was small, the heating effect was the main influence on the burning rate, but when the exhaust residual gas ratio was larger, the burning rate was reduced. Under idle conditions, the combustion stability and fuel consumption were improved with a larger residual gas ratio.

In summary, most previous studies did not present in detail the sensitive parameters that distribute exhaust residual mass trapped in the cylinder, such as intake and exhaust valve timing, engine speed, air-to-fuel ratio, combustion duration, engine load, and intake and exhaust pressure. That research only focused on adjusted intake and exhaust valve timing to control the exhaust residual, and this was specifically accomplished by modifying the engine's original valve mechanics system or manufacturing several camshafts. Those methods were limited because of high cost, lengthy manufacturing time, resource consumption, and difficulties in maintaining the same testing environmental conditions in the experiments. Further, because those experiments were conducted in limited experimental conditions with changing valve timings, the validation of the simulation model was also limited. This may results in largely inaccurate of the simulation model in prediction of the exhaust residual gas. All of these drawbacks are significant gaps in the extant literature, and we therefore seek to fill this gap through the work presented in this thesis.

2.4 Summary

This chapter gives an introduction of research engine and a literature review about the effect of combustion duration, bore-stroke ratio, valve port diameter-bore ratio, exhaust valve closing timing and exhaust residual gas on engine performance and emission characteristics.

All previous studies have focused on the heavy-duty engine with diesel fuel or alternative fuel as well as used dual fuel (hydrogen-ethanol) and LPG fuel. However, these results were difficult to apply in a small SI-engine since it failed to shed light on the combustion duration, bore-stroke ratio, valve port-diameter and exhaust valve closing timing effect on residual gas and effective release energy. Besides that, the previous studies due to the lack of control and ability to determine the precise combustion duration and exhaust residual gas inside the cylinder. These were the main reasons for the loss of time and researching cost. However, through combined experimental and simulative methods, author has been able to eliminate these drawbacks.

Thus, a laboratory system was established combines with a simulation model to study the small SI-engine behavior to control the combustion duration and investigated engine parameters were residual gas, effective release energy, BSFC, IMEP, BMEP, peak firing temperature, engine torque, engine power, NO_x, CO, and HC emissions. Also, the optimum combustion duration, bore-stroke ratio, valve port diameter–bore ratio, exhaust valve closing timing and exhaust residual gas for engine giving the optimal performance or at least harmful emission are investigated. The information of engine testing specification and basic performance parameters that will be used to valid the simulation model which will be introduced in the next parts.

3. EXPERIMENTAL SYSTEM

3.1 Introduction

This part introduces the research engine and experimental system. The research engine is a small SI engine that is equipped for the motorcycle. The purpose of the experimental setup just is support the basic engine behavior data such as ignition timing, air-mass flow, cylinder pressure, cylinder temperature and engine torque to valid simulation model. The detail of researching engine and experimental system will be introduced below.

3.2 Researching engine

A four-stroke, spark-ignition engine with 137 cm^3 in displacement volume of each cylinder was used. There are two intake valves and exhaust valves in each cylinder. Two different camshafts controlled the exhaust valves and intake valve.

The main specifications of the engine are summarized in Table 3.1.

Table 3.1 Engine specifications

Parameter	Unit	Value
Model	-	Four stroke, Spark ignition
Number of cylinder	-	2
Compression ratio	-	11.8:1
Bore	mm	57
Stroke	mm	53.8
Connecting rod	mm	107.9
Intake valve	-	Number : 2 valves Diameter: 22 mm Valve lift: 6.5 mm Opening: 40 deg BTDC, Closing: 200 deg ATDC.
Exhaust valve	-	Number: 2 valves Diameter: 22 mm Valve lift: 6.5 mm Opening time: 230 deg ATDC Closing: 30 deg ATDC.
Cooling system	-	Air cooled

3.3 Experimental condition

Fig 3.1 and Fig 3.2 show the experimental schematics and experimental system. The experiment was conducted with engine speed band of 2000 – 8000 rpm, 11.8:1 is the compression ratio of the engine, and the air/fuel ratio was kept at 13.6 and 29.5-30^{0}C of the temperature of intake air during experiments. Before doing the experiments, all the tested devices were calibrated. The system resistant moment was controlled by a Dynamometer Controller. During the engine performance the oil temperature was maintained at 80^{0}C and the engine was cooled by using air, and the oil temperature was determined and controlled by thermal couple and temperature sensors. The injector controller was used to maintain air-fuel ratio is 13.6. The steady state of engine performed was present in the experiments. At each engine speed the throttle angle was kept at 100% of opening. The pressure and temperature in the combustion chamber are determined by using pressure sensor is located on the engine head.

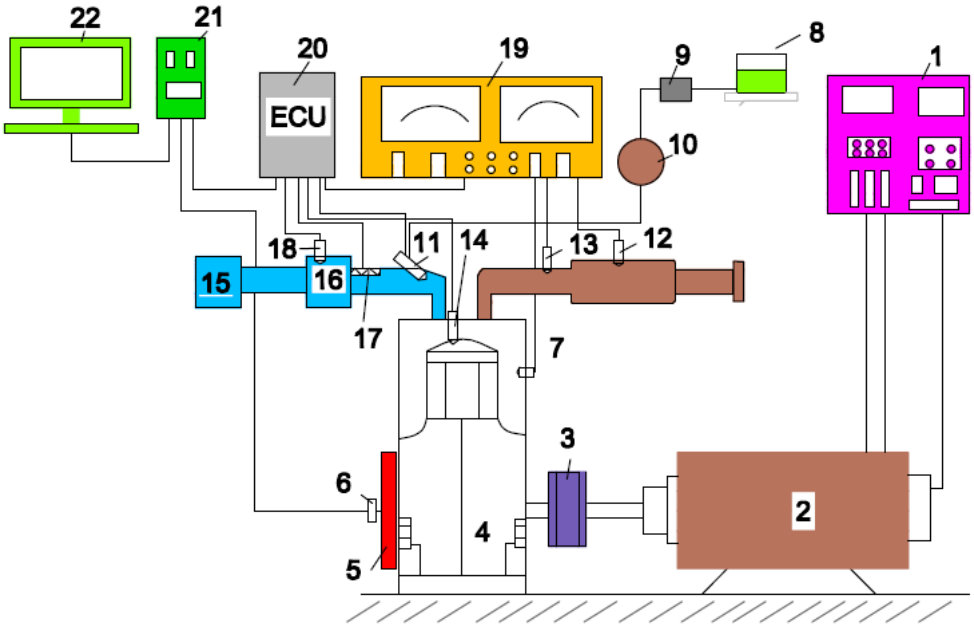

Fig. 3.1 Experimental schematics

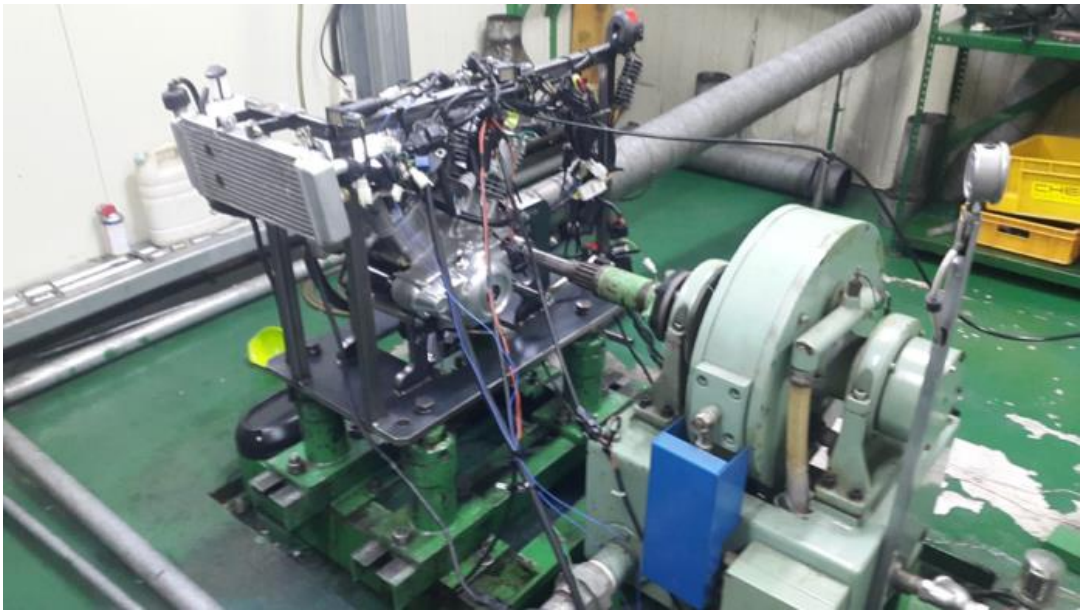

Fig. 3.2 Experimental system

The devices were used in the experiment system: A dynamo testing system controller (1), AVL's Hydraulic / Water Brake dynamometer with serial number is ZAG56907 (2), the connecting shaft (3) to connect the engine to the dynamometer. The experimental engine (4), the encoder Autonics E40S8-1800-3-T (6) is located on the flywheel (5). To prevent engine working in knocking condition a knocking sensor 30530-P2M-A01 (7) was employed. The fuel tank (8), fuel pump (9), fuel filter (10) and injector denso (16450-C12-235) (11) were the fuel system's parts. The sensors (12) and (13) were used to determine the exhaust gas temperature and oxygen in the exhaust gas. The cylinder pressure sensor Kistler 6056A (14) was located on the engine's head. The air cleaner box (15) and throttle (16), an air-heater (17) was used to remain temperature of air flow from 29.5-30^{0}C. The air flowing meter (18) and ECU (20) are used to determine air flow and control fuel mass. The monitor (19), encoder's signal convertor (21) and a computer (22) were used to observe and analyze input data. The main of experiment devices specification is shown in table 3.2.

Table 3.2 Experiment devices specification

Equipment	Parameter	Range [unit]	Accuracy
AVL's Hydraulic / Water Brake dynamometer (ZAG56907)	Speed	2000 – 8000 [rpm]	± 0.1%
	Power	0 – 150 [kW]	
Encoder Atonics E40S8-1800-3-T	Power supply	5 [VDC]	± 0.1%
A knocking sensor 30530-P2M-A01	Package Dimensions	4.7 x 3.45 x 1.85 [inches]	± 0.1%
Injector denso (16450-C12-235)	Power supply	4- holes,12[V]- 3[bar]	± 0.1 bar
Cylinder pressure sensor Kistler 6056A	Pressure range	0 - 250 [bar]	± 0.5 bar

Fig 3.3 shows the injection timing and ignition timing control system. Base on this this system, the ignition timing can be setup for various testing condition such as low or high engine speed and part load or full load condition. Base on this process, the effect of ignition timing and injection timing engine performance and emission characteristics can be investigated.

Fig. 3.3 Injection timing and ignition timing control system

Fig. 3.4 shows a computer was used to observe and analyze input data and output data as the cylinder pressure, engine speed, and engine torque can be observed during the experiments.

Fig. 3.4 dynamo controller and output data observed monitor

3.4 Summary

This chapter has detail explained about the engine testing specification, experimental system setup and experimental condition. Base on this experimental system, the engine ignition timing, air-mass flow, cylinder pressure, cylinder temperature and engine torque will be obtained under steady state and full load condition. This output experimental data will be used to valid the engine simulation model, which will be discussed in chapter 4.

4. SIMULATION MODEL SETUP

4.1 Introduction

It was complicated to determine the effective energy, trapped residual gases and pressure rise or to control combustion duration in the combustion chamber through experiments with the various testing conditions. Simulation method is powerful and effective tools to eliminate this problem, and AVL-Boost software was employed to estimate the influence of the hardware and software parameter on the engine performance and emission characteristics. This AVL-Boost software is well-known in the field of internal combustion engines. It helps researchers simulate various combustion engine types, such as SI engines [82], [83] compression ignition (CI) engines [84], diesel engine with turbocharger [85], [86] and engine using alternative fuel [87].

4.2 Numerical modeling

Fig. 4.1 presents the simulation model setup. The simulation model's elements represent the experimental engine parts. The engine part's characteristics were defined in simulation elements, this will be shown in appendix section. The steady state or transient state of the testing engine condition is selected in the element E1. The monitor MNT1 helps research observer interesting output data such as engine brake torque, residual gas, and effective energy. The system boundary conditions of the exhaust and intake tube were defined in elements SB1 and SB2. The air cleaner CL1 helps to filter air into the combustion chamber. The TH1 element helps to control the throttle angle. In the experiments, the throttle angle was kept at100%, and the restriction in the exhaust and intake tubes was defined by R1, R2, and R3. The junction (J1, J2, J3, J5, and J6) collects or distributes the air flow in the pipe. Measurements MP1 and MP2 on the exhaust and intake pipes defines the airflow characteristics. I1 and I2 is injector provides fuel to cylinders C1 and C2.

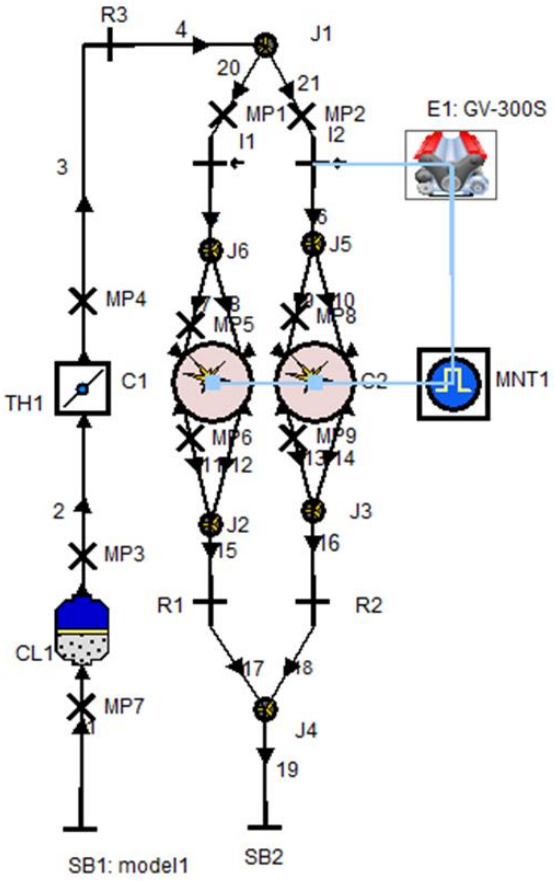

Fig. 4.1 Simulation model

Combustion model:

The Vibe function was used to determine heat release characteristics:

$$\frac{dx}{d\alpha} = \frac{a}{\Delta\alpha}(m+1)y^m . e^{-a.y(m+1)}$$

$$dx = \frac{dQ}{Q}; y = \frac{\alpha - \alpha_0}{\Delta\alpha_c} \quad (8)$$

Where

Q is total fuel heat input (W);

α is the crank angle (deg);

α_0 is the start of combustion (deg);

$\Delta\alpha_c$ is combustion duration (deg);

m is shaped parameter (-);

a is Vibe parameter a = 6.9 (-) for complete combustion.

The faction burned in mass ε can be calculated:

$$\boldsymbol{x = \int \frac{dx}{d\alpha} d\alpha = 1 - e^{-a.y(m+1)}} \quad (9)$$

The combustion chamber's heat transfer:

$$Q_T = A.q_{coeff}.(T_c - T_w) \quad (10)$$

Where

Q_T is heat lost to the wall (W/m^2);

A is the total surface area of the cylinder head, piston and cylinder (m^2);

q_{coeff} is heat transfer coefficient (W/m^2 K);

T_c is combustion gas temperature (K);

T_w is the wall temperature of the cylinder (K).

The residual gas fraction was calculated from the equation (11):

$$\boldsymbol{x_{SOC}^{cp} = \frac{\int_{V_c}^{V} \rho.x^{cp}.dV}{\int_{V_c}^{V} \rho.dV}} \quad (11)$$

ρ is local cylinder density (kg/m^3);

V is local cylinder volume (m^3);

x_{cp} is local cylinder combustion product mass fraction at SOC.

The effective release energy was calculated from equation (`12):

$$Q_{released,eff} = Q_{released} - Q_{CP} \quad (12)$$

The NO_x formation followed the six reactions [88] listed in Table 4.1:

Table 4.1. NO_x formative reactions

Stoichiometry	Rate $k_i = k_{0,i}. T^a.e^{(-TA_i/T)}$	k_0 [cm^3, mol, s]	a [-]	T_A [K]
$N_2 + O = NO + N$	$r_1 = k_1 . C_{N2}. C_O$	4.93E13	0.0472	38048.01
$O_2 + N = NO + O$	$r_2 = k_2 . C_{O2}. C_N$	1.48E08	1.5	2859.01
$N + OH = NO + H$	$r_3 = k_3 . C_{OH}. C_N$	4.22E13	0.0	0.0
$N_2O + O = NO + NO$	$r_4 = k_4 . C_{N2O}. C_O$	4.58E13	0.0	12130.6
$O_2 + N_2 = N_2O + O$	$r_5 = k_5 . C_{O2}. C_{N2}$	2.25E10	0.825	50569.7
$OH + N_2 = N_2O + H$	$r_6 = k_2 . C_{OH}. C_{N2}$	9.14E07	1.148	36190.66

The concentration of N_2O and the production rate of NO were determined by Equations (13) and (14):

$$C_{N_2O} = 1.1802.10^{-6}.T^{0.6125}.e^{\frac{9471.6}{T}}.C_{N_2}.\sqrt{P_{O_2}} \quad (13)$$

$$r_{NO} = 2.C_p.C_K.[1-\lambda^2].\frac{r_1}{1+\lambda.R_1}.\frac{r_4}{1+R_2} \quad (14)$$

$$\lambda = \frac{C_{NO,act}}{C_{NO,equ}}.\frac{1}{C_P};$$

$$R_1 = \frac{r_1}{r_2 + r_3}; R_2 = \frac{r_4}{r_5 + _6}$$

The CO formation followed the two reactions [89] in Table 4.2:

Table 4.2 CO formative reactions

Stoichiometry	Rate
$CO + OH = CO_2 + H$	$r_1 = 6{,}76 .10^{10}.e^{(T/1102)}.C_{CO}.C_{OH}$
$CO + O_2 = CO_2 + O$	$r_2 = 2{,}51 . 10^{12}. e^{(24055/T)}.C_{CO}.C_{O2}$

The production rate of CO emission was calculated by Equation (15):

$$r_{CO} = C_{Const}.(r_1 + r_2).(1-\varphi)$$

$$\varphi = \frac{C_{NO,act}}{C_{NO,equ}} \quad (15)$$

The unburned HC mass was calculated by Equation (16)

$$m_{HC} = \frac{P_C.V_{crevice}.M}{R.T_{piston}} \tag{16}$$

Air mass flow has a large impact on the performance of internal combustion engines. If the air mass flow into the cylinder in the limited band is increased while keeping the air-fuel ratio constant, the injected fuel into the cylinder increases. As a result, the maximum pressure in the cylinder would increase and the engine would perform at a higher torque. To improve the power of small SI-engines, several methods have been presented, such as reducing the restriction of the intake tube and reducing the bending tube in the intake tube system.

The air mass flow into the cylinder was calculated by Equation 17

$$\mathbf{\frac{dm}{dt} = A_{eff}.\, p_{01}.\sqrt{\frac{2}{R_g.T_{01}}}.\,\psi} \tag{17}$$

$\frac{dm}{dt}$ is mass flow rate;

$A_{eff}$is effective flow area;

p_{01} is upstream stagnation pressure;

T_{01} is upstram stagnation temperature;

R_g is gas constant.

For subsonic flow:

$$\psi = \sqrt{\frac{\mathbf{K}}{\mathbf{k-1}}\left[\left(\frac{\mathbf{p_{02}}}{\mathbf{p_{01}}}\right)^{\frac{2}{K}} - \left(\frac{\mathbf{p_{02}}}{\mathbf{p_{01}}}\right)^{\frac{K+1}{K}}\right]}$$

For sonic flow:

$$\psi = \left(\frac{2}{K+1}\right)^{\frac{1}{K-1}}.\sqrt{\frac{K}{k+1}}$$

K is ratio of specific heats;

p_{02} is downstream static pressure.

4.3 Model validation

The confidence of the simulated model was evaluated based on the comparison between the experimental results and simulated results. The black curves describe the experimental results while the red curves describe simulated results. Before using the simulated model to estimate the effect of parameters on engine performance and emission characteristics, this model was validated. The values of engine's specification and experimental data (bore, stroke, connecting length, intake and exhaust tube length and diameter, experimental conditions) were used as input data for the simulated model.

The ignition timing for each engine speed in both cases is shown in Fig. 4.2. Because the ignition timing is an input data for the simulation model so it can be seen that the experimental values for ignition timing were very close to the simulated values.

In the internal combustion engine with air-fuel ratio is constant, the air mass flow is a most sensitive factor which affects the fuel mass. Fig. 4.3 shows a comparison between experimental and simulated results in an air mass flow. The air-mass flow is changed while the air-fuel ratio is constant. The maximum difference between simulation and experimental result was 1.42% at 6000 rpm. It is acceptable because the experimental value of air mass flow is the average value.

The peak firing temperature is known as an important factor which has a strong effect on NO_x emission. Fig. 4.4 shows a comparison between experimental and simulated results for peak firing temperature. The values for the two cases are not much different at each engine speed. The maximum differential was 5.34% at 4000 rpm.

Fig. 4.5 shows the validation peak firing pressure rise. It can be seen that the values of peak firing pressure rise in the two cases are almost same at each engine speed. The maximum difference was 4.5% at 5000 rpm. During the combustion stroke, a better homogeneous air-fuel mixture leads to a full transient from chemical energy to the thermal energy and increase peak pressure in a shorter time to reduce heat loss and improve energy efficiency.

Fig. 4.6 shows a comparison between experimental and simulated results for engine torque. The maximum difference is 0.9% at 8000 rpm.

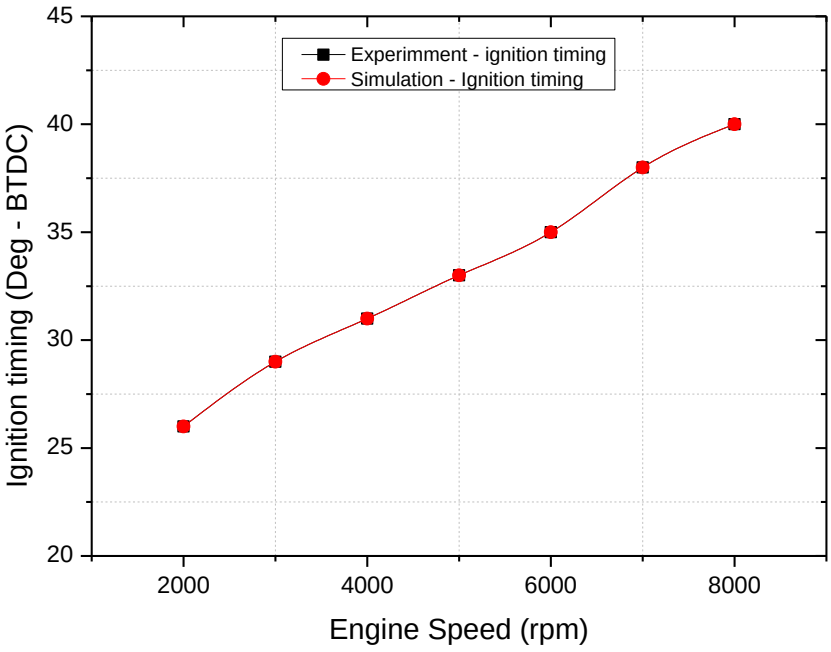

Fig. 4.2 Ignition timing versus engine speed

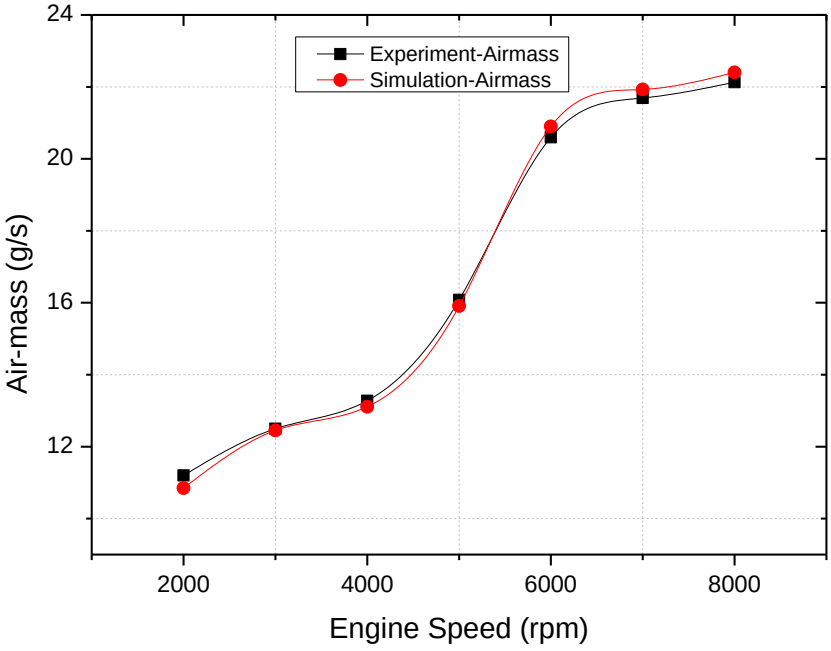

Fig. 4.3 Air mass flow versus engine speed

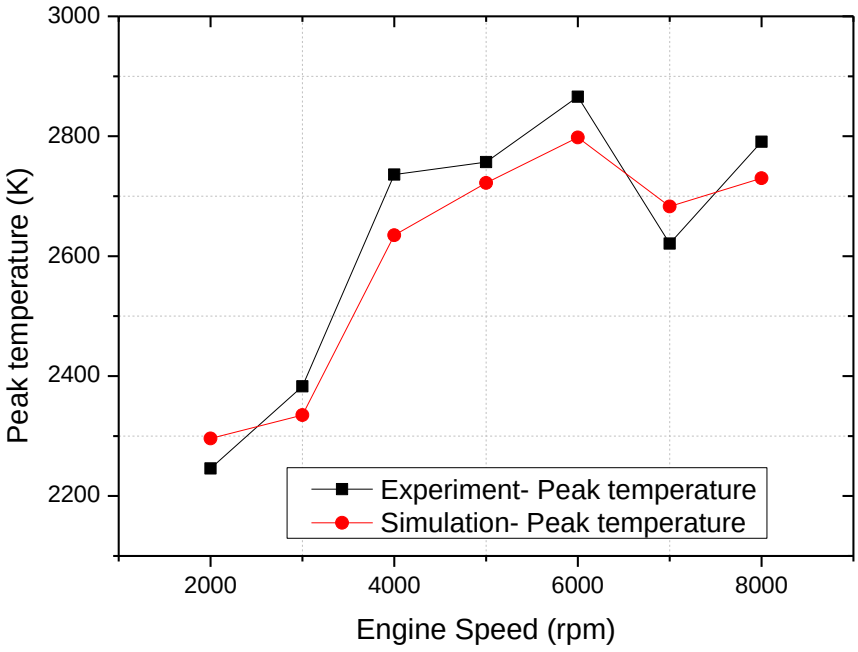

Fig. 4.4 Peak temperature flow versus engine speed

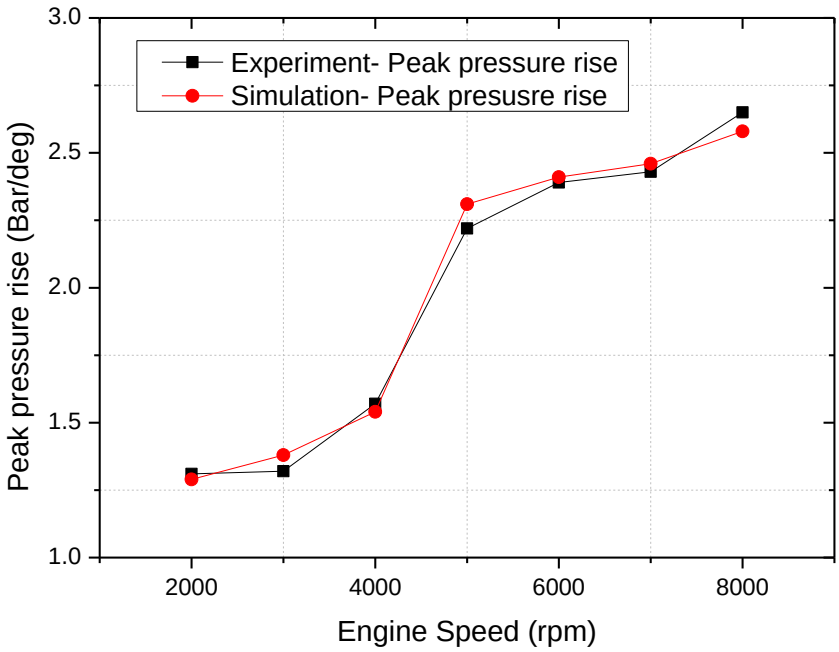

Fig. 4.5 Peak pressure rise flow versus engine speed

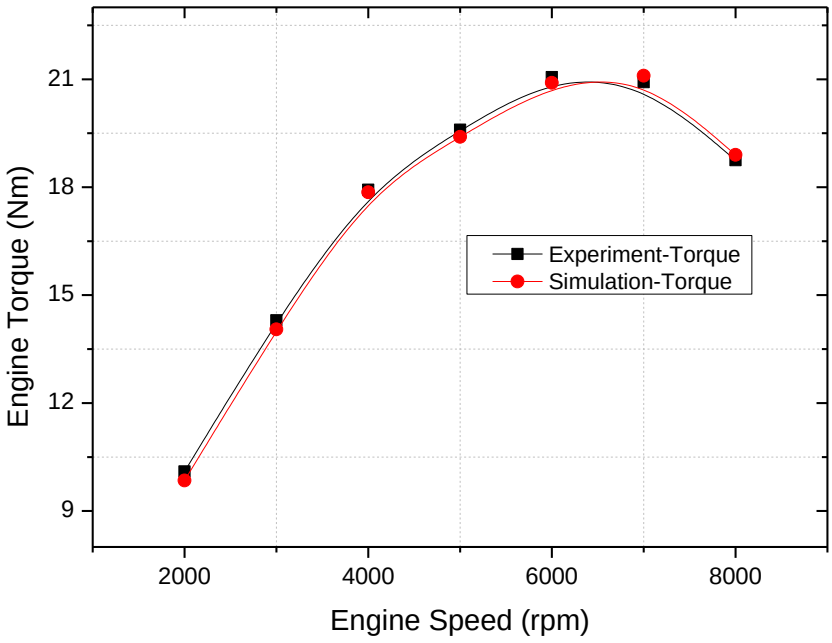

Fig. 4.6 Engine torque versus engine speed

From the comparison between experimental results and simulation results of the applied engine, all of the results in two cases are same, so the simulation model made by AVL-Boot software has a good accuracy in prediction of engine performance.

4.4 Summary

This chapter has explained the simulation modeling setup base on the AVL-boost software with version 2018. The simulation is validated base on the comparison between simulation results and experimental results in ignition timing, air-mass flow, peak cylinder pressure, peak cylinder temperature and engine torque. A steady base model was produced to support the simulated model, which had a more accurate method for predicting engine performance and emission characteristics. The investigation the effect of combustion duration, bore-stroke ratio, valve port diameter-bore ratio, exhaust valve closing timing and exhaust residual gas on engine performance and emission characteristics could be carried out via simulated approach.

A detail of optimization hardware and software parameters and determination of exhaust residual gas will be estimated in Chapter 5.

5. SIMULATION RESULTS AND DISCUSSION

Based on the simulation model made by AVL-Boot software has a good accuracy in prediction of engine performance in chapter 4. This chapter presents a study the effect of parameters such as: combustion duration, bore-stroke ratio, valve port diameter-bore ration, exhaust valve closing timing and exhaust residual gas on engine performance and emission characteristic. The drawback of the previous could be eliminated and from the results, the engine performance and emission could be improve with those optimal determination parameters.

5.1 Effects of combustion duration estimation

This part presents how combustion duration affects the performance and emission characteristics of motorcycle engines. From the results, the researcher is able to know the best combustion duration value that gives the target engine torque, NO_x, CO and HC. The investigated engine parameters were residual gas, effective release energy, BSFC, IMEP, BMEP, peak firing temperature, engine torque, engine power, NO_x, CO, and HC emissions. Also, the relationship between the optimum combustion duration at each engine speed, residual gas, effective release energy, and engine emission were discussed.

5.1.1 Effects of combustion duration on engine performance

This section described the effect of combustion duration on engine performance. The results show the relationship between combustion duration and some other parameters as like as residual gas, effective release energy, BSFC, IMEP, BSFC, peak firing temperature, brake torque, engine power and NO_x, CO and HC emission.

Fig 5.1 shows gross release energy versus combustion duration at different engine speeds. The gross release energy depends mostly on the air-fuel mass in the cylinder and the combustion conditions.

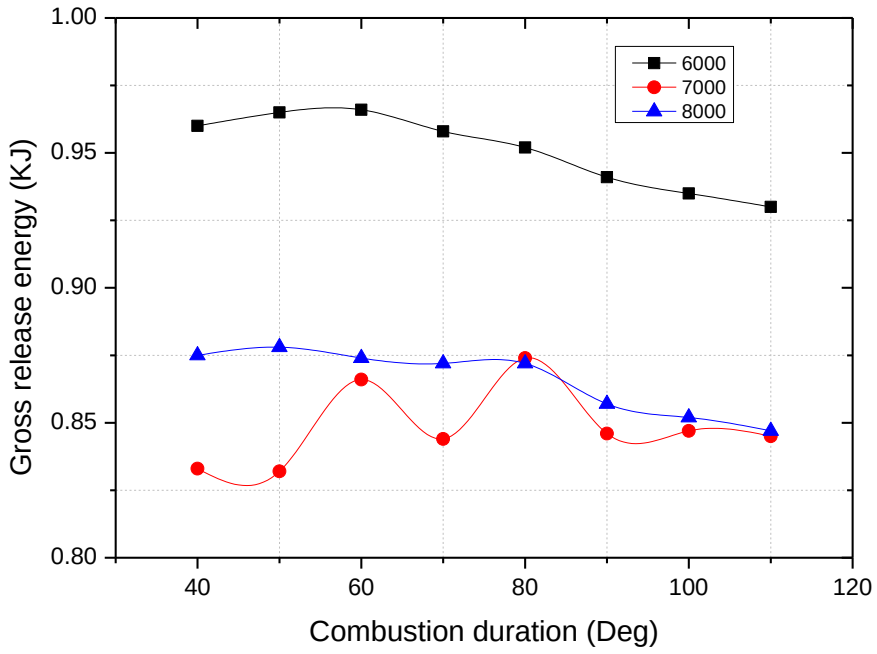

Fig. 5.1 Gross release energy versus combustion duration

Fig 5.2 shows the effect of combustion duration on the residual gas ratio. It can be seen that when combustion duration increase from 40 degrees to 110 degrees at engine speed was 7000 rpm and 8000 rpm. The residual gas ratio shows a downward trend from 0.25% – 0.13%. When the engine speed was 6000 rpm, the residual gas ratio decreases from 0.36% to 0.22% and then increase to 0.3%. The minimum residual gas ratio was 0.22% at 80 degrees combustion duration. It can be explain by that at a low and medium engine speed, an excessively long combustion duration can extend the burning process until the pistons are at BDC or even in the exhaust stroke. This process will affect the next intake stroke to reduce fresh air-fuel into the cylinder, thereby sweeping the exhausted gas outside.

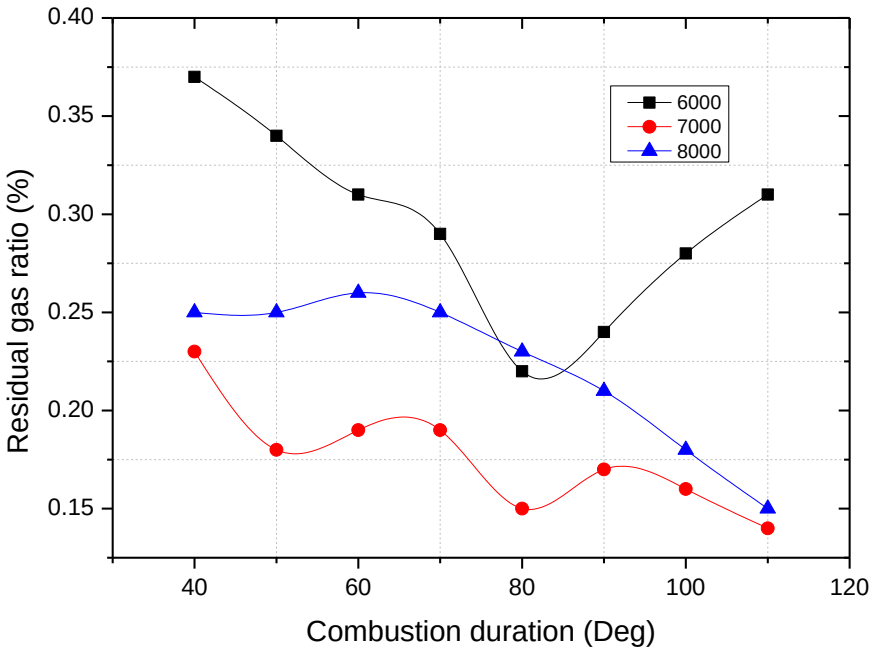

Fig. 5.2 Residual gas ratio versus combustion duration

Figure 5.3 shows the effect of combustion duration on peak firing temperature. The peak firing temperature decreases as the combustion duration increases. This is because the increase in combustion duration is due to the increased percentage of heat loss. On the other hand, if the combustion duration is too long then it will take more time for the heat transfer within the piston, cylinder and flowing out through the exhaust gas. This accounts for the decrease in the mean effective release energy has decreased (Fig 5.4).

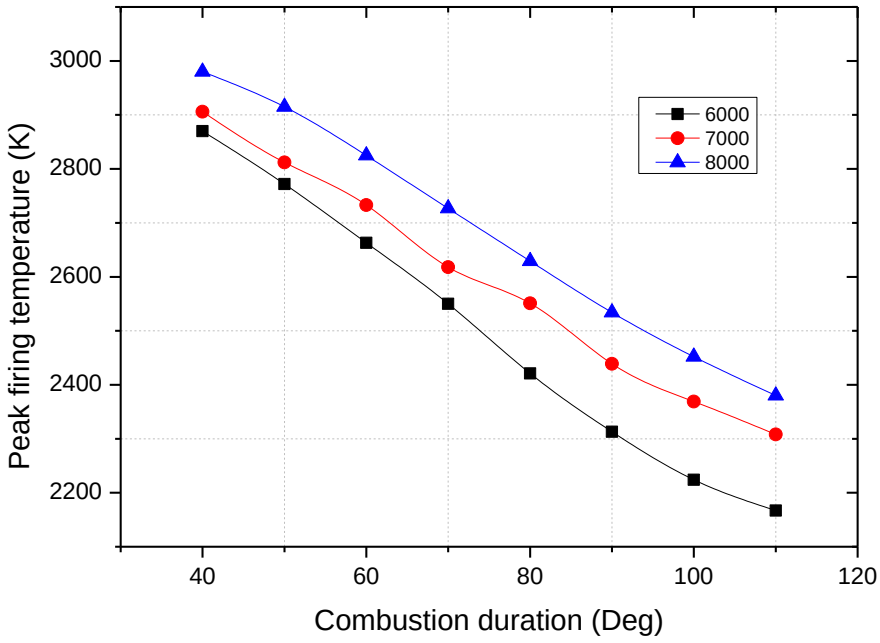

Fig. 5.3 Peak firing temperature versus combustion duration

As shown in Figure 5.4, as the combustion duration increases, the effective release energy increases until a maximum value was achieved after that, a subsequent decrease was observed. The maximum effective release energy was different at different engine speeds. This could be explained by following two aspect factors. Firstly, if the combustion duration is extremely short then the chemical energy of fuel could not be completely converted to thermal energy. Moreover, if the combustion duration is long, then more thermal energy loss will occur because of increased heat loss. That is why the effective release energy initially increased until a maximum value was achieved. After that, it was decease following the increase in combustion duration. Secondly, in a real SI engine, because the combustion reaction always takes some time, the heat release is conducted instantaneously at TDC. To increase thermal efficiency, a short duration is required for the total heat release energy to occur. Because it increases the frequency of heat release energy to make the real cycle resembles an Otto cycle better. The engine speed band has a strong effect on the time of total heat release energy which accounts for the different maximum release energy at gotten different engine speeds. In this research, at 6000 rpm, the maximum effective release energy was 0.826 KJ at 60 degrees combustion duration. At 80 degrees combustion duration, the maximum effective release energy at 7000 rpm and 8000 rpm was 0.831 KJ and 0.825 KJ, respectively.

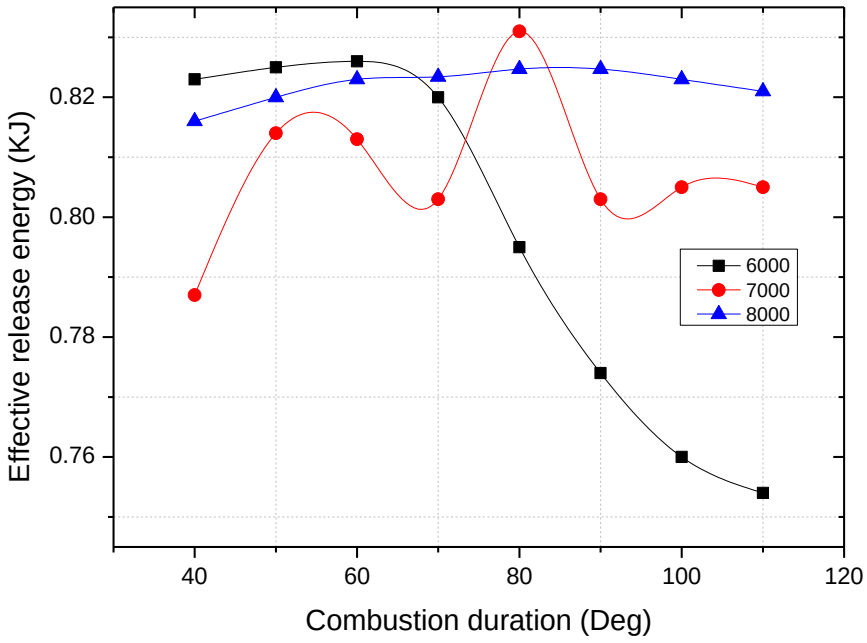

Fig. 5.4 Effective release energy versus combustion duration

Figures 5.5 and Fig 5.6 show the BMEP and IMEP versus combustion duration. The BMEP and IMEP increases until a maximum value was achieved before further decrease began to occur. At each engine speed, there was an optimal combustion duration value, at that value, the engine showed a higher BMEP and IMEP. Besides that, the engine achieves a maximum BMEP and IMEP at the same combustion duration. This is because the effect of combustion duration on BMEP and IMEP was same with effect on effective release energy. As shown in Fig 5.4, Fig 5.5 and Fig 5.6 similar trend of effective release energy, BMEP and IMEP was presented. The equation (18) shows the relationship between BMEP and IMEP. This equation explains why the maximum BMEP and maximum IMEP was dropped at the same combustion duration value.

BMEP=IMEP – FMEP – SMEP (18)

Where

FMEP is friction mean effective pressure, Bar;

SMEP is scavenging mean effective pressure, Bar.

In this research, at 6000 rpm and 60 degrees combustion duration, the maximum BMEP was 10.55 bar and maximum IMEP was 12.6 bar. At 7000 rpm and 80 degrees combustion

duration, the maximum BMEP was 10 bar, and the maximum IMEP was 12.20 bar. At 8000 rpm, the maximum BMEP was 9.24 bar, and maximum IMEP was 11.85 bar.

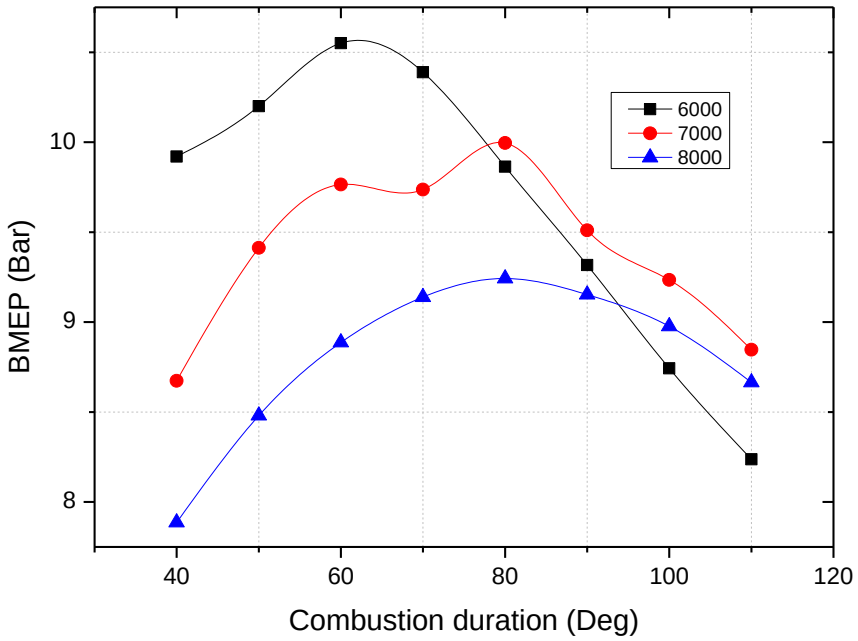

Fig 5.5 BMEP versus combustion duration

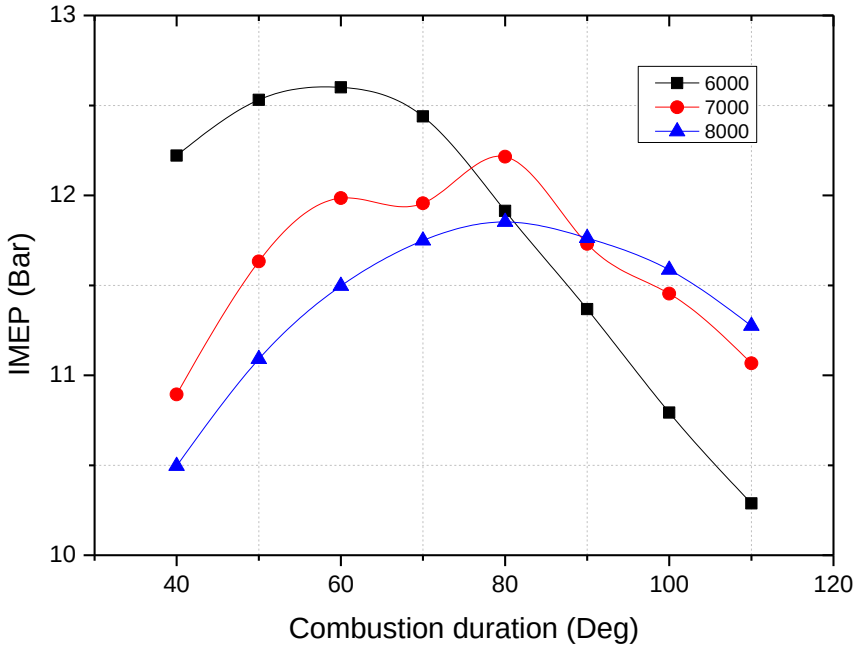

Fig. 5.6 IMEP versus combustion duration

Figure 5.7 shows the combustion duration effect on BSFC. Initially, the BSFC was decreasing until a minimum value was achieved after that, an increase began to occur. At each engine speed, a combustion duration value for optimal fuel consumption was identified. At 6000 rpm and 60 degrees combustion duration, the minimum BSCF was 319.8 g/KWh. At 7000 rpm and 80 degrees combustion duration, the minimum BSFC was 373.5 g/KWh. At 8000 rpm and 80 degrees combustion duration, the minimum BSFC was 385.7 g/KWh. The effect of combustion duration on BSFC, engine effective torque and engine effective power all suggest that the BMEP has a strong effect on BSFC, engine effective torque, and engine effective power.

Equation 19 shows the relationship between BMEP and engine effective torque.

$$\mathbf{T_{eff}} = \frac{\mathbf{BMEP.V_D}}{\mathbf{k_{cycle}.\pi}} \quad (19)$$

Where

T_{eff} is engine effective torque (Nm);

V_D is displacement (m^3);

k_{cycle} is a simulation cycle parameter, cycle.

The relationship between BMEP and engine effective power

$$P_{eff} = BMEP.V_D.n_{cycle} \quad (20)$$

Where

P_{eff} is engine effective power (kW);

n_{cycle} is a number of cycle per second, cycle/sec.

The relationship between BSFC and engine power

$$BSFC = \frac{\varepsilon}{\mathbf{P_{eff}}} \quad (21)$$

Where

ε is the fuel consumption rate in grams per second (g/s).

From equation (19), (20), (21) it can be seen that the increase of BMEP helps improve engine effective torque, engine effective power, and BSFC.

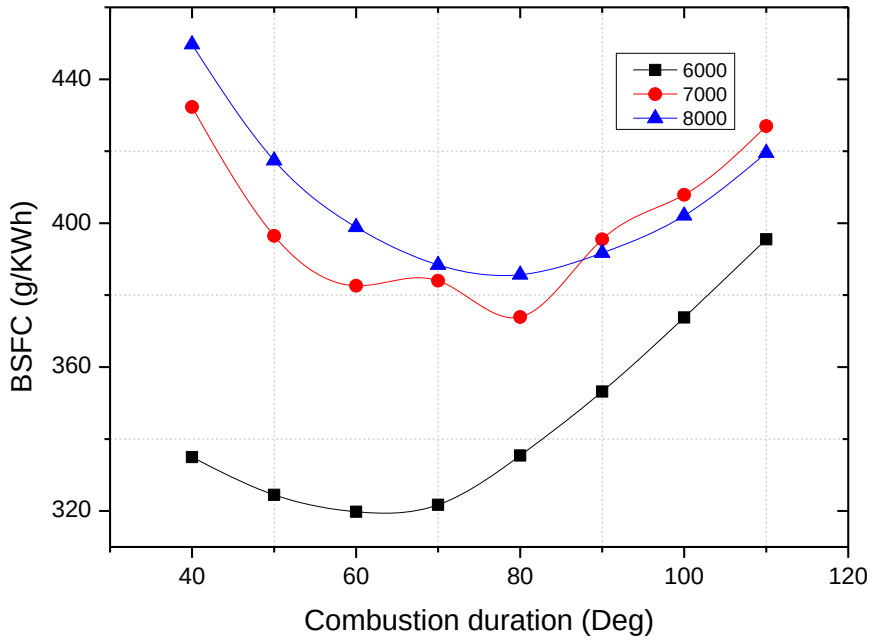

Fig. 5.7 BSFC versus combustion duration

Figures 5.8 and Fig. 5.9 show the combustion duration effect on engine brake torque and engine power. Following the increased combustion duration, the BMEP, engine brake torque and engine power had the same fluctuating trend. The engine brake torque and engine power increases until a maximum value was achieved after that, a decrease was observed as the combustion duration keeps increasing. At each engine speed, the optimal combustion duration value at that the engine shows an optimal performance. The maximum engine brake torque and engine power dropped at the same combustion duration value. At 6000 rpm and 60 degrees combustion duration, the maximum brake torque was 22.7 Nm and maximum power 14.48 KW. At 7000 rpm and 80 degrees combustion duration, the maximum brake torque was 21.55 Nm, and maximum power was 16.01 KW. At 8000 rpm and 80 degrees combustion duration, the maximum brake torque was 20.25 Nm, and maximum power was 16.92 kW. In case of the engine speed at 7000 rpm and 70 degrees combustion duration, the values fluctuated because of the combustion duration on the mixing air-fuel homogeneity at 70 degrees was not better than that at 60 degrees and 80 degrees. The homogeneous air-fuel mixing in the combustion chamber was reflected through the residual gas and CO emission. With a combustion duration of 70 degrees, the residual gas was bigger than that at 60 degrees and 80 degrees.

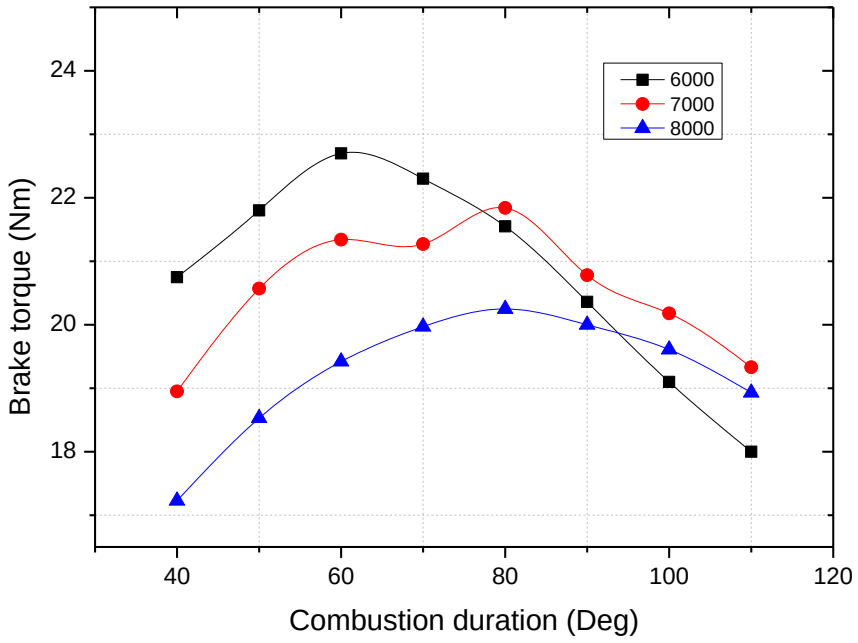

Fig. 5.8 Brake torque versus combustion duration

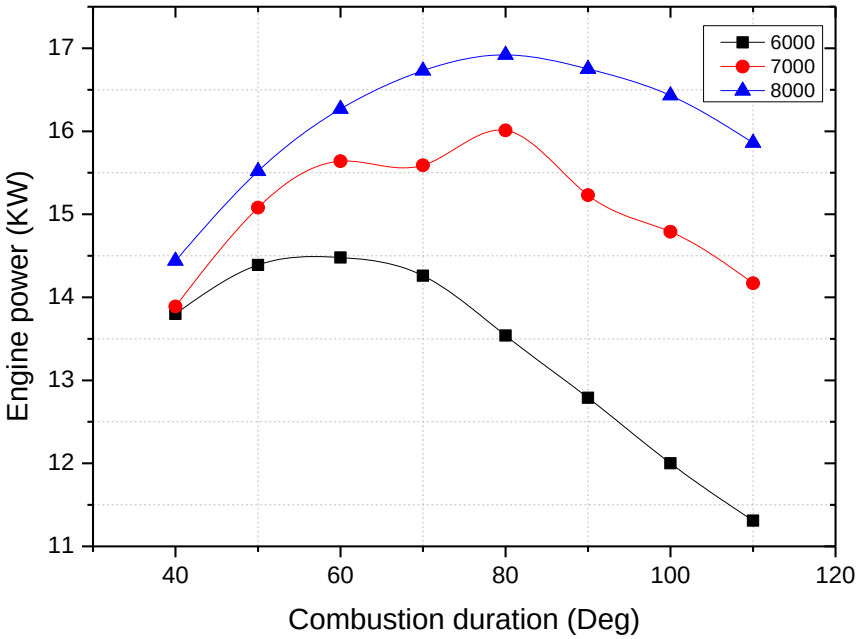

Fig 5.9 Engine power versus combustion duration

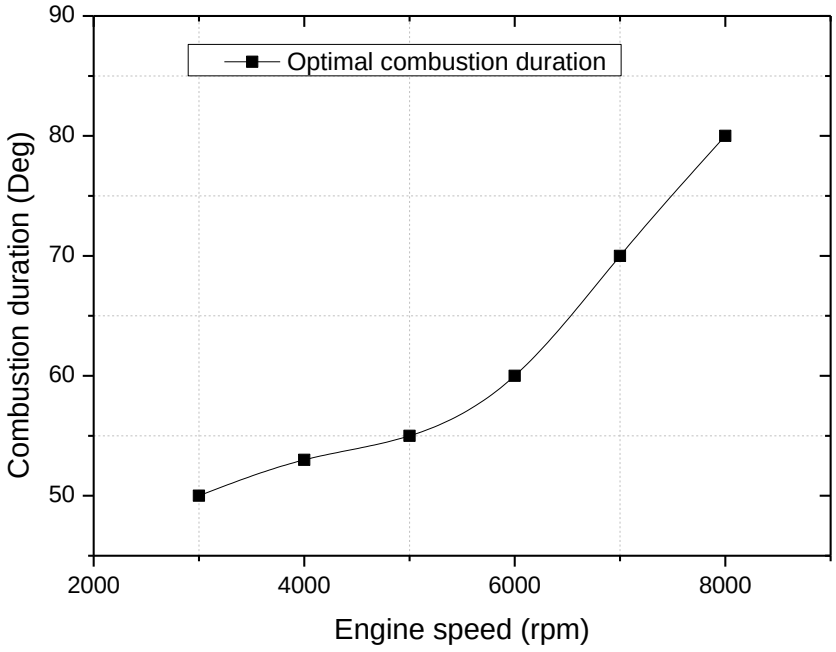

Fig 5.10 Optimal combustion duration at each engine speed

Figure 5.10 shows the optimal combustion duration at each engine speed. The optimal combustion duration has increased trend with increasing engine speed. This suggest that when engine run at higher speed, parameter such as air-fuel ratio, spark advance, and compression ratio should be adjusted to extend the combustion duration. When the engine is operated at the optimal combustion durations, the engine torque is at maximum value and BSFC is at a minimum value.

5.1.2 Effects of combustion duration on engine emission

Figure 5.11 shows the effect of combustion duration on the NO_x emission. The NO_x emission decreases with increasing combustion duration because of the decreased peak firing temperature (Fig. 5.3). The peak firing temperature has the greatest effect on NO_x emission. The decrease in peak firing temperature is said to reduce NO_x emission and vice versa.

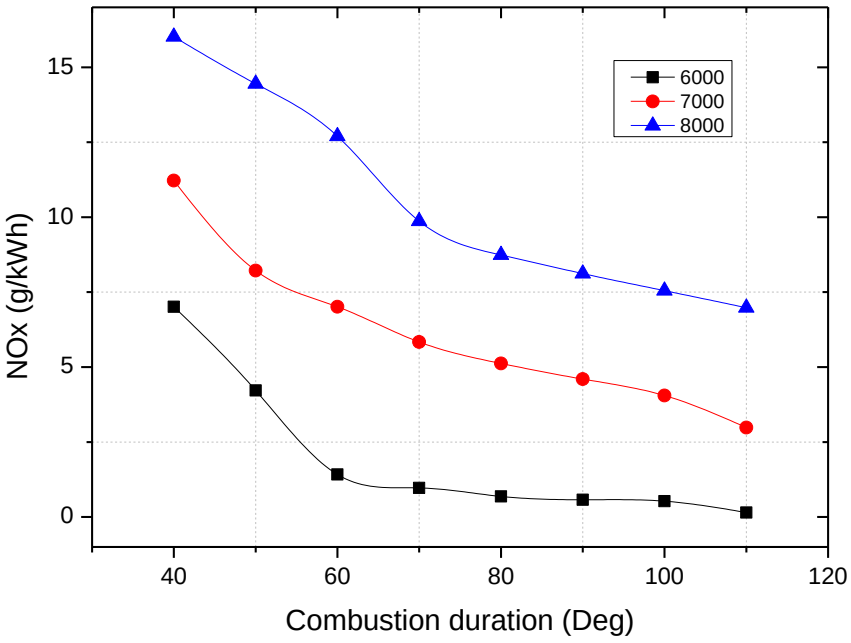

Fig 5.11 NO_X emission versus combustion duration

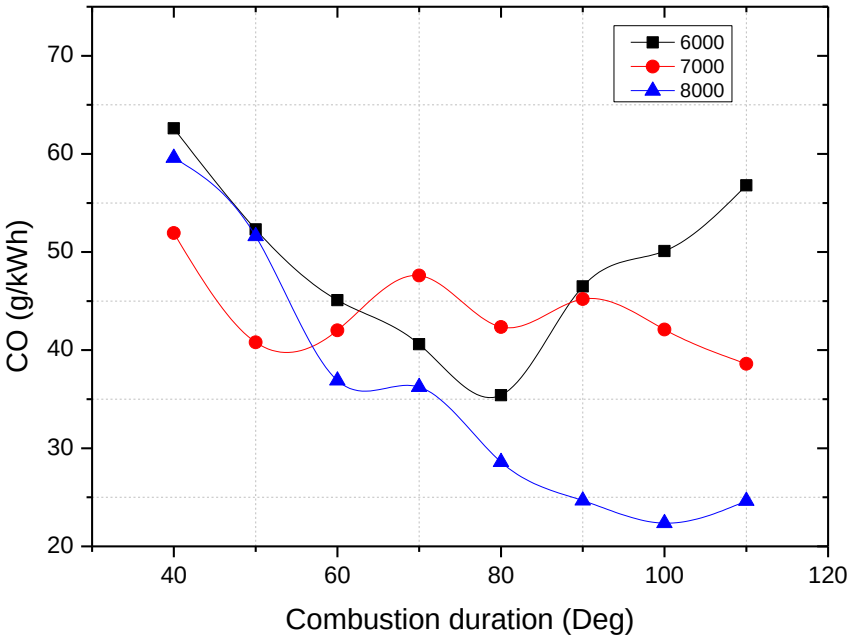

Fig 5.12 NO_x emission versus combustion duration

Figure 5.12 shows that the trend of CO emission was not maintained, this trend was like that of the residual gas ratio. At 6000 rpm, the CO emission decreased while the combustion duration increased from 40 degrees to 80 degrees. At 7000 rpm and 8000 rpm, the CO emission trend decreases while engine combustion duration increases from 40 degrees to 80 degrees. This suggests that the residual gas had a huge effect on the CO emission characteristics because when the residual gas increases, the amount of fresh air in the next intake stroke decreases. Thus, the CO emission increases with an increase in the residual gas.

Figure 5.13 shows that HC emission decreases as the combustion duration increases because of the increase in the time needed for complete combustion of the fuel to occur.

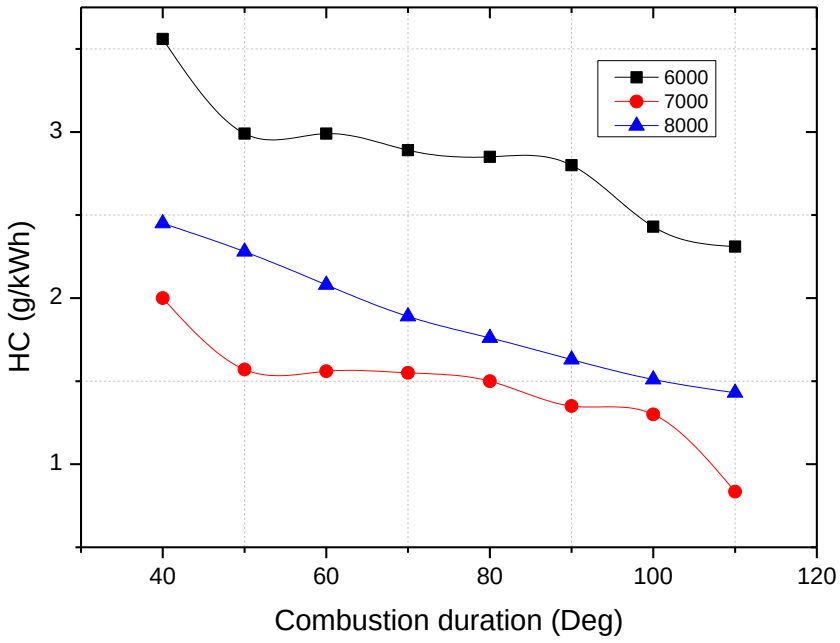

Fig 5.13 HC emission versus combustion duration

The above result reveals the importance of combustion duration in a small SI-engine. In addition, how this parameter influences the residual gas ratio, effective release energy, BSFC, engine torque, and engine emission characteristics were discussed.

5.1.3 Summary

This section has presented a solution for solving the lack of control and the inability to precisely determine the combustion duration. For the very first time, the effect of combustion duration was totally presented in a motorcycle engine. With an engine testing speed band ranging from 3000 rpm – 8000 rpm, the combustion duration increased from 40 degrees to 110 degrees crank angle. Through combined experimental and simulated methods, this is an accurate method for predicting the effect of combustion duration on engine performance and engine emission characteristic. The optimal combustion duration at each engine speed was also determined. At that optimal combustion duration value, the engine displays superior performance. By varying the combustion duration, we were able to control both the NO_x and CO emission in the limited band.

The results were summarized below:

1) The combustion duration has a significant effect on residual gas and the effective release energy. In various engine speeds, the effect of combustion duration on residual gas, and effective release energy varied. Following increased of combustion duration, at an engine speed was 7000 rpm and 8000 rpm the residual gas and effective release energy decreased. The minimum residual gas ratio was 0.14% and 0.15%, respectively. When engine speed was 6000 rpm, the residual gas decreases initially and increases thereafter. Likewise, at 80 degrees combustion duration, the minimum residual gas ratio was 0.22% while the maximum effective release energy was 0.826 KJ at 60 degrees combustion duration.

2) The optimal value of effective release energy, BMEP, IMEP, and BSFC was achieved at the same combustion duration value of each engine speed. At an engine speed of 6000 rpm and 8000 rpm, the optimal value of effective release energy, BMEP, IMEP, and BSFC drops at 60 degrees and 80 degrees combustion duration.

3) At each engine speed, an optimal combustion duration value was found. According to the result of the research, the engine gives the best performance at 6000 rpm and 60 degrees combustion duration. In this case, the engine was able to achieve the maximum brake torque at 22.7 Nm and minimum BSCF at 319.8 g/KWh.

4) The combustion duration affected heat loss in the cylinder because the increased combustion duration gave rise to an increased heat transfer within the cylinder and piston. As

the combustion duration increases from 40 degrees to 110.0 degrees, the peak firing temperature decreases from 2900 K to 220 K.

5) The residual gas affected the released energy and CO emission. The trend of residual gas was opposite to trend of effective release energy. As the residual ratio increases, the effective release energy decreases while the CO emission increase, and vice versa.

6) The NOx and HC emission decrease when the combustion duration increases from 40 degrees to 110.0 degrees. At engine speed of 6000 rpm, the NOx and HC decreases from 7 g/kWh to 0.2 g/kWh and 3.56 g/kWh to 3.1 g/Kwh respectively. When engine speed was 7000 rpm, the NOx and HC decrease from 11.22 g/kWh to 2.98 g/kWh and 2 g/kWh to 0.835 g/Kwh respectively. When the engine speed was 8000 rpm, the NOx and HC decrease from 16.2 g/kWh to 6.9 g/kWh and 2.45 g/kWh to 1.43 g/Kwh in respectively.

5.2 Effects of bore-stoke ratio (BTR) estimation

In the continual effort to develop an improved performance of a small SI engine, this part presents the effects of bore-stroke ratio on residual gas, peak firing pressure rise, combustion duration and effective release energy of a motorcycle engine. A laboratory system was established, and studied a small SI-engine via a simulation model. Through combined experimental and simulative methods, the drawbacks of the experimental in optimization of bore-stroke ratio parameter were eliminated.

5.2.1 Effects of BTR on engine performance

Figure.5.14 depicts the volume efficiency as a function of bore-stroke ratio. When the bore-stroke ratio increased from 0.8 to 1.1, the volume efficiency increased from 0.78 to 0.83. The minimum volume efficiency was 0.78 at a 0.8 bore-stroke ratio and the maximum value was 0.83 at a 1.1 bore-stroke ratio. This can be explained by that beside the intake port configuration and engine speed have sensitive effect on air mass flow and air-fuel mixture turbulent in the combustion chamber, the combustion chamber shape also effects on air mass flow and turbulent fluctuations of air-fuel flow. With increasing of bore-stroke ratio, the space between inlet port and cylinder wall was increased. A large space between inlet port and cylinder wall help increasing ventilating space behind inlet ports, a reduction of collision

between air-fuel flows with cylinder wall led to reduce the reverse flow, allowing higher air–fuel mass and reduce the turbulence of air-fuel mixture flow in the cylinder. This accounts for the reason why the volumetric efficiency increases as the bore-stroke ratio increases. The decrease of turbulence fluctuations of air-fuel flow in the combustion chamber led to increase the air-fuel mixing time and reduce the homogeneous of air-fuel mixture. As the results, the increase of ignition timing and combustion duration when bore-stroke ratio increases was observed in Fig. 5.15 and Fig. 5.16. The ignition timing and combustion duration were increased from 15 to 35 deg BTDC and from 70 to 100 deg CA respectively.

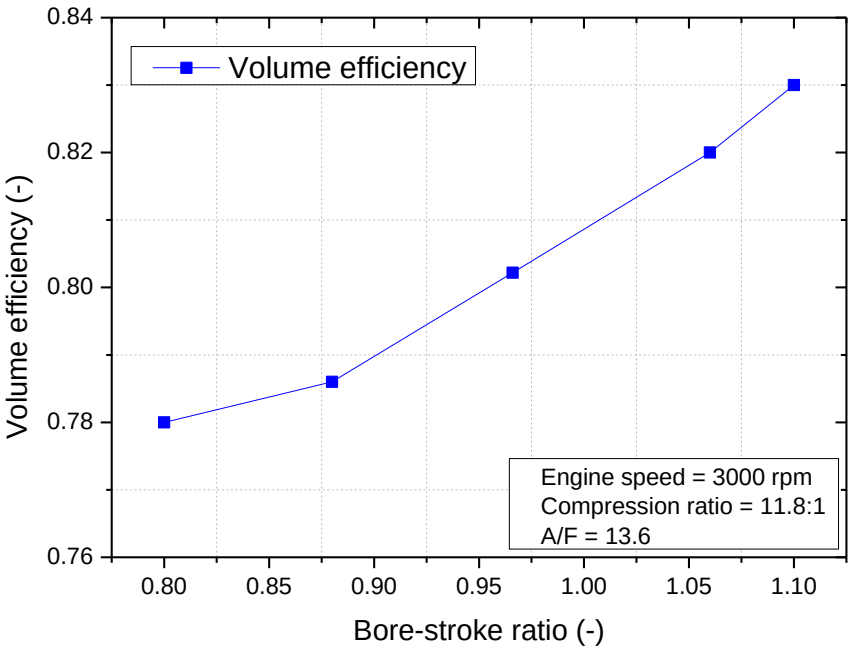

Fig 5.14 The effect of BTR on volume efficiency

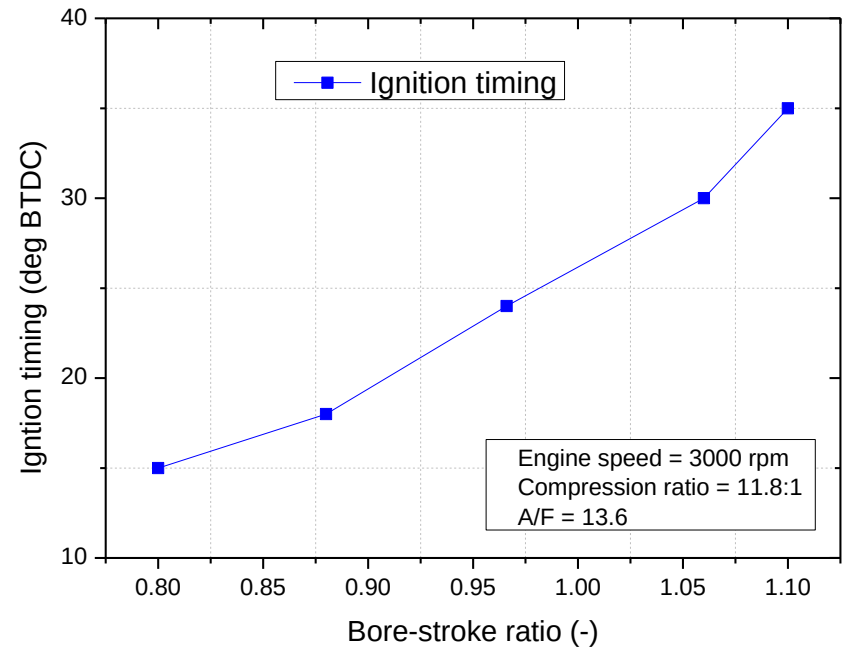

Fig 5.15 The effect of BTR on ignition timing

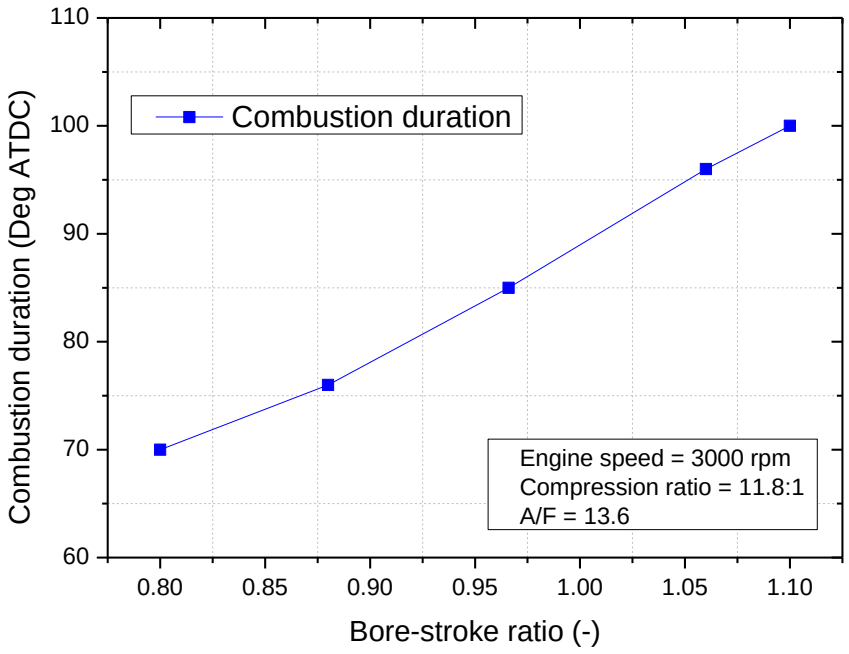

Fig 5.16 The effect of BTR on combustion duration

In the internal combustion engine: valves lift, valve overlap, ignition timing and engine speed were the most sensitive parameters effect on residual gas. In this section, how bore-stroke ratios effect on residual gas will be learned. Figure 5.17 shows the residual gas ratio as a function of the bore-stroke ratio. When the bore-stroke ratio increased from 0.8 to 1.1, the residual gas ratio declined from 7.5% to 5.6 %. The variation of residual gas ratio was within 2% when bore-stroke ratio changed that means the bore-stroke ratio had quite effect on residual gas. The minimum residual gas ratio was 5.6% at a 1.06 bore-stroke ratio and the maximum residual gas ratio was 7.5% at a 0.8 bore-stroke ratio. This can be explained by an increase of bore-stroke ratio helping to increase the air-fuel mass flow and combustion duration. This process helps to reduce the multiform molecular of exhaust gases, and the subsequent effect of the intake stroke by introducing fresher air fuel to sweep the exhausted gas out of the cylinder. This accounts for the reason why the residual gas ratio decreases as the bore-stroke ratio increases.

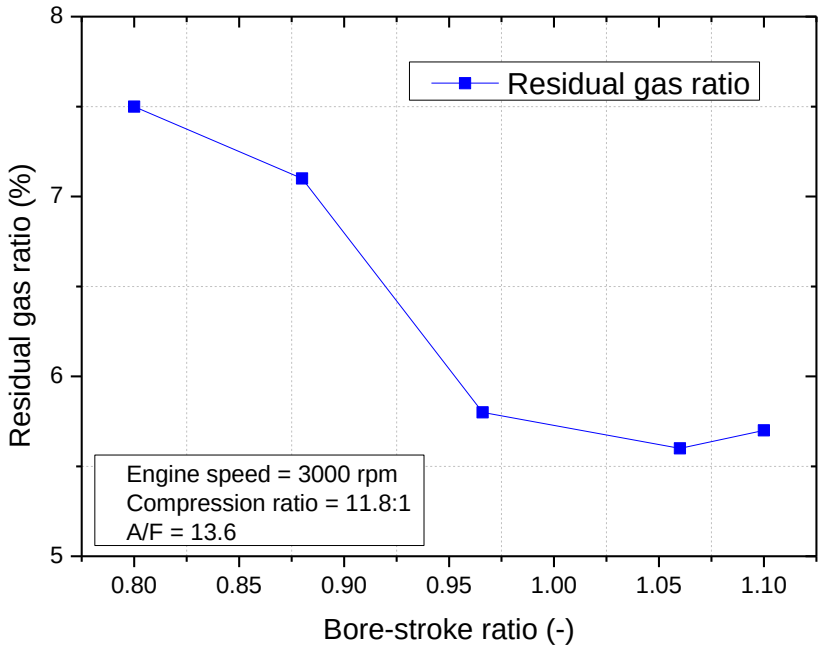

Fig 5.17 The effect of BTR on residual gas ratio

The bore-stroke ratio has a significant effect on peak firing pressure rise and peak firing temperature. As shown in Figs. 5.18 and 5.19, the peak firing temperature de-creased when bore-stroke ratio increased. This is because the increase in bore-stroke ratio was due to the increase in heat loss. On the other hand, the peak firing pressure rise trend was not stable. At a bore-stroke ratio of 0.966, the peak firing pressure rise achieved its maximum value of 3.05 bars/deg. This pressure rise value was bigger than that when compared to reference bore-stroke ratio case (1.06). This could be explained by that, at 0.966 of bore-stroke ratio a better homogeneous air-fuel mixture was performed, this led to a full transient from chemical energy to the thermal energy and increase peak pressure in a shorter time.

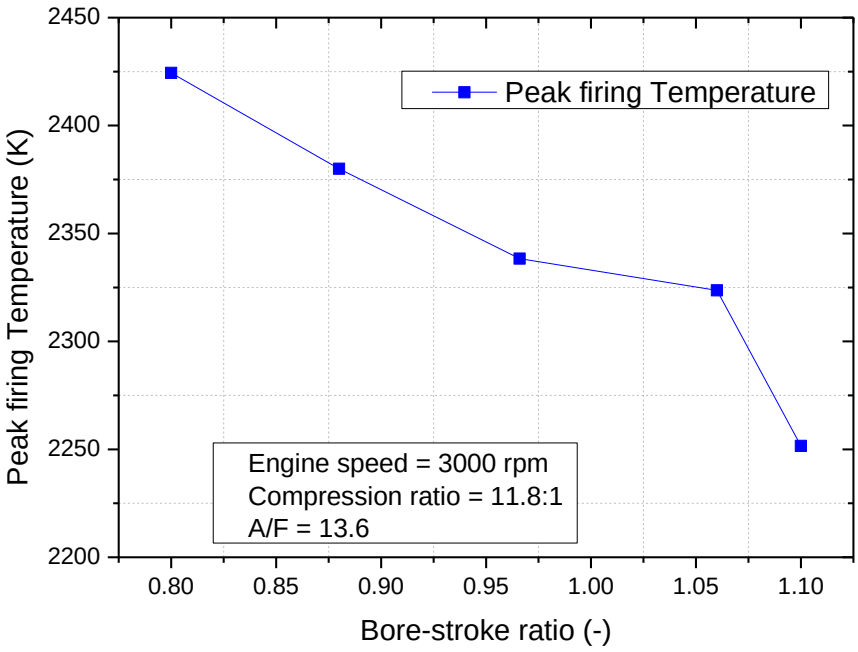

Fig 5.18 The effect of BTR on peak firing temperature

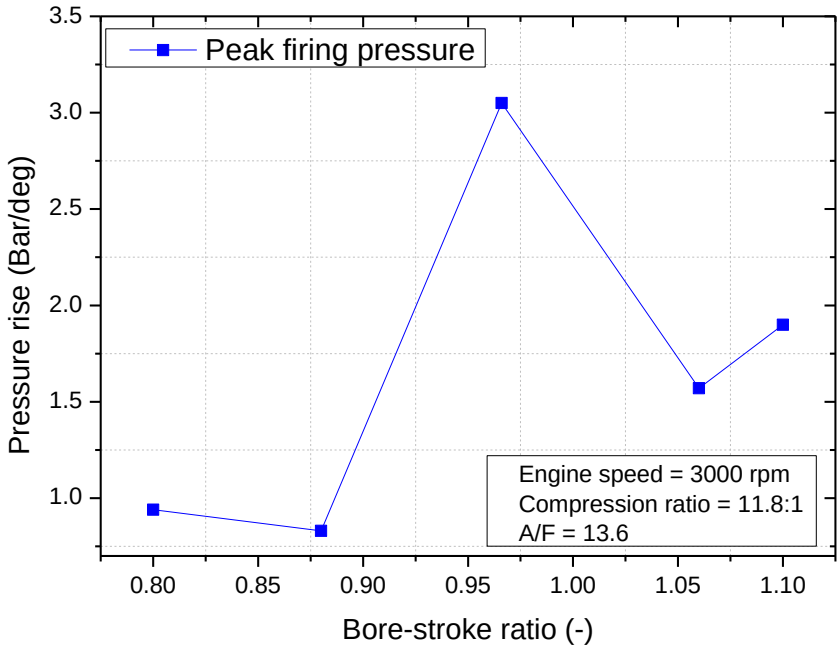

Fig 5.19 The effect of BTR on peak firing pressure rise

In the combustion stroke of the internal combustion engine, the chemical energy of fuel trapped in the cylinder was released into heat energy. An amount of loss heat energy was from heat transfer, pumping loss and energy that is not effectively released in the cylinder but is going into the combustion products so the remaining amount energy is effective release energy (Fig 5.20). The heat loss and combustion duration of an internal combustion engine have a large effect on effective release energy. In our study, the increases in the bore-stroke ratio were due to increases of the heat transfer loss, so we observed a decline in effective release energy. This could be because, combustion reaction does not occur instantaneously in a typical SI engine. However, heat is instantaneously released at top dead center (TDC). In order to increase the thermal efficiency, the burn time is expected to be short and the faster the release of the heat energy. As this was, the increased heat energy between the real cycle and a typical Otto cycle would be similar. Because a larger bore-stroke ratio leads to a longer burn time so a lower effective release energy was as a consequence. In this study, the effective release energy decreased from 0.606 kJ to 0.567 kJ when the bore-stroke ratio increased from 0.8 to 1.1.

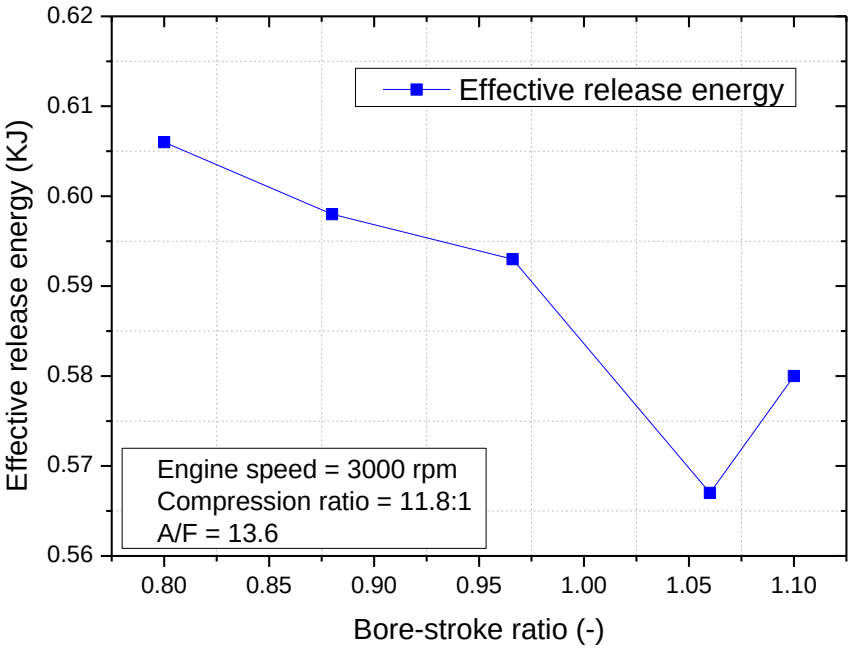

Fig 5.20 The effect of BTR on effective release energy

Figures 5.21 brake mean effective pressure (BMEP) versus bore-stroke ratio. The BMEP decreased when the bore-stroke ratio increased, because the bore-stroke ratio had the same impact on BMEP and effective release energy. Figures 5.20 and 5.21 present similar trends of effective release energy and BMEP. Equation (18) depicts the relationship between BMEP and IMEP, explaining why the maximum and minimum values of BMEP and IMEP declined at the same bore-stroke ratio value. When the bore-stroke ratio was 0.8, the engine achieved its maximum BMEP (6.92 bar) and maximum IMEP (9.09 bar). At the bore-stroke ratio was 1.06, the minimum values of BMEP and IMEP were 6.42 bar and 8.61 bar, respectively.

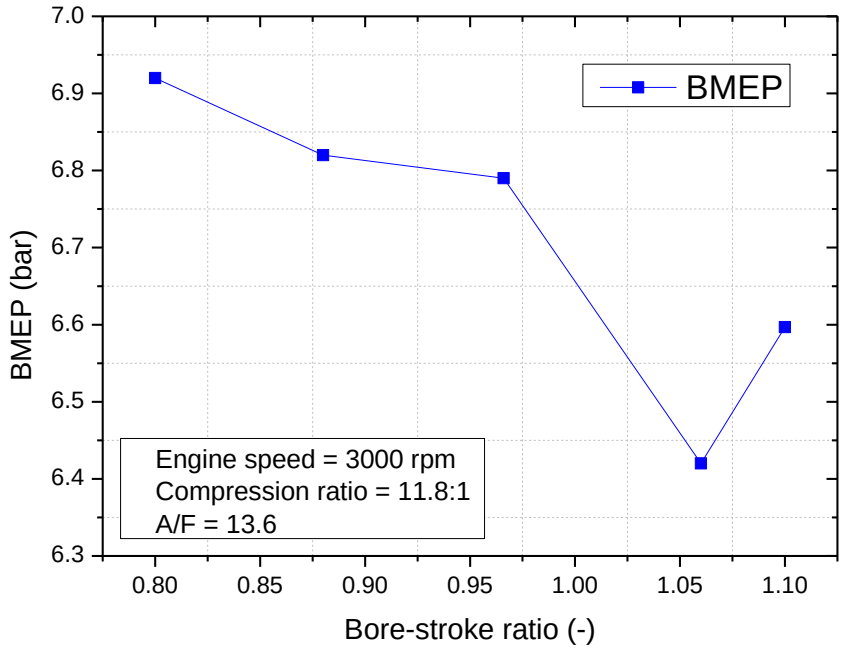

Fig 5.21 The effect of BTR on effective release energy

Fig. 5.22 shows that the BSFC was influenced by bore-stroke ratios, trending upward when the bore-stroke ratio increased from 0.8 to 1.1. In test conditions with constant the engine speed and constant air-fuel ratio, the BMEP had the greatest effects on the BSFC. The relationship between BMEP and BSFC is described in Equation (22):

$$BSFC = \frac{m_{air}.n_c.2.16.10^9}{AFR.BMEP.V_D.n} \qquad (22)$$

Fig. 5.23 shows the impact of bore-stroke ratio on the engine brake torque. With increasing bore-stroke ratio, the BMEP and engine brake torque showed the same downward trends. At a bore-stroke ratio of 0.8, the engine's maximum brake torque was 15.13 Nm, a 7.68% improvement when compared to reference bore-stroke ratio case (1.06).

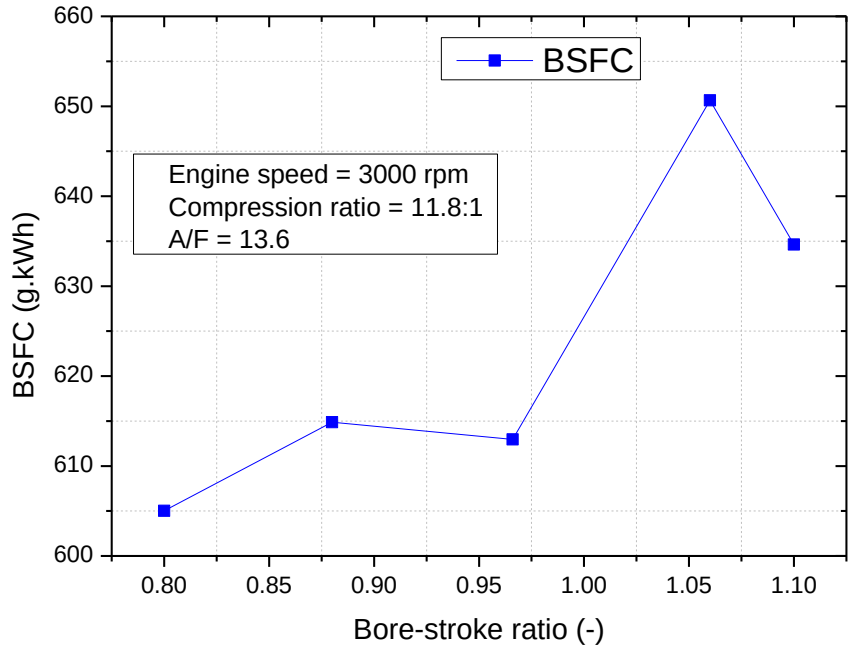

Fig 5.22 The effect of BTR on BSFC versus bore-stroke ratio

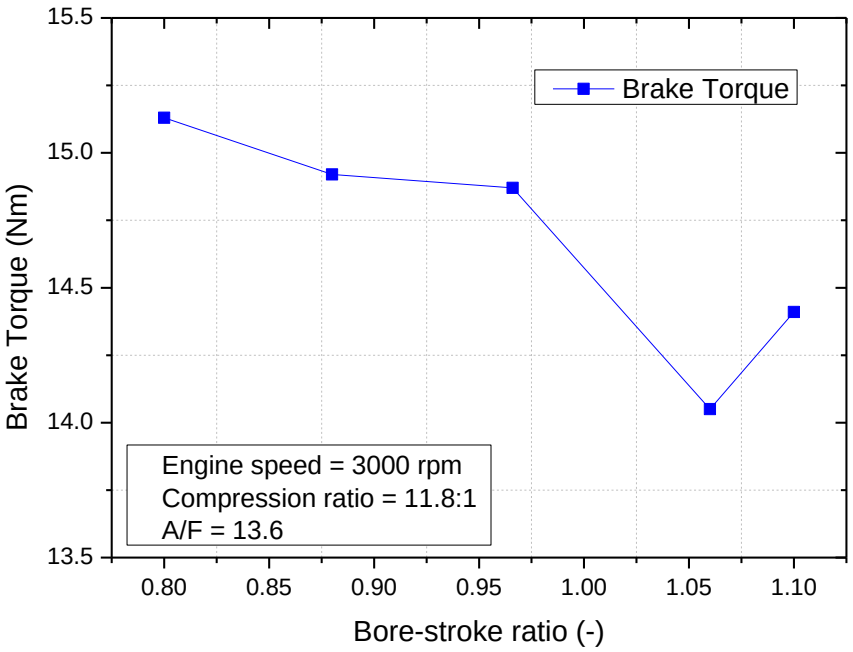

Fig 5.23 The effect of BTR on BSFC versus bore-stroke ratio

5.2.2 Effects of BTR on engine emission

Figure 5.24 shows the NO_x emission versus bore-stroke ratio. The NO_x emissions tend to increase with increasing bore-stroke ratio due to two reasons. First reason was the increased in the bore-stroke ratio to increase air filling and reduce the homogeneous of air-fuel mixture in the cylinder to increase the level of Oxygen concentrate area. The increase in level of Oxygen concentrate led to increase NO_x emission in combustion stroke. The second reason because residual gas has the sensitive effect on NO_x emission. In diesel engines, the exhaust gas recirculation (EGR) method is an excellent approach to decrease the NO_x emissions. The increase of residual gas in the cylinder leads to reduced NO_x emissions. In this study, two above reasons explained why the NO_x tended to increase with increasing bore-stroke ratio. The minimum NO_x emission was 1.08 g/kWh at a 0.88 bore-stroke ratio and the maximum NO_x emission was 16.91 g/kWh at a bore-stroke ratio of 0.966.

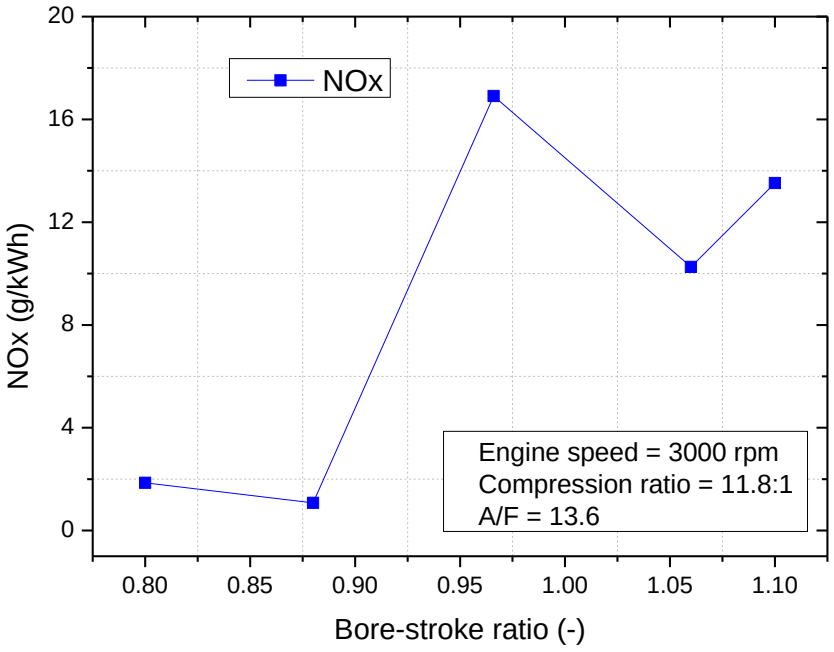

Fig. 5.24 The effect of BTR on NO_x emission

Figures. 5.25 and 5.26 show the CO and HC emissions versus bore-stroke ratio. An increased bore-stroke ratio leads to longer burn time and increases air filling. The longer combustion duration helps to completely burn the fuel to reduce HC emissions, while the increased air filling adds more oxygen to decrease the CO formed. This explains why the HC and CO

emissions decreased as of bore-stroke ratio increased. The HC and CO emission are not accurately predicted even by three dimensional, hence the HC and CO emission values were as referential values but the trend of HC and CO emission were accurately predicted when bore-stroke ratio increased.

These results demonstrate in detail the investigation of residual gas, peak pressure rise, combustion duration and effective release energy with various bore-stroke ratios and explain the effect of residual gas on NO_x emission of a small SI-engine.

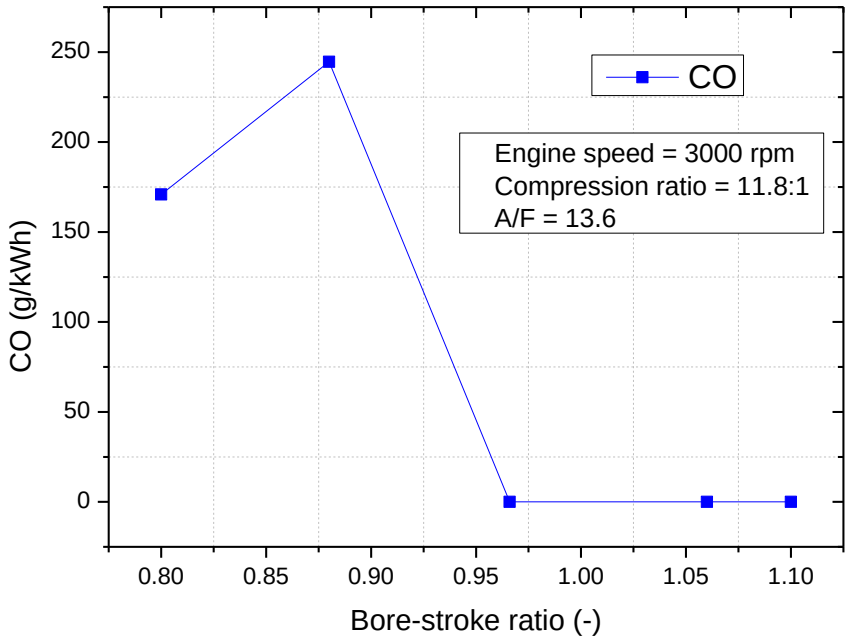

Fig. 5.25 The effect of BTR on CO emissions

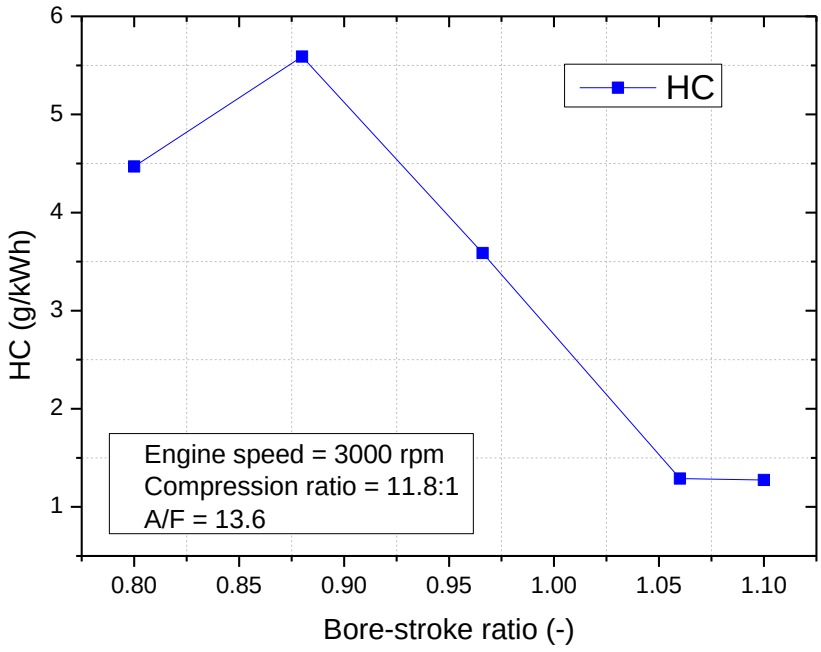

Fig. 5.26 The effect of BTR on HC emissions

5.2.3 Summary

In this part, the residual gas, peak firing pressure rise, combustion duration and effective release energy of a Small SI-engine were discussed. And the effects of residual gas on effective release energy and NO_x emission are also described.

The results were summarized below:

1) When the bore-stroke ratio increased from 0.8 to 1.1, the residual gas ratio decreased from 7.5% to 5.6 %. The volume efficiency increased from 0.78 to 0.83, the ignition timing increased from 15 to 35 deg BTDC and the combustion duration increased from 70 to 100 deg CA. The peak firing temperature and effective release energy declined. At a bore-stroke ratio of 0.966, the peak firing pressure achieved its maximum value of 3.05 bar/deg. The effective release energy decreased from 0.606 kJ to 0.567 kJ.

2) The NO_x emission tended to increase as the bore-stroke ratio increased. The minimum NO_x emission was 1.08 g/kWh at the bore-stroke ratio of 0.88, and the maximum was 16.91

g/kWh at the bore-stroke ratio of 0.966. The HC and CO emissions decreased as the bore-stroke ratio increased.

3) In this study, the engine performed at its optimal efficiency when the bore-stroke ratio was 0.8. At this ratio, the residual gas and BSFC were minimal, the IMEP, BMEP and engine torque were at maximum, and the maximum engine torque improved by 7.68% compared to the reference bore-stroke ratio of 1.06.

5.3 Effects of valve port diameter-bore (VPD/B) ratio estimation

Above sections have presented detailed the effect of combustion duration and bore-stroke ratio on the engine performance and emission characteristics. Two effective factors are engine effective release energy and residual gas was highlighted. However, the engine effective release energy and residual gas are effected by other factors, such as valve port diameter-bore ratio and exhaust valve closing timing. In the section 5.3 and 5.4 the effect of valve port diameter –bore ratio and exhaust valve closing timing on engine effective release energy and exhaust residual gas was completely presented.

5.3.1 Effects of VPD/B on engine performance

The results were studied of two VPD/B ratio cases:

Case 1: intake port diameter changes while the exhaust port diameter is 22 mm.

Case 2: exhaust port diameter changes while the intake port diameter is 22 mm.

The various of intake and exhaust port diameters were presented in Table 5.1:

Table 5.1 VPD/B ratio of two cases

VPD/B ratio	0.3	0.35	0.4	0.45	0.5
Intake and exhaust port diameter (mm)	17.1	20	22	25.7	28.5

Figure 5.27 depicts the volumetric efficiency as a function of VPD/B ratio. A contrary effect on engine volumetric efficiency of two cases (intake port-bore ratio (case 1) and exhaust port-bore ratio (case 2)) can be observed. When the VPD/B increased from 0.3 to 0.5:

In case 1: the volumetric efficiency decreased from 0.695 to 0.653. The minimum volumetric efficiency was 0.653 at a 0.5 VPD/B and the maximum value was 0.695 at a 0.3 VPD/B. This can be explained by that at a constant engine speed, an increase of VPD/B led to decrease the swirl ratio and acceleration of air flow into the cylinder. This was cause to reduce amounts of air fill into the cylinder as the subsequent effect of the intake stroke by decreasing fresh air fuel to sweep the exhausted gas out of the cylinder. This accounts for the reason why the volumetric efficiency decreases and the residual gas fraction ratio increases as the VPD/B increases (Fig. 5.28). The residual gas fraction increased from 11 to 14%. The minimum value was 0.107% at a 0.3 VPD/B and the maximum value was 0.144% at a 0.5 VPD/B.

In case 2: the volumetric efficiency increase from 0.656 to 0.688 the minimum volumetric efficiency was 0.656 at a 0.30 VPD/B and the maximum value was 0.688 at a 0.5 VPD/B. This can be explained by that an increase of VPD/B led to decrease the reverse of exhaust gas back to the combustion chamber. This was cause to charge fresh air-fuel mixture more into the cylinder and reduce exhaust residual. This accounts for the reason why the volumetric efficiency increases and the residual gas fraction ratio decreases as the VPD/B increases (Fig. 5. 28). The residual gas fraction decreased from 13.82 to 11.25%. The minimum value was 11.25% at a 0.5 VPD/B and the maximum value was 13.82% at a 0.3 VPD/B.

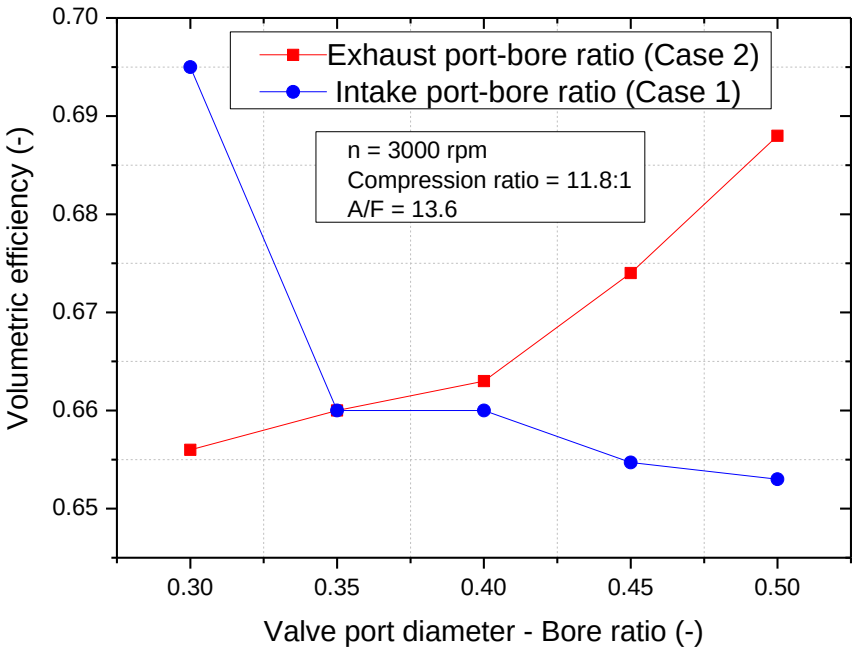

Fig 5.27 Volumetric efficiency versus VPD/B

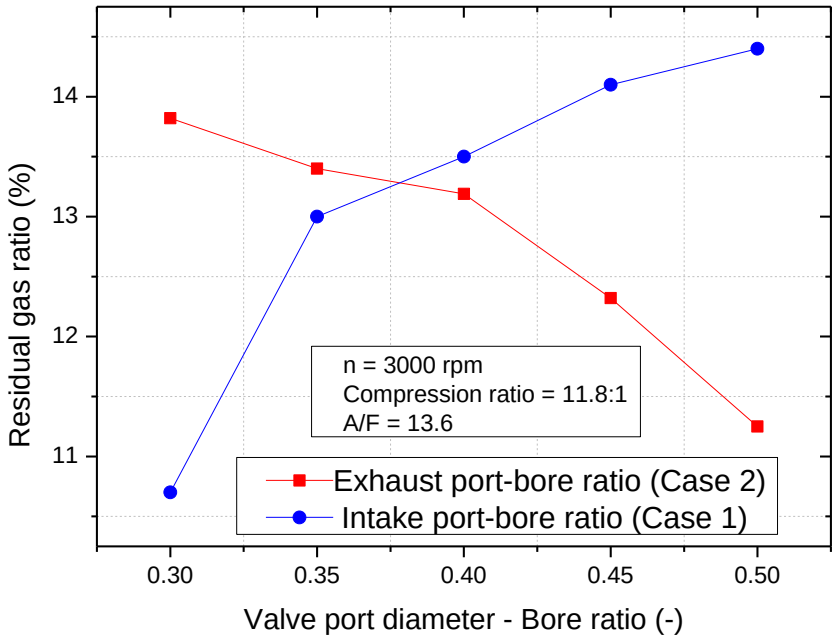

Fig 5.28 Residual gas fraction versus VPD/B

As shown in Figs. 5.29 and 5.30, the peak temperature and pressure rise present the similar trend in both cases. As the increase of VPD/B, the peak temperature and pressure rise

increase after achieving a maximum value and then decreases. This is because a higher VPD/B was due to the increase or decrease in the residual gas fraction (Fig. 5.28). A suitable an amount of high temperature exhaust gases trapped in the cylinder to raise the evaporation and homogeneity in the air-fuel mixture. The homogeneous air-fuel mixture helped the thermal energy can be released in a shorter time to improve peak temperature and pressure rise. However, when too much exhaust gas gets trapped in the combustion chamber it may restrict the fresh air-fuel mixture into the combustion chamber and due to poor combustion. This is the reason why the pressure rise and peak temperature both decreased after achieving a maximum value.

In this research:

In case 1: the maximum peak temperature and maximum peak pressure rise achieved maximum values of 2047 K and 0.87 bar, respectively at 0.4 VPD/B.

In case 2: the maximum peak temperature and maximum peak pressure rise achieved maximum values of 2056 K and 0.87 bar, respectively at 0.3 VPD/B.

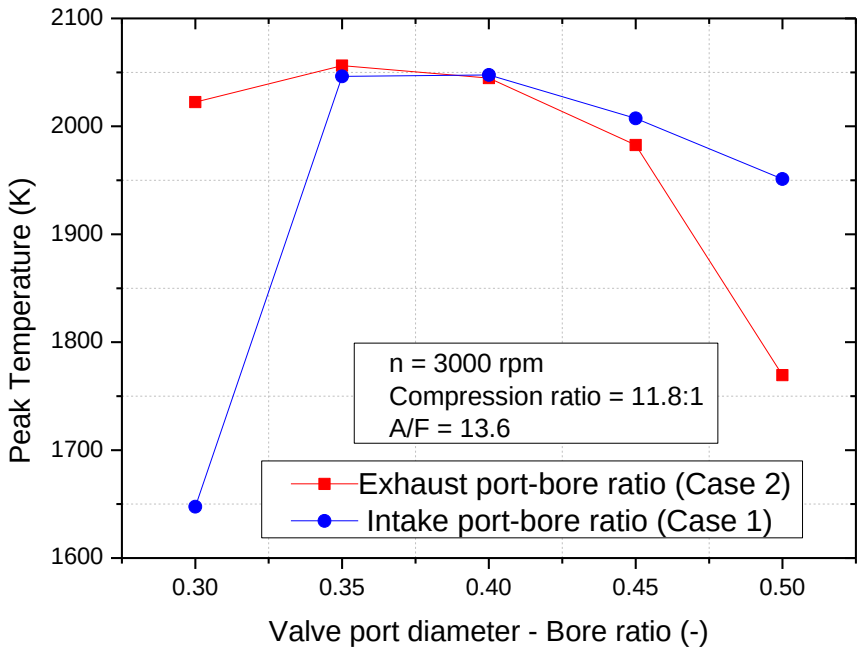

Fig. 5.29 Peak firing temperature versus VPD/B

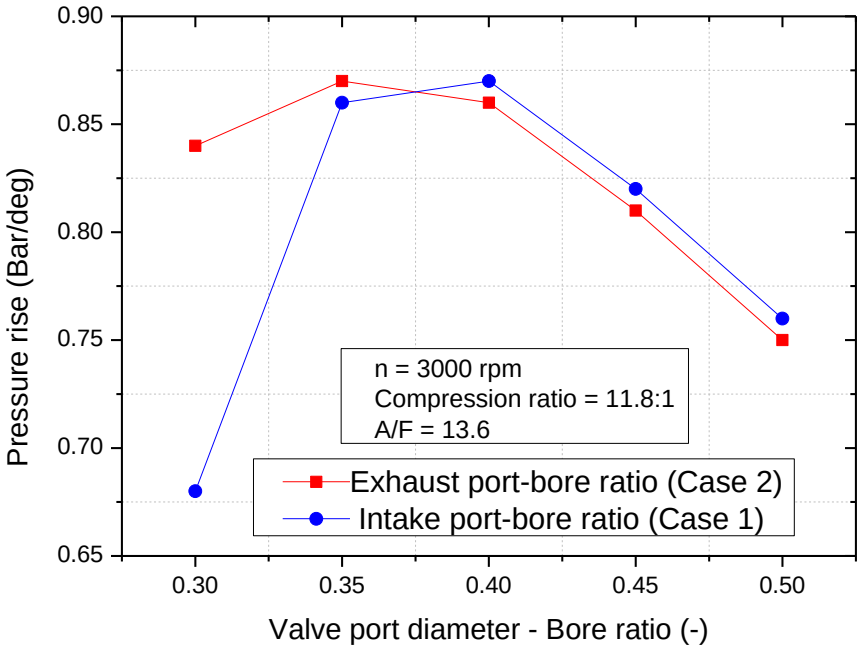

Fig. 5.30 Pressure rise versus VPD/B

As discussed above, the residual gas fraction in combustion chamber has a big effect on homogeneous of air-fuel mixture. The influence of the residual gas fraction on the peak pressure rise, peak temperature and effective energy can be seen though figures 5.28, 5.29 and 5.30. As the increase of VPD/B, the effective release energy increase until a maximum value after that decrease as shown in Fig. 5.31. The maximum value was 0.45 kJ at 0.4 VPD/B in case 1; and 0.451 kJ at 0.35 VPD/B in case 2. From this result, we know that the engine performs optimal efficiency when the exhaust residual gas fraction ratio is from 13 to 14%.

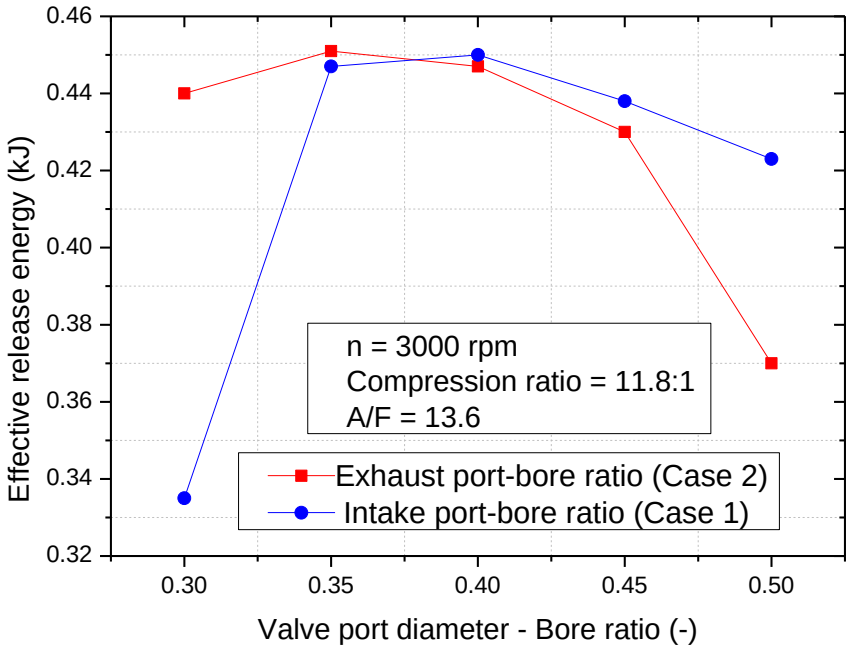

Fig. 5.31 Effective release energy versus VPD/B

Fig. 5.32 and 5.33 shows the IMEP and BMEP at each VPD/B ratio. Because the cylinder pressure of power stroke has a sensitive effect on IMEP from the equation (23), and the effective release energy effect on BMEP. So the similar trend of IMEP and pressure rise, BMEP and effective release energy can be observed.

$$IMEP = \frac{1}{V_D}\int P_c.dV \qquad (23)$$

The IMEP and BMEP was achieved the maximum value of 6.63 bar and 4.5 bar at 0.4 VPD/B in case 1, and in case 2 these values are 6.66 bar, 4.53 bar at 0.35 VPD/B, respectively.

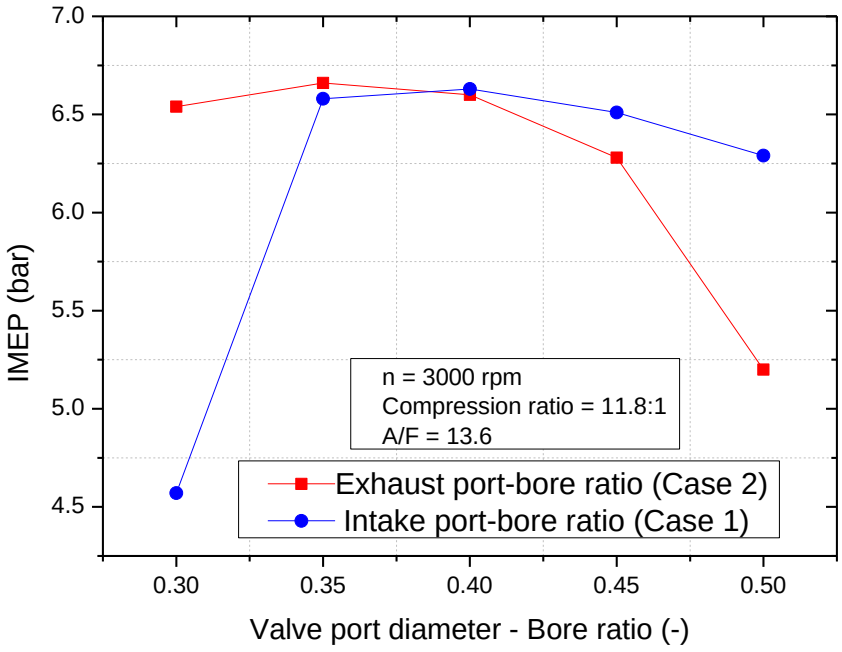

Fig. 5.32 IMEP versus VPD/B

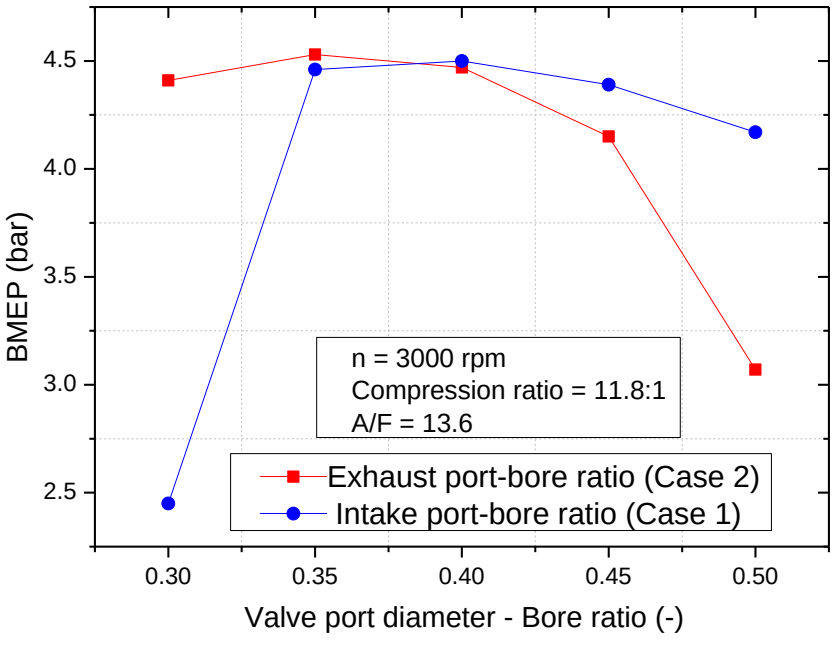

Fig. 5.33 BMEP versus VPD/B.

Figure 5.34 shows that the BSFC decrease when VPD/B ratio increase from 0.3 to 0.5. With a constant the engine speed and constant air-fuel ratio, BMEP had the greatest effect on BSFC. The influence of BMEP and BSFC to each other is shown in Equation (24):

$$BSFC = \frac{m_{air}.n_c.2.16.10^9}{AFR.BMEP.V_D.n} \quad (24)$$

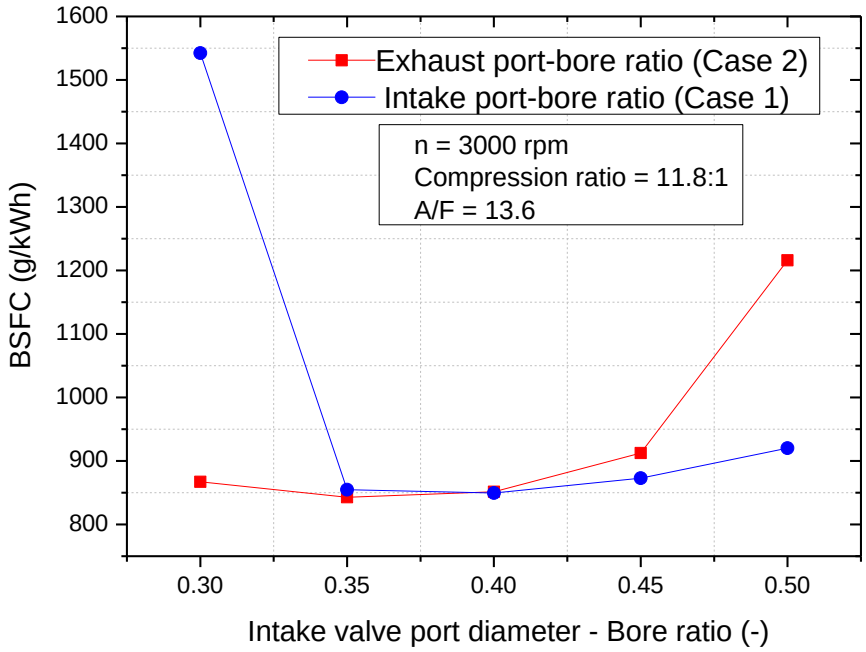

Fig. 5.34 BSFC versus VPD/B

The opposite trends of BMEP and BSFC are depicted in Figs 5.33 and 5.34. The minimum BSFC is 849.5 g/kWh in case 1 and 842.8 g/kWh in case 2.

It can be seen that, at the intake port-bore ratio is smaller than 0.35 or exhaust port-bore ratio is bigger than 0.45 the missing firing may happen because of this band of VPD/B ratio, the BSFC value, HC emission (Fig. 5.37) were very high and NO_x emission was nearly zero (Fig. 5.36). So with the intake port-bore ratio is smaller than 0.35 or exhaust port-bore ratio is bigger than 0.45, it is not a good condition to engine operate.

The similar trend between BMEP and engine effective torque can be observed through Fig. 5.33 and 5.35. The effect of BMEP on engine effective torque is presented in equation (25). Equation (25) shows that a higher BMEP due to an enhanced engine torque.

$$T_{eff} = \frac{BMEP.V_D}{k_{cycle}.\pi} \quad (25)$$

Fig. 5.35 shows the engine brake torque was achieved the maximum value of 9.85 Nm in case 1 and 9.91 Nm in case 2. This means the engine torque can be improved by adjusting the exhaust valve port diameter.

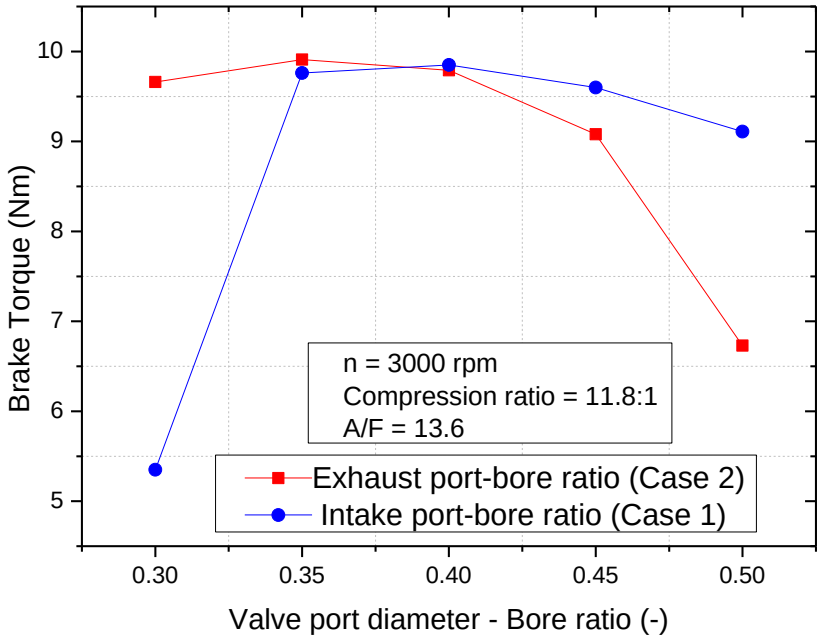

Fig. 5.35 Brake torque versus VPD/B

5.3.2 Effects of VPD/B on engine emission

The peak firing temperature is a factor which has a strong effect on NO_x emission, in this research, the peak firing temperature increases to a maximum value, after that decrease event VPD/B was still increasing. As a result, with both cases: the NO_x shows the similar trend with peak firing temperature. Fig. 5.36 shows the NO_x emission increases until achieved a maximum value after that decrease even VPD/B was still increasing. The maximum NO_x emission was 6.6 g/kWh, at 0.4 VPD/B of case 1, and this value was 7.07 g/kWh at 0.35

VPD/B of case 2. This result shows that the exhaust valve port-bore ratio has a more sensitive effect on NO_x emission than intake valve port-bore ratio.

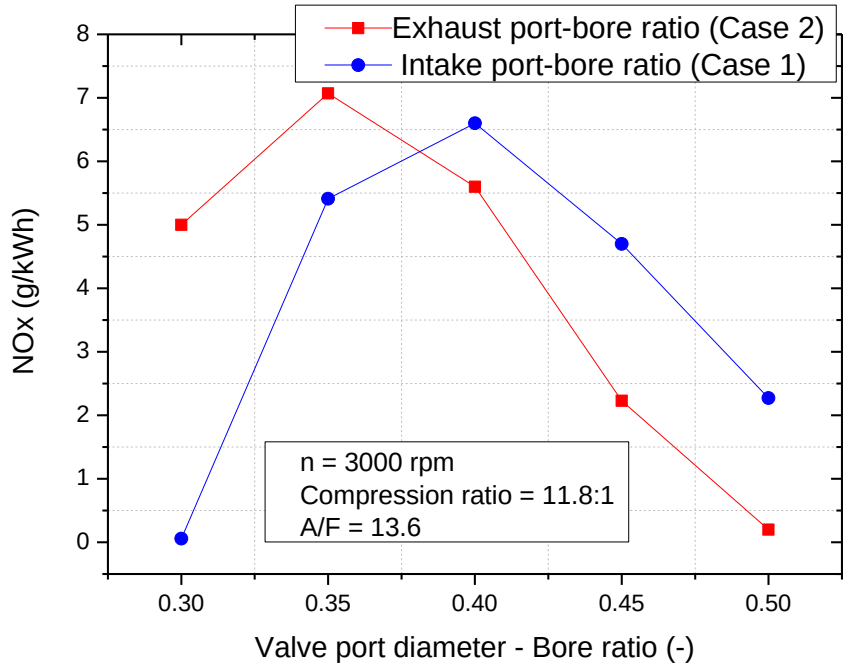

Fig. 5.36 NO_x emission versus VPD/B

Fig. 5.37 and 5.38 shows that with intake port-bore ratio is smaller than 0.35 and exhaust valve port–bore ratio is bigger than 0.45. The high HC emission and low CO emission was presented. This is because the poor combustion and miss firing occurred. With a VPD/B ratio of 0.35 to 0.4 the engine has stable performance.

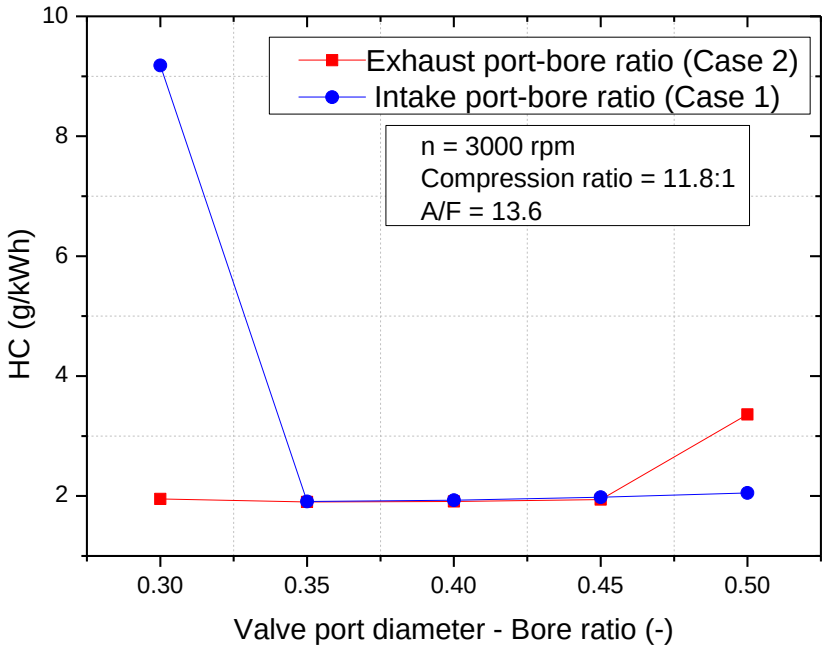

Fig. 5.37 HC emission versus VPD/B

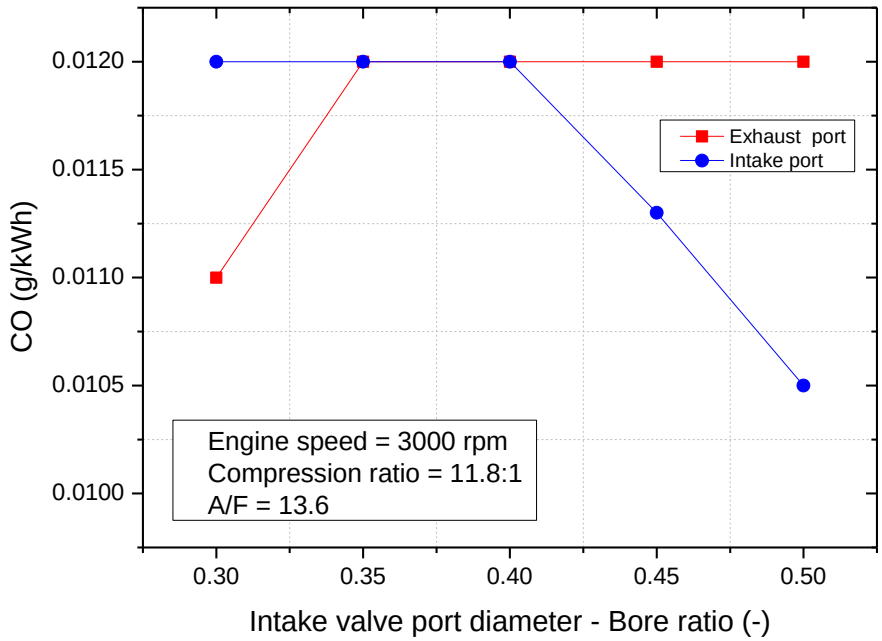

Fig. 5.38 CO emission versus VPD/B

5.3.3 Summary

This section shows a study to determine the effective release energy, peak pressure rise and residual gas fraction of a spark-ignition engine with various VPD/B. Through our approach, the disadvantages of experimental methods were solved, producing a confident method to determine the effective energy, residual gas, peak temperature and pressure rise.

The results were summarized below:

1) A lager intake port diameter causes to decrease of volumetric efficiency, while volumetric efficiency increases with the lager exhaust port diameter.

2) The VPD/B ratio gets large influence on residual gas fraction, effective energy and engine emission. As the increase of VPD/B ratio of 0.3 to 0.5 the residual gas fraction increases 27.3% with larger intake port and decrease 18.6 % with larger exhaust port. The engine will perform optimal efficiency when the exhaust residual gas fraction is from 13 to 14%. The maximum effective release energy was 0.45 kJ at 0.4 intake port-bore ratio, and 0.451 kJ at 0.35 exhaust port-bore ratio.

3) The maximum peak firing temperature and peak pressure rise was 2047 K and 0.87 bar at 0.4 intake port–bore ratio. This value was 2056 K and 0.87 bar at 0.3 exhaust port-bore ratio.

4) The optimal effective release energy and BSFC was achieved at the same VPD/B value. When VPD/B from 0.35 to 0.4, the engine performs the maximum effective release energy and the minimum BSFC. The engine operates not well with VPD/B ratio value is smaller than 0.35 or bigger than 0.45 because the misfiring may happen.

5) This result shows that the exhaust valve port-bore ratio has a more sensitive effect on NOx emission than intake valve port-bore ratio.

6) With the intake port-bore ratio is smaller than 0.35 and exhaust valve port–bore ratio is bigger than 0.45. The high HC emission and low CO emission were presented.

5.4 Effects of exhaust valve closing timing (EVCT) estimation

In the continual effort to improved engine performance and engine emission characteristics, the effect of exhaust valve closing timing will be estimated in this part. In the combustion engine, the intake valve timing is known as an effective factor which effects on inlet airflow into the cylinder, in the other hand the exhaust valve timing is a factor has strong effect on the exhaust gas flow. The intake and exhaust valve timing are the sensitive factors which has strong effect on valve overlap. An optimal valve overlap allowed for fresh air-fuel mixture into the cylinder and carried more exhaust gas out of the combustion chamber. An early valve overlap may cause the exhaust gas to be expelled into the intake port, and a late valve overlap may result in the reverse flow, which would bring exhaust gas flow back into the cylinder. In this part, the residual gas, effective release energy and peak firing pressure rise with exhaust valve closing timing will be discussed in detail.

5.4.1 Effects of EVCT on engine performance

Figure 5.39 shows that the EVTC had a significant effect on the residual gas in the combustion chamber. When the EVCT increased from 10 to 90 deg ATDC, the residual gas ratio increased from 0.2 to 1.7%. The minimum residual gas ratio was 0.2% when the EVCT was 10 deg ATDC, and the maximum residual gas ratio was 1.7% at when the EVCT was 90 deg ATDC. It could be explained by that: In this researching section, because the intake valve opening timing was fixed at 40 deg BTDC and the exhaust valve closing timing was increased. The increase of exhaust valve closing timing from 10 to 90 deg led valve overlap value increased from 50 to 130 deg. The level of late valve overlap increased with increasing of EVCT. This accounted for the increased in the reverse exhaust gas flow and increase residual gas in the cylinder as a consequence.

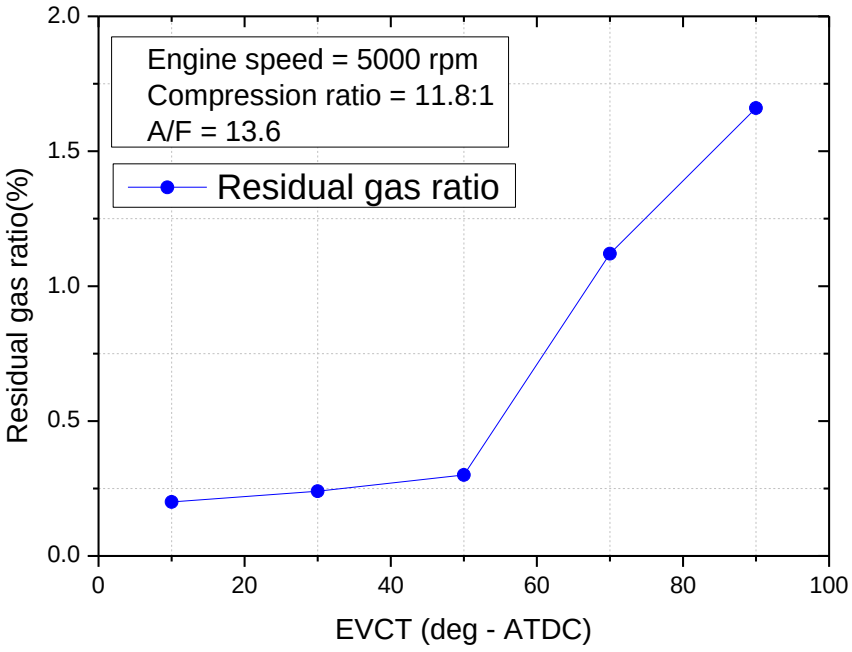

Fig. 5.39 Residual gas ratio versus EVCT

In Figures 5.40 and 5.41, the same trend of the peak firing pressure rise and peak firing temperature can be observed with the increase of EVCT.

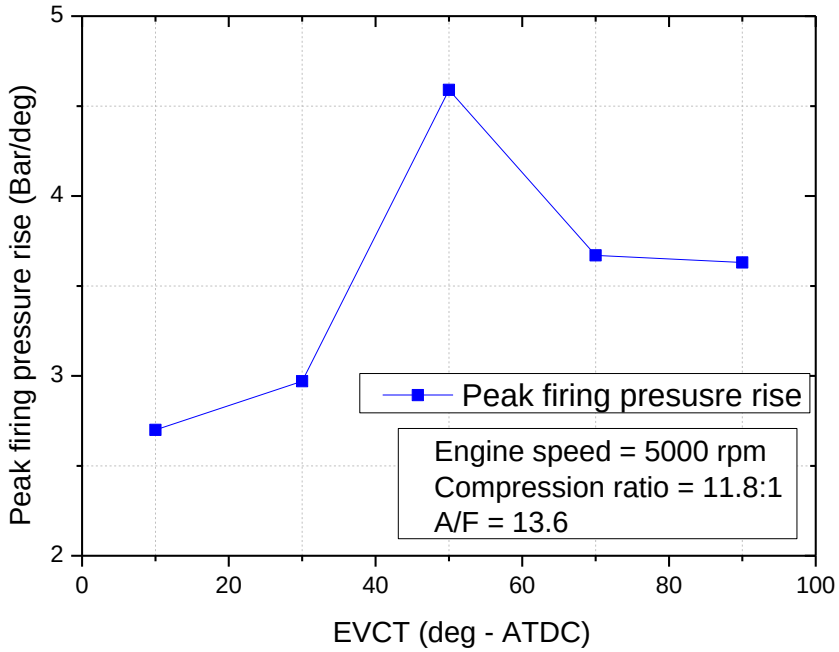

Fig. 5.40 Peak firing pressure rise versus EVCT

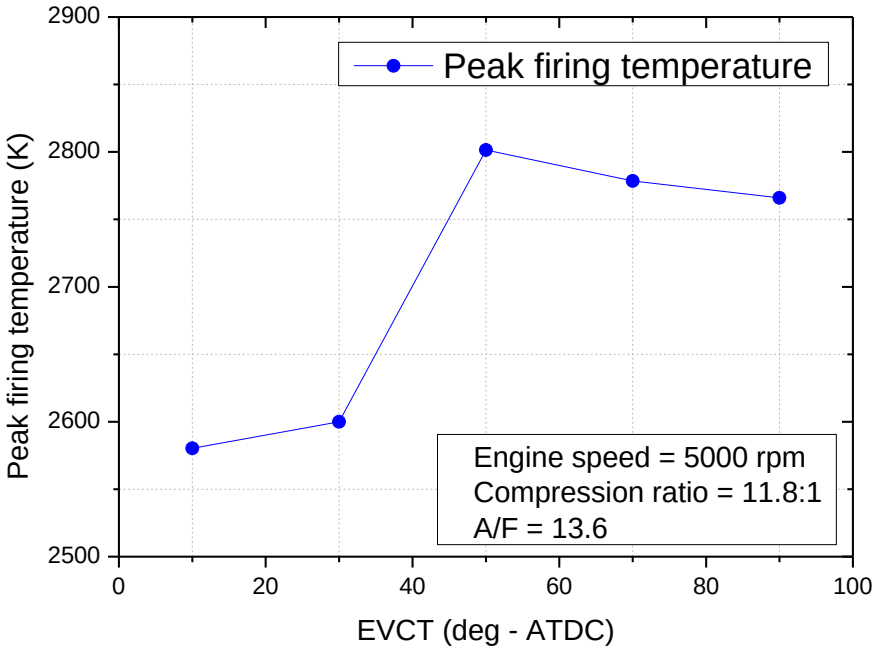

Fig. 5.41 Peak firing temperature versus EVCT

The EVCT had a strong effect on peak firing pressure rise and peak firing temperature. The peak firing pressure rise and peak firing temperature were increased until maximum values were achieved, after which a decrease began to occur. This is because the increase in EVCT was due to an increase of exhaust gas drawn back into the combustion chamber. A suitable an amount of exhaust gas trapped in the cylinder with high temperature to increase the homogeneity of the fresh air-fuel mixture in the combustion chamber of the next intake stroke. The homogeneous air-fuel mixture in the combustion chamber helped the chemical energy of fuel could be completely converted to thermal energy in a short time to increase peak firing temperature and peak pressure rise. However, when too much exhaust gas gets trapped in the cylinder it may reduce the fresh air-fuel mixture into the cylinder and cause poor combustion. This is the reason why the peak firing pressure rise and peak firing temperature both decreased after achieving a maximum value. In this research, when the EVCT was 50 deg ATDC, the peak firing pressure rise and peak firing temperature achieved maximum values of 4.59 bar/deg ATDC and 2801.45 K respectively.

In the SI-engine typical, the combustion reaction does not occur instantaneously. In order to improve the thermal efficiency, the combustion duration is expected to be short and the faster release of the heat energy to reduce heat loss transfer to piston and cylinder wall. So a better homogeneous in air-fuel mixture is the main factor to reduce combustion duration and increase the heat release energy rise. As discussed above, the residual gas has a large effect on homogeneous of air-fuel in the cylinder. A similar effect of residual gas on peak firing pressure rise, peak firing temperature and effective release energy can be observed though figures 5.40, 5.41 and 5.42. As the increase of EVCT, the effective release energy increase until a maximum value after that decrease as shown in Fig. 5.42. The maximum value was 0.64 KJ at 50 deg ATDC of EVCT.

Fig. 5.43 shows the brake mean effective pressure (BMEP) versus EVCT. The BMEP reflected the effective release energy of the internal combustion engine because higher effective release energy led to an increase in the cylinder pressure. The increase of cylinder pressure helped improved BMEP. This explains why the changing of BMEP was similar to the effective release energy with an increase of EVCT. The maximum effective release energy and maximum BMEP (9.3 bar) both dropped at the same 50 deg ATDC of EVCT.

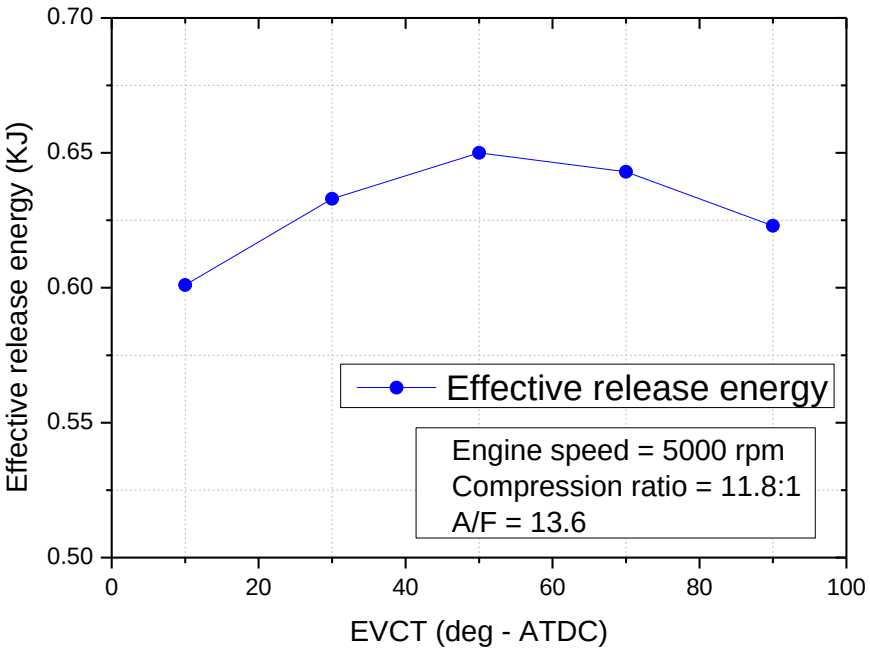

Fig. 5.42 Effective release energy versus EVCT

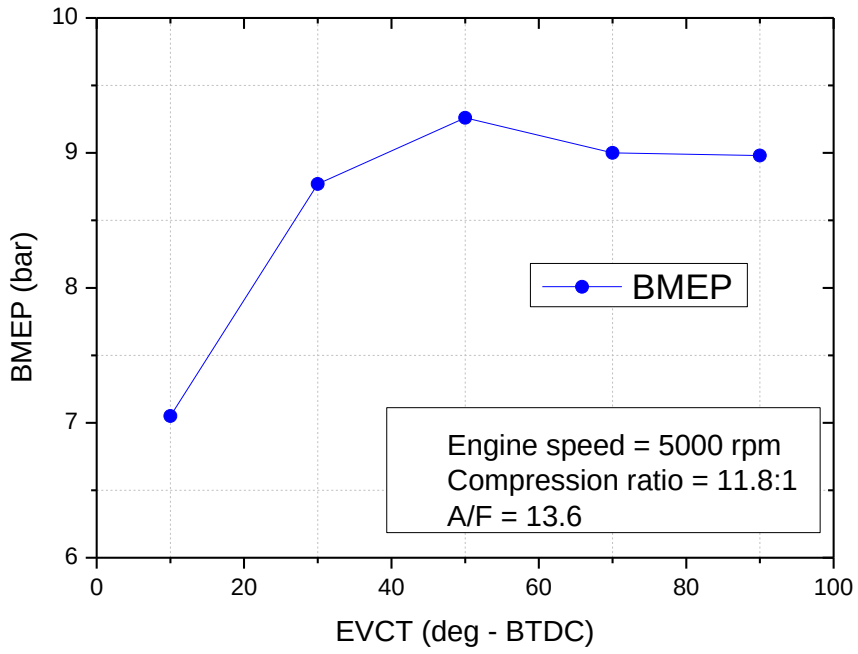

Fig. 5.43 BMEP versus EVCT

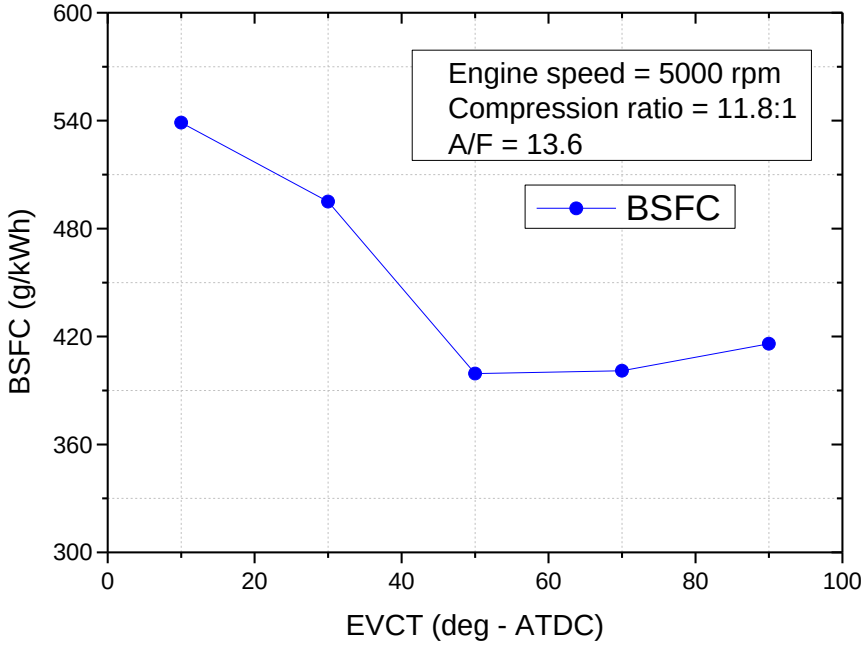

Fig. 5.44 BSFC versus EVCT

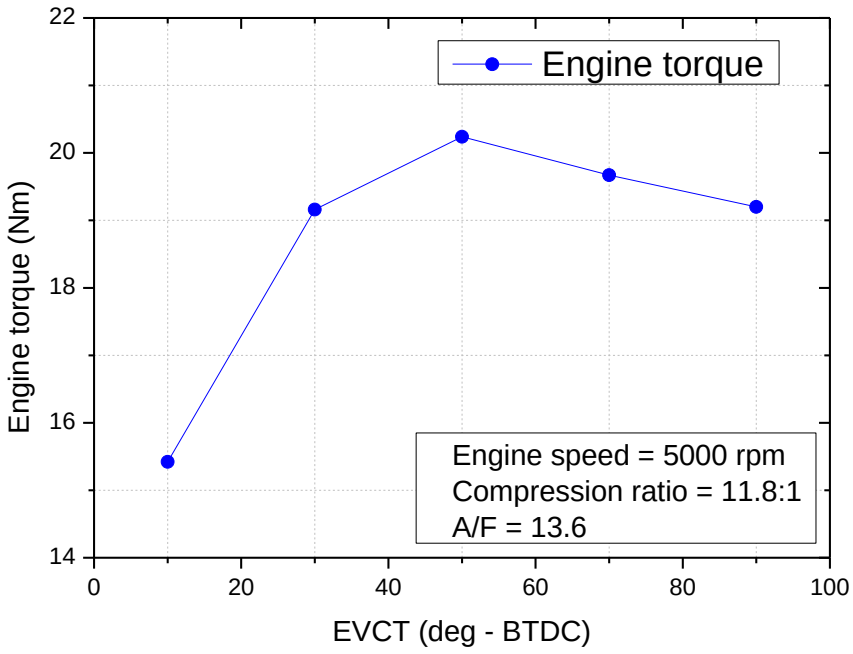

Fig. 5.45 Engine brake torque versus EVCT

Figure 5.44 shows that the brake specific fuel consumption (BSFC) declined when EVCT was increased from 10 to 90 deg ATDC. In testing conditions with a constant the engine speed and air-fuel ratio, BMEP had the greatest effect on BSFC. The contrary trends of BMEP and BSFC are depicted in Figs. 5.43 and 5.44. The engine achieved its minimum BSFC (399.35g/kWh) and maximum value of BMEP at the same 50 deg ATDC of EVCT.

An increase of BMEP led to an enhanced engine effective torque. Fig. 5.45 shows the engine brake torque versus EVCT. With increasing EVCT, the BMEP and engine brake torque showed the same trends. At an EVCT of 50 deg ATDC, the engine's maximum brake torque was 20.4 Nm.

5.4.2 Effects of EVCT on engine emission

Figure 5.46 shows the effect of EVCT on NO_x emissions. The NO_x emission increased until it achieved a maximum value and then decreased as the EVCT continued to increase. This could be explained by that: the combustion temperature and exhaust gas re-circulation are two main causes effect on NO_x emission.

When EVCT increased from 10 to 50 deg ATD, the peak firing temperature increased from 2580 to 2801 K, the residual gas ratio slightly increase, and the NO_x emission increased from 7.5 to 12 (g/kWh). In this case the increase of NO_x emission was the main function of combustion chamber temperature.

When EVCT increased from 50 to 70 deg ATD, the peak firing temperature decreased and residual gas ratio suddenly increased, but NO_x emission still increased to 13.5 (g/kWh). This is because the combustion temperature still remained at high temperature (2779 K decreased 0.82%), while residual gas ratio increased 273.3%. This amount of residual gas combined with air-fuel mass in the next intake stroke to increase total mass of air-fuel in the combustion chamber. The increased mass of air-fuel in the combustion chamber led increase N_2 and O_2 concentration area, under the high combustion temperature, this condition was speed up the chemical reaction between N_2 and O_2 (table 1) to increase NO_x emission. In this case, the increase of NO_x emission was the function of temperature and air-fuel mass in the combustion chamber.

When EVCT was bigger than 70 deg ATD, two possible explanations for the decrease of NO_x emission, first reason was the strong decreased in the peak firing temperature to reduce NO_x emission. The second reason was the strong increase in the level of residual gas. The effect of an increase in residual gas would lead to a reduction of NO_x emission such as the effect of exhaust gas recirculation (EGR) in the diesel engines. The combination of two above reasons explained why NO_x emission decreased when EVCT was bigger than 70 deg ATDC. In our study, the minimum NO_x emission was 7.54 g/kWh at a 30 deg ATDC of EVCT and the maximum NO_x emission was 13.45 g/kWh at 70 deg ATDC of EVCT.

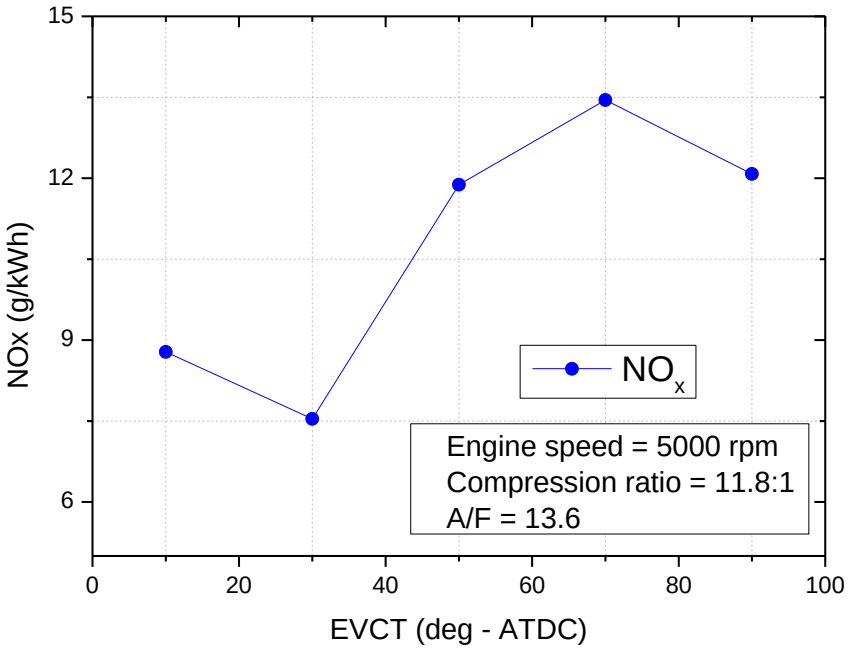

Fig. 5.46 NO_x emission versus EVCT

Fig. 5.47 shows the HC emission versus EVCT. The HC emission increased slightly when the EVCT increased from 10 to 50 deg ATDC. In contrast, after 50 deg ATDC of EVCT the HC emission increased quickly. This could be explained by that: the HC emission rose quickly because the increased level of residual gas hindered the movement of the fresh air into the cylinder such that there was lack of oxygen for complete combustion of the HC. The increase of the HC emission also led to a decrease in CO emission, as observed in Fig. 5.48

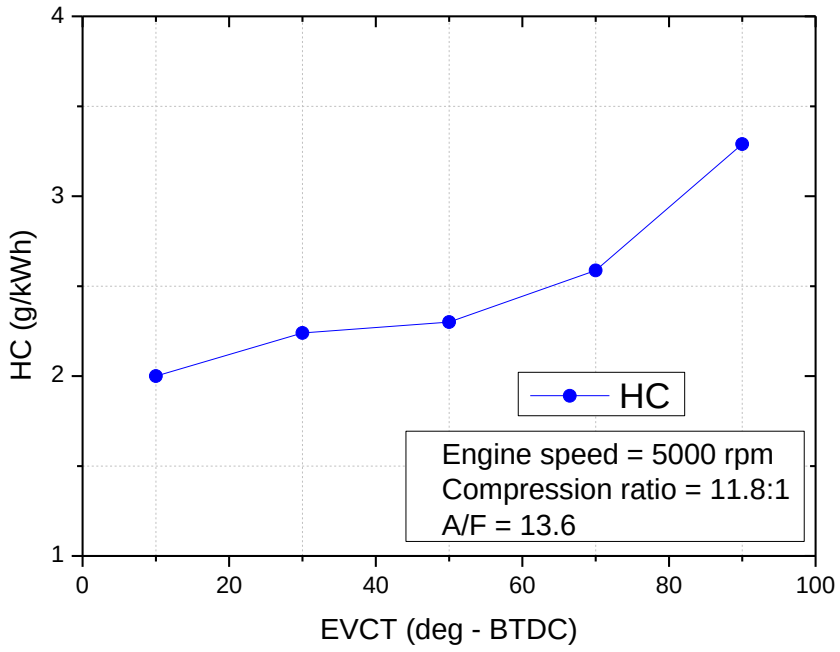

Fig. 5.47 NO_x emission versus EVCT

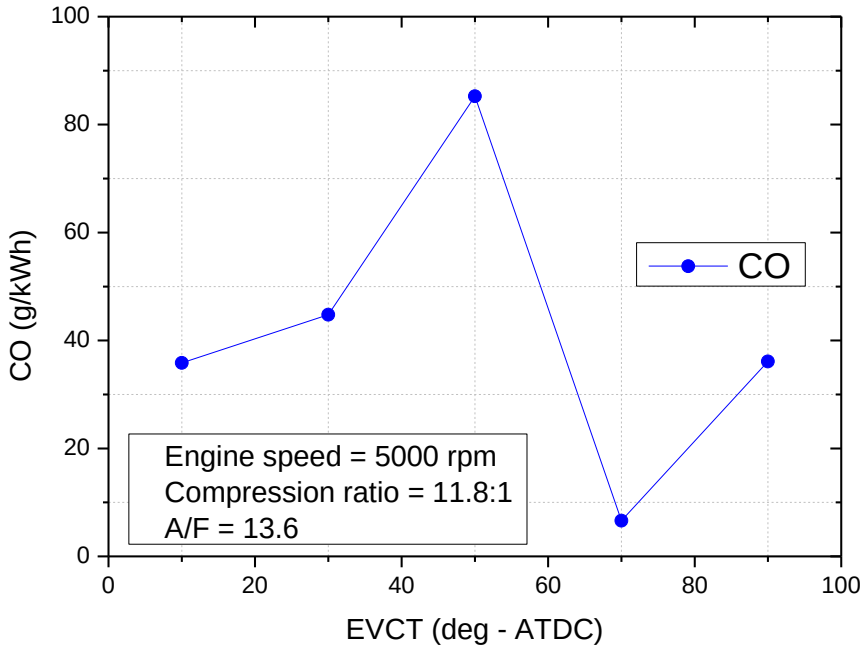

Fig. 5.48 NO_x emission versus EVCT

These results demonstrate the value in determining the effective release energy, residual gas, and peak firing pressure rise of a the engine for different EVCT values. The effect of each parameter on engine performance and engine emission characteristics were also discussed.

5.4.3 Summary

This section presents a study to determine the effective release energy, residual gas, and peak firing pressure rise of the engine over a range of EVCT values. For the first time, the effect of EVCT on residual gas, peak firing pressure rise, effective release energy and engine emission characteristics are completely discussed. The effect of residual gas on effective release energy and NO_x emission are also described. Through our approach, the usual drawbacks of experimental methods were eliminated, producing an accurate method to determine the effective release energy, residual gas, and peak firing pressure rise.

The results were summarized below:

1) The EVCT had a large effect on residual gas. When the EVCT increased from 10 to 90 deg ATDC, the residual gas ratio was increased from 0.2 to 1.7%. At an engine speed of 5000 rpm, the intake valve opening timing was 40 deg BTDC. Increasing EVCT beyond 70 deg ATDC increased the level of internal EGR with a corresponding reduction in NO_x emissions.

2) The residual gas had a significant effect on the homogeneity of the air-fuel mixture in the cylinder, which influenced the peak firing pressure rise and effective release energy. In this research, at an engine speed of 5000 rpm and an EVCT of 50 deg ATDC, the peak firing pressure rise and effective release energy achieved maximum values of 4.59 bar/deg and 0.64 KJ respectively.

3) The engine performed at its optimal efficiency when the EVCT was at 50 deg ATDC. Here the maximum BMEP was 7.74 bar, the minimum BSFC was 399.35g/kWh and the maximum engine brake torque was 16.92 Nm.

4) The NO_x emissions tended to increase with increasing EVCT because of the increased peak firing temperature. The NO_x emission increased until it achieved a maximum value, after which it decreased because the decrease of combustion chamber temperature and the increase in level of residual gas. The minimum NO_x emission was 7.54 g/kWh at a 30 deg ATDC of EVCT and the maximum value was 13.45 g/kWh at 70 deg ATDC of EVCT.

5.5 Effects of exhaust residual gas estimation

In the previous sections discussion, the influence of exhaust residual gas on the engine emission was introduced. And the parameters such as: combustion duration, bore-stroke ratio, valve port diameter – bore ratio and exhaust valve closing timing influences on the exhaust residual gas also was presented. However, other parameters that also influences on exhaust residual gas were not mentioned. Therefore, this part will summarize, discuss in completely detail the parameters effect on exhaust residual gas and the effects of exhaust residual gas on engine performance and engine emission characteristics. Because of the rising number of motorcycles in the world and the higher emission standards required such as EURO-5 and EURO-6, the residual gas, peak firing pressure rise, effective release energy and engine emission characteristic are worth investigating.

This research utilized an SI engine which had two separate camshafts, one for controlling the intake valve and the other for controlling the exhaust valve. This studies with changing valve timing were conducted without the limited experimental conditions described above. As a result, this simulation model produced more accurate predictions and we were able to thoroughly assess and discuss those parameters which have sensitive effects on exhaust residual gas.

This currently part for further studies the estimation parameters which have sensitive effects on exhaust residual gas, and the influence of residual gas on the effective release energy, peak firing pressure rise, and engine emission characteristics.

5.5.1 Parameters effect on exhaust residual gas estimation

This part thoroughly discusses and summarizes the parameters affected in internal exhaust residual gases recirculation of an engine, which has not been presented elsewhere in the literature. Figure 5.49 shows the residual gas ratio as a function of engine speed. The engine speed has a sensitive effect on the residual gas ratio; in our study, when the engine speed increased from 3000 to 8000 rpm, the residual gas ratio decreased from 4.52% to 1.54%. This can be explained by the fact that the increase of engine speed led to increases in the velocity and inertia of the exhaust and intake gas flows. In the exhaust stroke, the increased velocity and inertia of the exhaust gas flow expelled more exhaust gas from inside the cylinder to the

outside. In the intake stroke, the increased velocity and inertia of the intake air flow introduced fresher air-fuel mixture to sweep the exhausted gas out of the cylinder. This is why the residual gas ratio decreased as the engine speed increased.

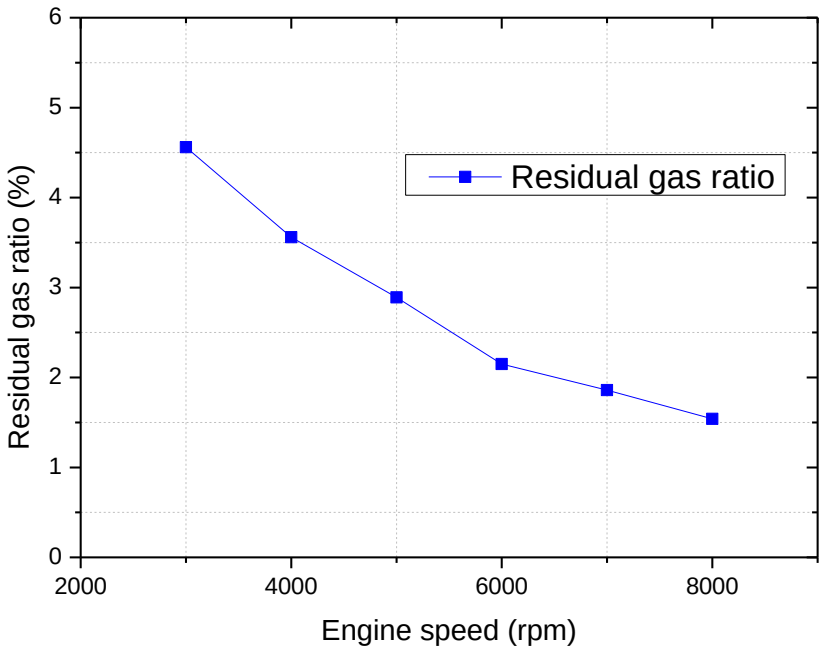

Fig. 5.49 Exhaust residual gas ratio versus engine speed

Figure 5.50 shows the residual gas ratio as a function of the air-fuel ratio (A/F ratio). The A/F ratio has a significant effect on the residual gas ratio; here, the residual gas ratio decreased from 3.18% to 2.58% when the A/F ratio increased from 12.5 to 15. This can be explained by the fact that the increase in the A/F ratio introduced fresh air mass into the cylinder while the fuel mass was kept constant. The increase in fresh air mass in the cylinder not only swept the exhausted gas out of the cylinder, but also helped to reduce the molecularly multiform exhaust gases. This is why the residual gas ratio decreased as the A/F ratio increased.

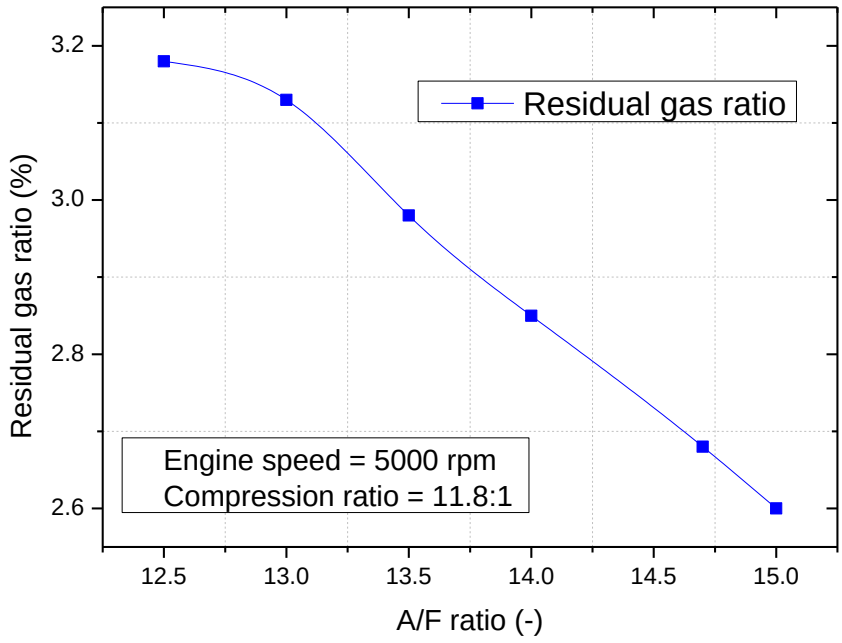

Fig. 5.50 Exhaust residual gas ratio versus A/F ratio

There are three positive valve overlap configurations (Fig. 5.51): intake valve early opening (IVEO); exhaust valve late closing (EVLC), and combined IVEO&EVLC.

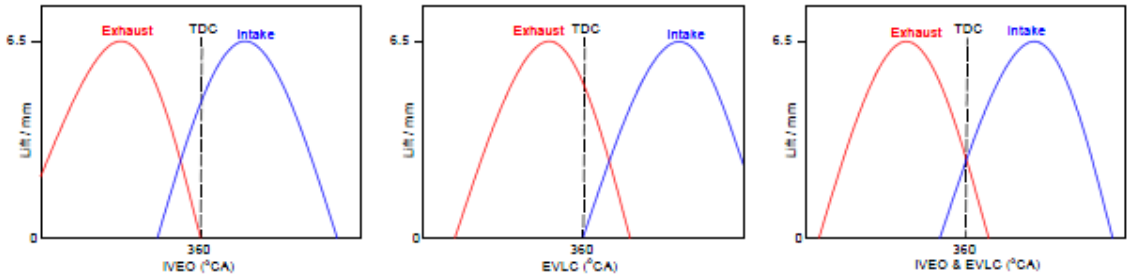

Fig. 5.51 Positive valve overlap configurations

Here, the effect of each valve timing configuration on the residual gas ratio is presented. As shown in Fig. 5.52, when the valve overlap increased, all three configurations showed an uptrend in the residual gas ratio. In a combustion engine the intake valve timing is known to affect the inlet air flow into the cylinder; conversely, the exhaust valve timing strongly affects the exhaust gas flow. An optimal valve overlap allows a fresh air-fuel mixture into the cylinder and carries more exhaust gas out of the combustion chamber. An early valve overlap may cause the exhaust gas to be expelled into the intake port, and a late valve overlap may

result in the reverse flow, which would bring the exhaust gas flow back into the cylinder. This explains why the IVEO&EVLC configuration of valve overlap has a greater effect on the residual gas ratio than the other configurations.

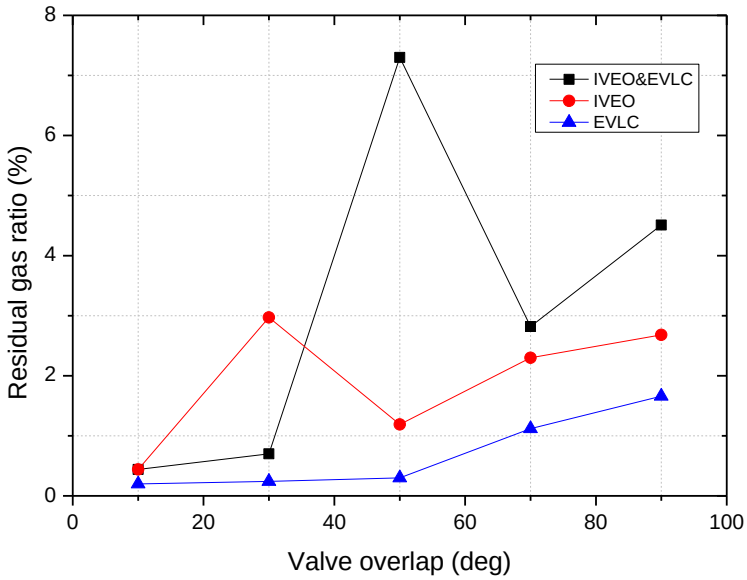

Fig. 5.52 Exhaust residual gas ratio versus valve overlap

The section 5.1 discussed the effect of combustion duration on performance and emission characteristics of a small SI-engine engine at engine speeds of 6000 rpm, 7000 rpm, and 8000 rpm. In this part, to avoid duplicating the effect of combustion duration on the exhaust residual gas ratio, the data were taken at 5000 rpm (Fig. 5.53). The increase in combustion duration was due to the increased residual gas ratio because an excessively long combustion duration can extend the burning process until the pistons are at bottom dead center (BDC) or even in the exhaust stroke. This process increases the pressure and temperature in the exhaust tube, and may result in a reverse flow which would bring the exhaust gas flow back into the cylinder. This explains why the exhaust residual gas ratio increased from 0.9% to 1.53% when combustion duration increased from 30 to 100 deg CA.

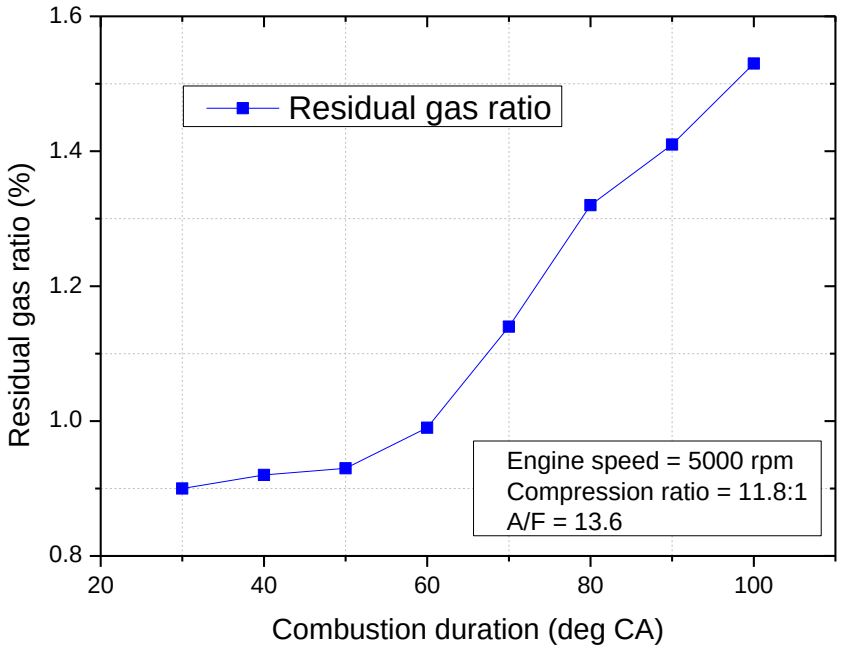

Fig. 5.53 Exhaust residual gas ratio versus combustion duration

Figure 5.54 shows the effect of intake port diameter-bore ratio (IPD/B ratio) on the residual gas. Here the IPD/B ratio ranged from 0.3 to 0.5, with the original intake valve port diameter at 22 mm as the reference value. With each change of the intake valve port diameter value, the bore diameter was kept constant at 57 mm. When the IPD/B ratio increased from 0.3 to 0.5, the residual gas ratio decreased from 2.96% to 2.7% the increased IPD/B ratio at high engine speed led to decreased airflow restriction of the inlet port. The subsequent effect of the intake stroke was to increase the amount of fresh air fill into the cylinder, which swept the exhausted gas out of the cylinder. This is why the residual gas ratio decreased as the IPD/B ratio increased.

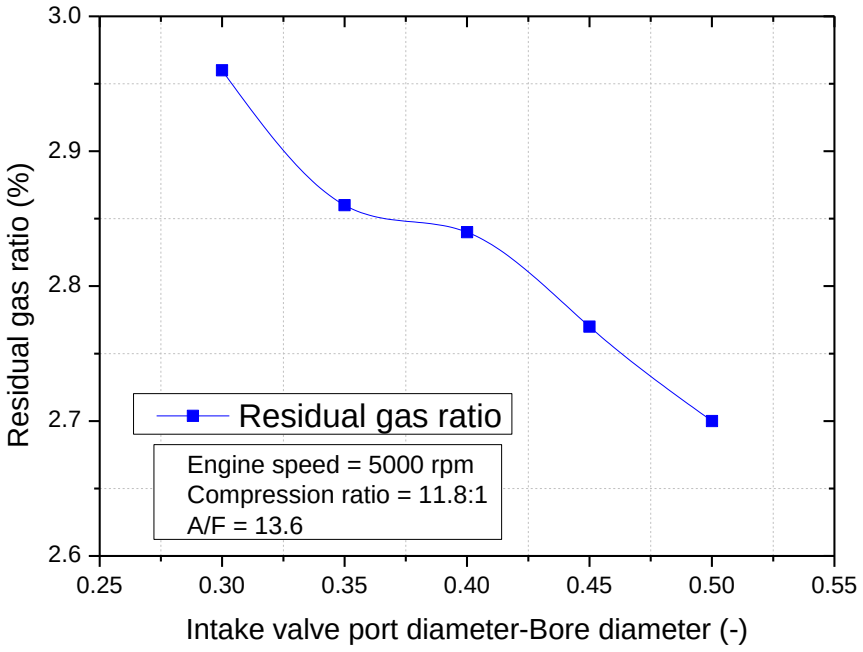

Fig. 5.54 Exhaust residual gas ratio versus IPD/B ratio

Figure 5.55 shows the residual gas ratio as a function of the bore-stroke ratio. Here the bore-stroke ratio ranged from 0.8 to 1.1, with the original bore-stroke ratio of 1.06 as the reference value. Following each change of bore and stroke value, the connecting rod length was adjusted to maintain a constant engine compression ratio. When the bore-stroke ratio increased from 0.8 to 1.1, the residual gas ratio fluctuated within 5%, which means the bore-stroke ratio had quite an effect on the residual gas. The minimum residual gas ratio was 2.8% at a 0.8 bore-stroke ratio, and the maximum residual gas ratio was 2.85% at a 0.88 bore-stroke ratio. This can be explained by the increase of bore-stroke ratio promoting increased air-fuel mass flow and longer combustion duration. The increased air-fuel mass was due to the decreased residual gas ratio, but the increased combustion duration was due to the increased residual gas ratio. This is why the residual gas ratio fluctuated significantly as the bore-stroke ratio increased.

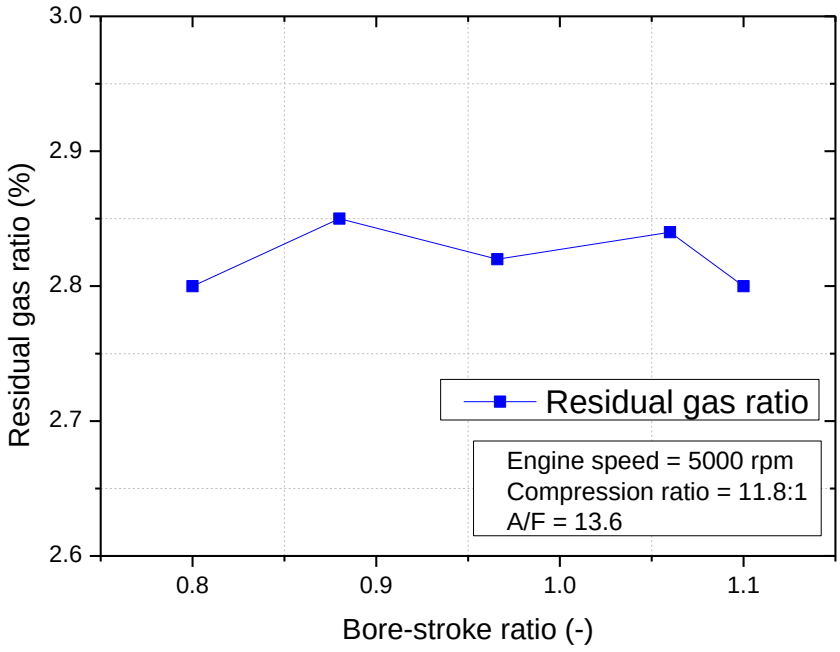

Fig. 5.55 Exhaust residual gas ratio versus Bore-Stroke ratio

5.5.2 Effects of exhaust residual gas on engine performance

The exhaust residual gas ratio has a significant effect on peak firing temperature and peak firing pressure rise. As shown in Figs. 5.56 and 5.57, the peak firing temperature and peak firing pressure rise decreased when the exhaust residual gas increased. This is because the increase in exhaust residual gas in the cylinder was due to a diluted and less homogeneous air-fuel mixture and an increased area that lacked fuel or oxygen. As a result, when the residual gas ratio increased from 1% to 5%, the peak firing temperature decreased from 2900 K to 1250 K and the peak pressure rise decreased from 8 to 5.5 bar/deg.

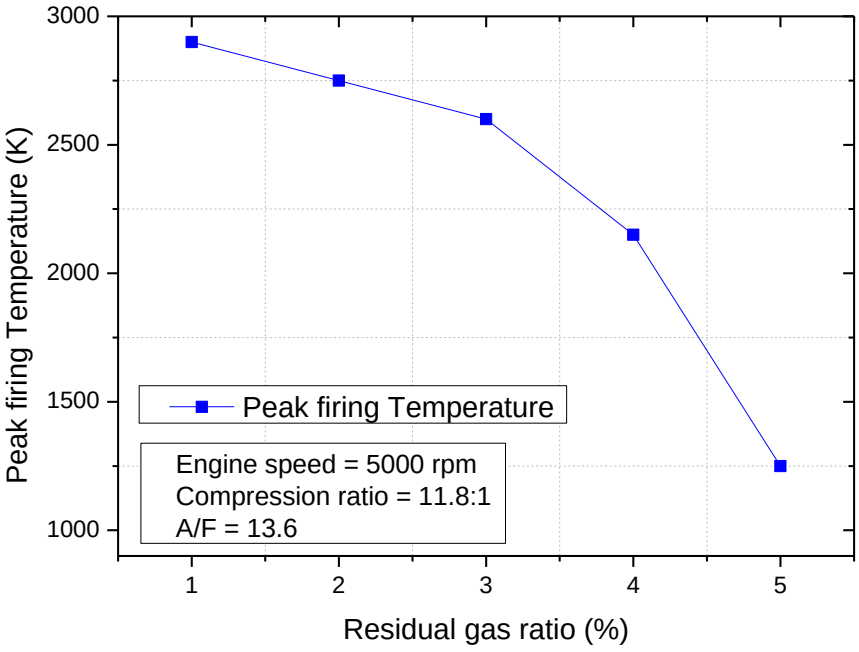

Fig. 5.56 Peak firing temperature versus residual gas ratio

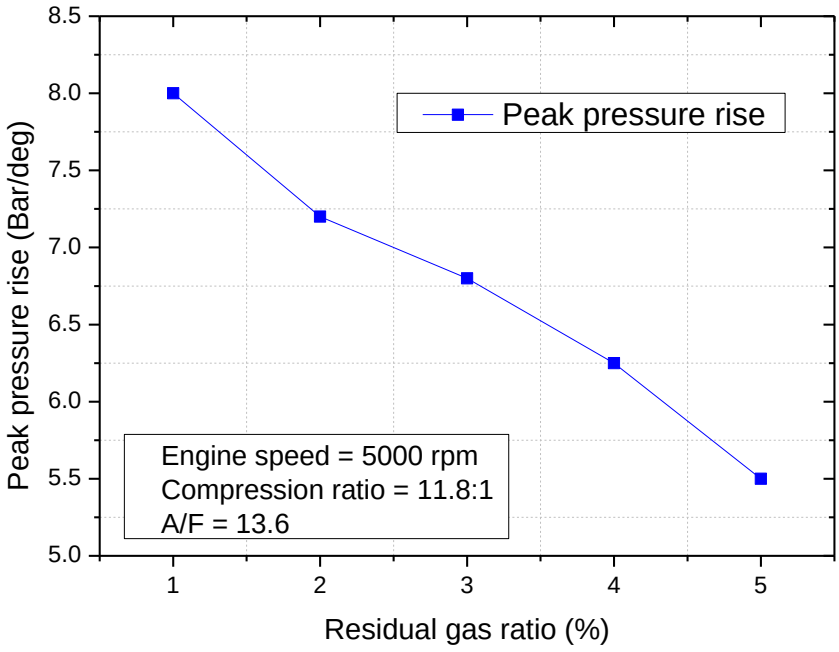

Fig. 5.57 Peak firing pressure rise versus residual gas ratio

The heat transfer loss and combustion duration have a large effect on the effective release energy. We observed a decline in effective release energy (Fig. 5.58) as the exhaust residual gas increased. This could have been because the combustion reaction does not occur instantaneously in a typical SI engine so the heat isn't instantaneously released at the top dead center (TDC). To increase the thermal efficiency, a short burn time leads to the faster release of the heat energy. When this is the case, the increased heat energy released in an actual cycle and a typical Otto cycle would be similar. Conversely, the increase of residual gas in the cylinder due to a longer burn time, lower peak firing pressure rise, and lower peak firing temperature leads to a lower effective release energy. In this study, the effective release energy decreased from 0.85 KJ to 0.53 KJ when the residual gas ratio increased from 1% to 5%.

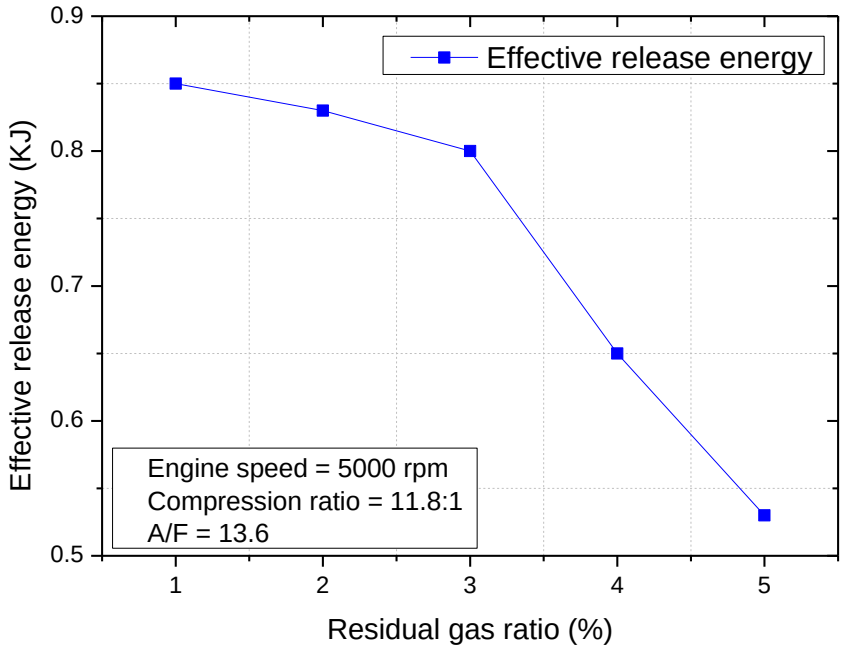

Fig. 5.58 Effective release energy versus residual gas ratio

Figures 5.59 and 5.60 show the indicated mean effective pressure (IMEP) and brake mean effective pressure (BMEP) versus residual gas ratio. Both the BMEP and IMEP decreased when the residual gas ratio increased because the latter had the same impact on BMEP, IMEP, and the effective release energy. Figures 5.58, 5.59, and 5.60 present similar trends of effective release energy, IMEP and BMEP. When the residual gas ratio was 1%, the engine

achieved its maximum BMEP (9.48 bar) and maximum IMEP (11.6 bar). At the residual gas ratio of 5%, the minimum values of BMEP and IMEP were 4.3 bar and 6.5 bar, respectively.

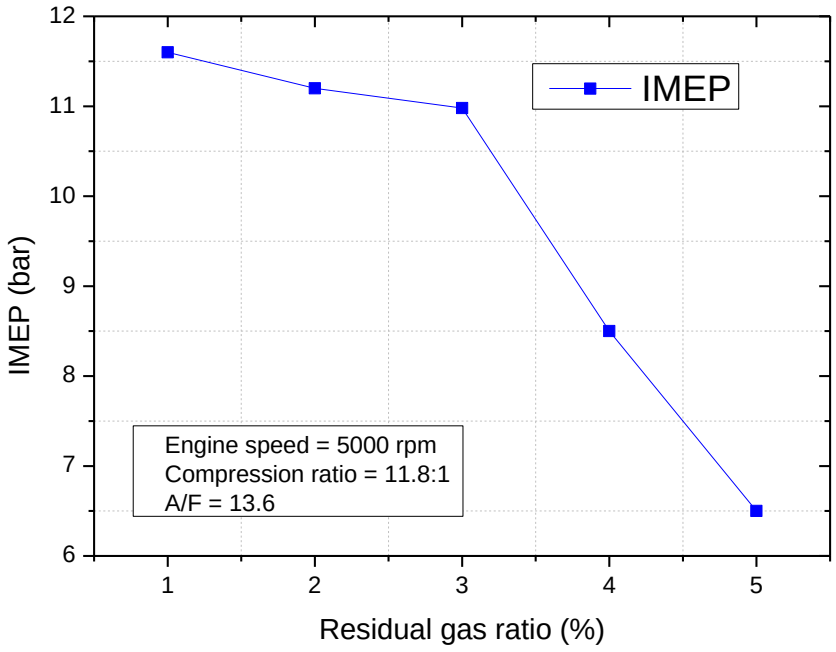

Fig. 5.59 IMEP versus residual gas ratio

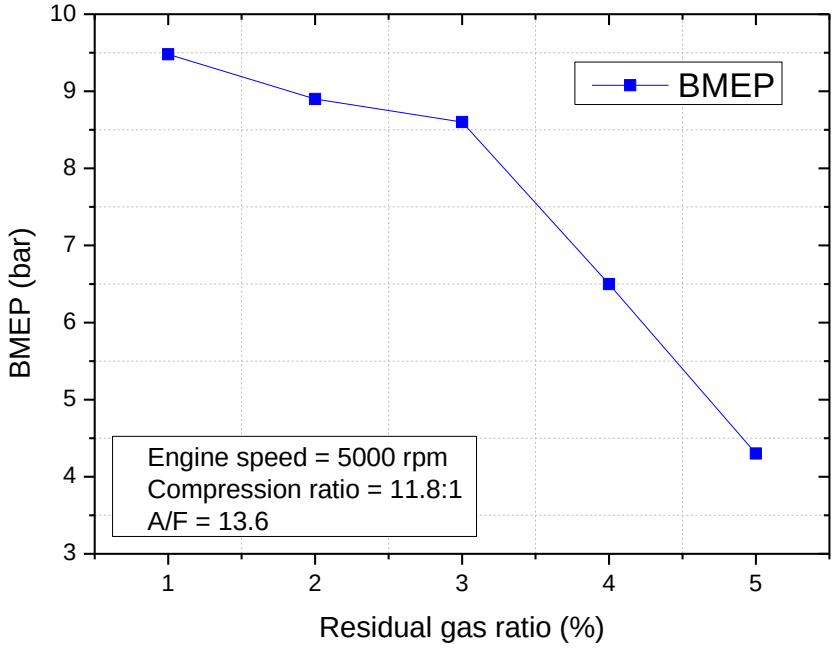

Fig. 5.60 BMEP versus residual gas ratio

Figure 5.61 shows that the brake-specific fuel consumption (BSFC) was influenced by the residual gas ratio, trending downward when the residual gas ratio increased from 1% to 5%. In testing conditions with constant engine speed and a constant air-fuel ratio, the BMEP had the greatest effects on the BSFC.

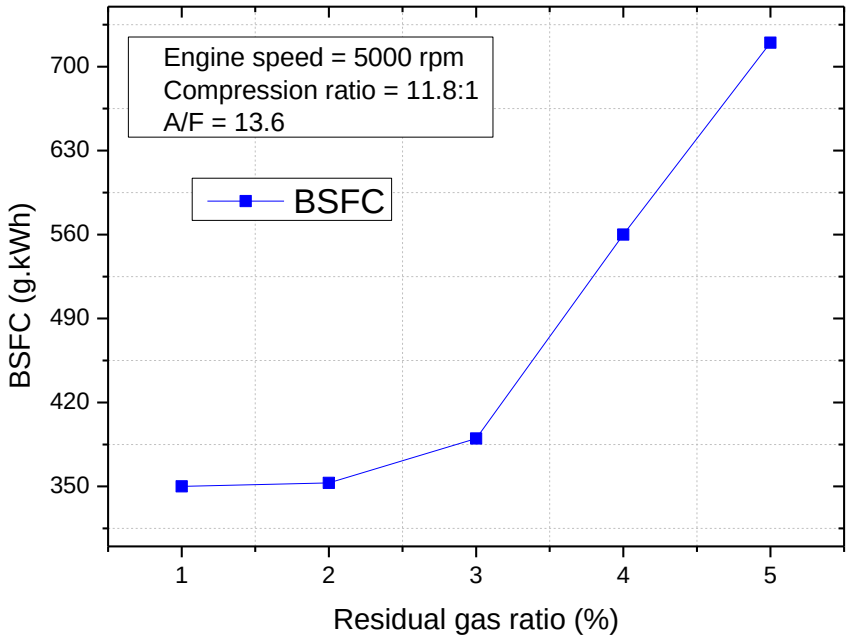

Fig. 5.61 BSFC versus residual gas ratio

Figure 5.62 shows the impact of the residual gas ratio on the engine brake torque. With an increasing residual gas ratio, the BMEP and engine brake torque showed the same downward trends. At a residual gas ratio of 1%, the engine's maximum brake torque was 20.3 Nm.

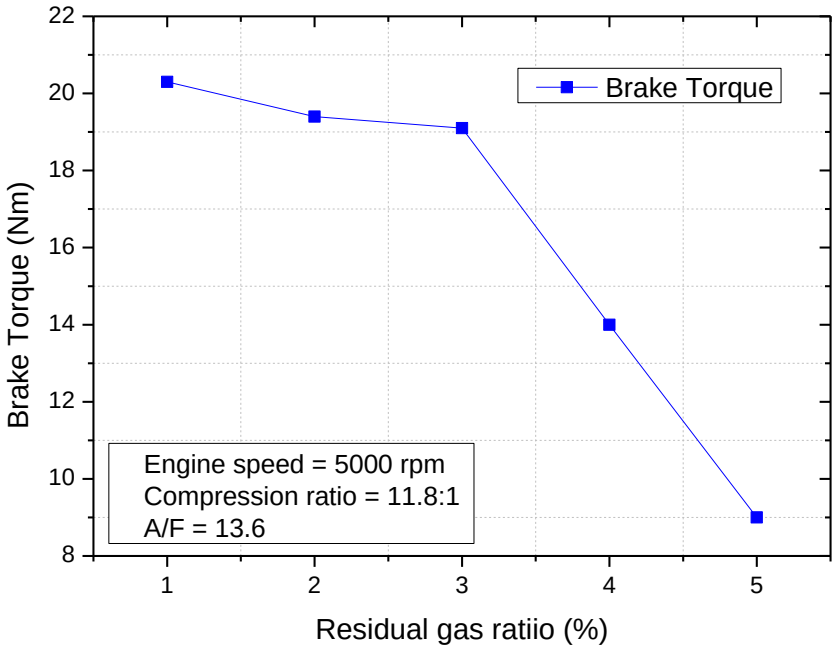

Fig. 5.62 Brake torque versus residual gas ratio

5.5.3 Effects of exhaust residual gas on engine emission

Figure 5.63 shows the NO_x emission versus residual gas ratio. The NO_x emissions tend to decrease with an increasing residual gas ratio for two reasons. First, an increased residual ratio is associated with a decreased peak firing temperature. And second, an increase in the residual gas is caused by a diluted air-fuel mixture and a lower level of oxygen concentrate. The decreased oxygen concentrate leads to decreased NO_x emissions in the combustion stroke. In our study, these two factors explain why the NO_x tended to decrease with an increasing residual gas ratio. The minimum NO_x emission was 2.12 g/kWh at a 5% residual gas ratio.

Figures 5.64 and 5.65 show the CO and HC emissions versus residual gas ratio. An increased residual gas ratio leads to a diluted air-fuel mixture and increased areas lacking oxygen. In this study, the dilution of the air-fuel mixture and the lack of oxygen increased the unburned HC and CO emissions from 3.65 to 18.2 g/kwh and from 139 to 450 g/kwh, respectively.

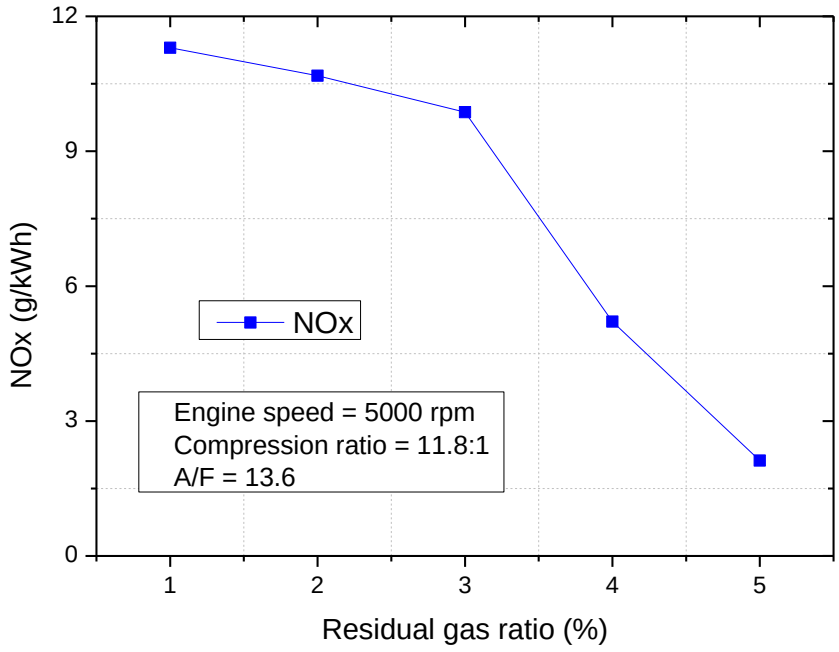

Fig. 6.63 NO_x emission versus residual gas ratio

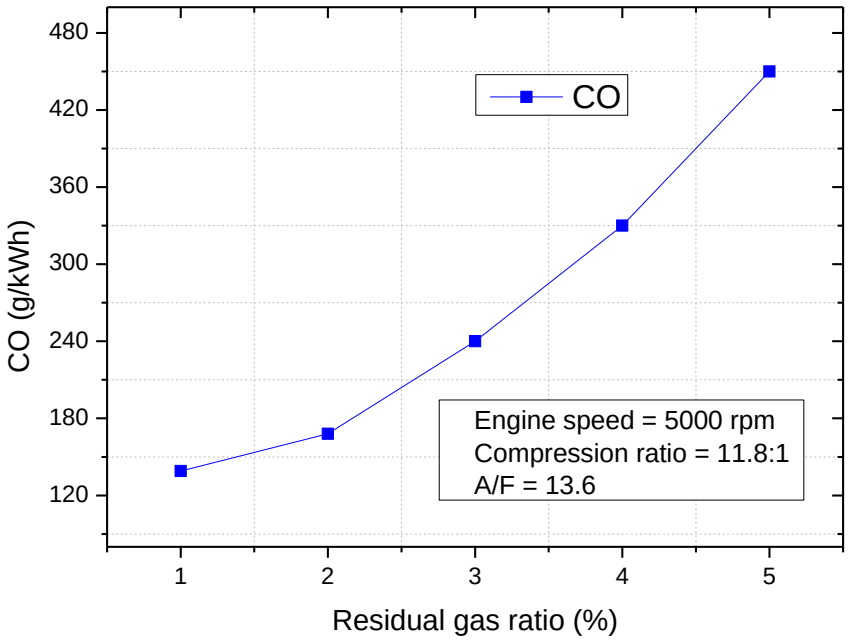

Fig. 5.64 CO emissions versus residual gas ratio

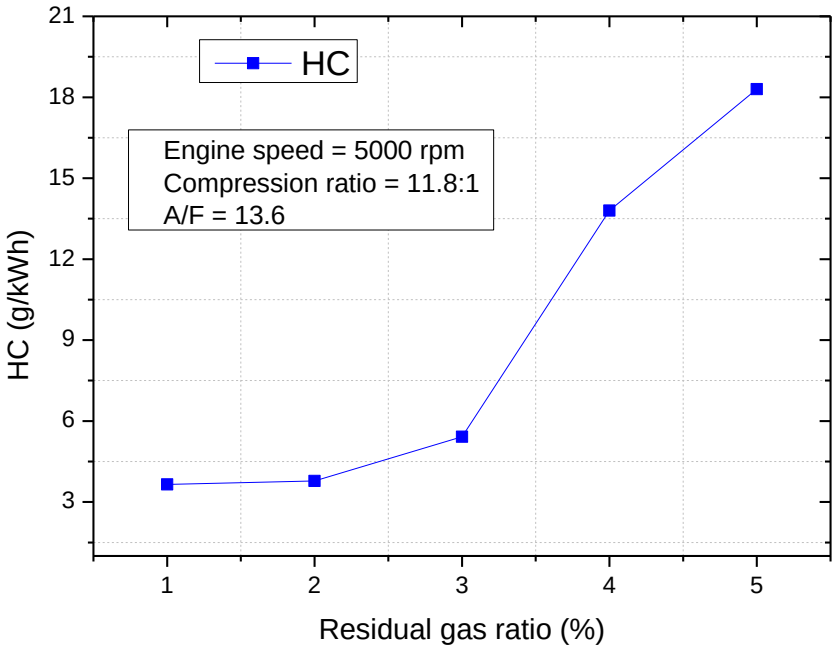

Fig. 5.65 HC emissions versus residual gas ratio

5.5.4 Summary

This section thoroughly investigated the parameters which have sensitive effects on internal exhaust residual gas recirculation, as well as the influence of exhaust residual gas on the effective release energy and engine emission characteristics of an SI engine.

The results were summarized below:

1) The increase of engine speed was due to the increase in velocity and inertia of the exhaust gas flow and intake air flow; this caused more exhaust gas inside the combustion chamber to be expelled to the outside in the exhaust-stroke, and introduced a fresh air-fuel mixture to sweep the exhausted gas out of the cylinder in the intake-stroke. As a result, the residual gas ratio decreased from 4.52% to 1.54% when the engine speed increased from 3000 to 8000 rpm.

2) The A/F ratio and valve overlap had sensitive effects on the residual gas ratio, which decreased from 3.18% to 2.58% when the A/F ratio increased from 12.5 to 15. Also, an optimal valve overlap allowed a fresh air-fuel mixture into the cylinder and carried more

exhaust gas out of the combustion chamber. An early valve overlap may cause the exhaust gas to be expelled into the intake port, and a late valve overlap may result in the reverse flow, which would bring exhaust gas flow back into the cylinder. These potentialities explain why the IVEO&EVLC case of valve overlap had a greater effect on the residual gas ratio than did the IVEO case and the EVLC case.

3) When the IPD/B ratio increased from 0.3 to 0.5, the residual gas ratio decreased from 2.96% to 2.7%. But when the bore-stroke ratio increased from 0.8 to 1.1, the residual gas ratio was fluctuated within 5%, which means the bore-stroke ratio had quite an effect on the residual gas. The minimum residual gas ratio was 2.8% at a 0.8 bore-stroke ratio, and the maximum residual gas ratio was 2.85% at a 0.88 bore-stroke ratio.

4) The exhaust residual gas ratio had a significant effect on the peak firing temperature and peak firing pressure rise. When the residual gas ratio increased from 1% to 5%, the peak firing temperature decreased from 2900 to 1250 K and the peak pressure rise decreased from 8 to 5.5 bar/deg.

5) An increase in the exhaust residual gas in the cylinder was due to a longer burn time, lower peak firing pressure rise, and lower peak firing temperature, which in turn caused a lower effective release energy. The effective release energy decreased from 0.85 KJ to 0.53 KJ when the residual gas ratio increased from 1% to 5%.

6) The NO_x emission tended to decrease as the exhaust residual gas increased because an increase of residual gas in the cylinder led to a decreased peak temperature and less oxygen concentrate. Thus, the NO_x emission declined from 11.3 to 2.12 g/kwh when the exhaust residual gas increased from 1% to 5%. An increased residual gas ratio led to a diluted air-fuel mixture and larger areas that lacked oxygen. The dilution of the air-fuel mixture and the lack of oxygen were due to increases in unburned HC and CO emissions from 3.65 to 18.2 g/kwh and from 139 to 450 g/kwh, respectively.

7) Declines in the IMEP, BMEP, and engine torque accompanied an increase in the residual gas ratio. Here, the IMEP decreased from 11.6 to 6.5 bar, the BMEP decreased from 9.48 to 4.3 bar, and the engine brake torque decreased from 20.3 to 9 Nm as the residual gas ratio increased from 1% to 5%.

6. SUMMARY AND CONCLUSION

All of the target objectives have discussed and obtained through this thesis works. The drawback of the experimental method in the scope of hardware optimization was eliminated through experimental and simulation approach method. The effects of combustion, bore-stroke ratio, valve port diameter-bore ratio, exhaust valve closing timing and exhaust residual gas were completely investigated. From the results the optimal hardware and software parameters also determined to improve engine efficiency and emission characteristics.

The importance results were summarized below:

- A small SI engine simulation modeling was provided to produce more accurate predictions and able to thoroughly assess and discuss those parameters which have sensitive effects on engine efficiency and emission characteristics.

- The combustion duration has a significant effect on residual gas and the effective release energy. Following increased of combustion duration, at an engine speed was 7000 rpm and 8000 rpm the residual gas and effective release energy decreased. The minimum residual gas ratio was 0.14% and 0.15%, respectively. When engine speed was 6000 rpm, the residual gas decreases initially and increases thereafter. Likewise, at 80 degrees combustion duration, the minimum residual gas ratio was 0.22% while the maximum effective release energy was 0.826 KJ at 60 degrees combustion duration. At each engine speed, an optimal combustion duration value was found. The NO_x and HC emission decrease when the combustion duration increases from 40 degrees to 110.0 degrees. At engine speed of 6000 rpm, the NO_x and HC decreases from 7 g/kWh to 0.2 g/kWh and 3.56 g/kWh to 3.1 g/Kwh respectively. When engine speed was 7000 rpm, the NO_x and HC decrease from 11.22 g/kWh to 2.98 g/kWh and 2 g/kWh to 0.835 g/Kwh respectively. When the engine speed was 8000 rpm, the NO_x and HC decrease from 16.2 g/kWh to 6.9 g/kWh and 2.45 g/kWh to 1.43 g/Kwh in respectively. According to the result of the research, the engine gives the best performance at 6000 rpm and 60 degrees combustion duration. In this case, the engine was able to achieve the maximum brake torque at 22.7 Nm improved 4.1% and minimum BSCF at 319.8 g/KWh improved 14.4% . By increasing the combustion duration, the engine harmful emission could be improved.
- When the bore-stroke ratio increased from 0.8 to 1.1, the residual gas ratio decreased from 7.5% to 5.6 %. The volume efficiency increased from 0.78 to 0.83, the ignition timing

increased from 15 to 35 deg BTDC and the combustion duration increased from 70 to 100 deg CA. The peak firing temperature and effective release energy declined. The engine performed at its optimal efficiency when the bore-stroke ratio was 0.8. At this ratio, the residual gas and BSFC were minimal, the IMEP, BMEP and engine torque were at maximum, and the maximum engine torque improved by 7.68% compared to the reference bore-stroke ratio of 1.06. The NO_x emission tended to increase as the bore-stroke ratio increased. The minimum NO_x emission was 1.08 g/kWh at the bore-stroke ratio of 0.88. The HC and CO emissions decreased as the bore-stroke ratio increased.

- The VPD/B ratio gets large influence on residual gas fraction, effective energy and engine emission. As the increase of VPD/B ratio of 0.3 to 0.5 the residual gas fraction increases 27.3% with larger intake port and decrease 18.6 % with larger exhaust port. When VPD/B from 0.35 to 0.4, the engine performs the maximum torque 9.91Nm improved 3.2%. The engine operates not well with VPD/B ratio value is smaller than 0.35 or bigger than 0.45 because the misfiring may happen. This result shows that the exhaust valve port-bore ratio has a more sensitive effect on NO_x emission than intake valve port-bore ratio. With the intake port-bore ratio is smaller than 0.35 and exhaust valve port–bore ratio is bigger than 0.45. The high HC emission and low CO emission were presented.
- When the EVCT increased from 10 to 90 deg ATDC, the residual gas ratio was increased from 0.2 to 1.7%. At an engine speed of 5000 rpm, the intake valve opening timing was 40 deg BTDC. Increasing EVCT beyond 70 deg ATDC increased the level of internal EGR with a corresponding reduction in NO_x emissions. The engine performed at its optimal efficiency when the EVCT was at 50 deg ATDC. Here the maximum engine brake torque improved 0.4%. The NO_x emissions tended to increase with increasing EVCT because of the increased peak firing temperature. The NO_x emission increased until it achieved a maximum value, after which it decreased because the decrease of combustion chamber temperature and the increase in level of residual gas. The minimum NO_x emission was 7.54 g/kWh at a 30 deg ATDC of EVCT and the maximum value was 13.45 g/kWh at 70 deg ATDC of EVCT.
- The residual gas ratio decreased from 4.52% to 1.54% when the engine speed increased from 3000 to 8000 rpm. The A/F ratio and valve overlap had sensitive effects on the residual gas ratio, which decreased from 3.18% to 2.58% when the A/F ratio increased from 12.5 to 15. When the IPD/B ratio increased from 0.3 to 0.5, the residual gas ratio decreased from 2.96% to 2.7%. But when the bore-stroke ratio increased from 0.8 to 1.1,

the residual gas ratio was fluctuated within 5%, which means the bore-stroke ratio had quite an effect on the residual gas.

- The exhaust residual gas ratio had a significant effect on the peak firing temperature and peak firing pressure rise. When the residual gas ratio increased from 1% to 5%, the peak firing temperature decreased from 2900 to 1250 K and the peak pressure rise decreased from 8 to 5.5 bar/deg. The NO_x emission tended to decrease as the exhaust residual gas increased. The NO_x emission declined from 11.3 to 2.12 g/kwh when the exhaust residual gas increased from 1% to 5%. An increased residual gas ratio led to a diluted air-fuel mixture and larger areas that lacked oxygen. The dilution of the air-fuel mixture and the lack of oxygen were due to increases in unburned HC and CO emissions from 3.65 to 18.2 g/kwh and from 139 to 450 g/kwh, respectively. Declines in the IMEP, BMEP, and engine torque accompanied an increase in the residual gas ratio. Here, the IMEP decreased from 11.6 to 6.5 bar, the BMEP decreased from 9.48 to 4.3 bar, and the engine brake torque decreased from 20.3 to 9 Nm as the residual gas ratio increased from 1% to 5%.

For the further work, the optimal engine operation condition and parameters in the transient sate will be estimated. In addition, a study to estimate the pure methanol and ethanol as fuel for small SI-engine will be conducted.

REFERENCES

[1] G. R. de Souza, C. de C. Pellegrini, S. L. Ferreira, F. Soto Pau, and O. Armas, “Study of intake manifolds of an internal combustion engine: A new geometry based on experimental results and numerical simulations,” *Therm. Sci. Eng. Prog.*, vol. 9, no. December 2018, pp. 248–258, 2019, doi: 10.1016/j.tsep.2018.12.003.

[2] L. Shi, G. Shu, H. Tian, and S. Deng, “A review of modified Organic Rankine cycles (ORCs) for internal combustion engine waste heat recovery (ICE-WHR),” *Renew. Sustain. Energy Rev.*, vol. 92, no. April, pp. 95–110, 2018, doi: 10.1016/j.rser.2018.04.023.

[3] W. Sui, J. P. González, and C. M. Hall, “Combustion Phasing Modelling of Dual Fuel Engines,” *IFAC-PapersOnLine*, vol. 51, no. 31, pp. 319–324, 2018, doi: 10.1016/j.ifacol.2018.10.067.

[4] H. Wei, A. Shao, J. Hua, L. Zhou, and D. Feng, “Effects of applying a Miller cycle with split injection on engine performance and knock resistance in a downsized gasoline engine,” *Fuel*, vol. 214, no. June 2017, pp. 98–107, 2018, doi: 10.1016/j.fuel.2017.11.006.

[5] D. Jung and N. Iida, “An investigation of multiple spark discharge using multi-coil ignition system for improving thermal efficiency of lean SI engine operation,” *Appl. Energy*, vol. 212, no. September 2017, pp. 322–332, 2018, doi: 10.1016/j.apenergy.2017.12.032.

[6] J. Rajeevan, M. H. Hans, A. Joseph, T. S. Kiran, and G. K. Thampi, “Hybrid Turbocharged SI engine with Cooled Exhaust Gas Recirculation for Improved Performance,” *Procedia Technol.*, vol. 24, pp. 444–451, 2016, doi: 10.1016/j.protcy.2016.05.061.

[7] Y. Zhenzhong, W. Jianqin, F. Zhuoyi, and L. Jinding, “An investigation of optimum control of ignition timing and injection system in an in-cylinder injection type hydrogen fueled engine,” *Int. J. Hydrogen Energy*, vol. 27, no. 2, pp. 213–217, 2002, doi: 10.1016/S0360-3199(01)00096-9.

[8] M. M. Rahman, M. Kamil, and R. A. Bakar, “Engine performance and optimum injection timing for 4-cylinder direct injection hydrogen fueled engine,” *Simul. Model. Pract. Theory*, vol. 19, no. 2, pp. 734–751, 2011, doi: 10.1016/j.simpat.2010.10.006.

[9] J. Cho, S. Park, and S. Song, “The effects of the air-fuel ratio on a stationary diesel

engine under dual-fuel conditions and multi-objective optimization," *Energy*, vol. 187, p. 115884, 2019, doi: 10.1016/j.energy.2019.115884.

[10] S. K. Hotta, N. Sahoo, K. Mohanty, and V. Kulkarni, "Ignition timing and compression ratio as effective means for the improvement in the operating characteristics of a biogas fueled spark ignition engine," *Renew. Energy*, vol. 150, no. x, pp. 854–867, 2020, doi: 10.1016/j.renene.2019.12.145.

[11] ASIA, "No Title," *https://data.aseanstats.org/indicator/ASE.TRP.ROD.* .

[12] P. Brequigny, F. Halter, C. Mounaïm-Rousselle, and T. Dubois, "Fuel performances in Spark-Ignition (SI) engines: Impact of flame stretch," *Combust. Flame*, vol. 166, pp. 98–112, 2016, doi: 10.1016/j.combustflame.2016.01.005.

[13] C. E. C. Alvarez, G. E. Couto, V. R. Roso, A. B. Thiriet, and R. M. Valle, "A review of prechamber ignition systems as lean combustion technology for SI engines," *Appl. Therm. Eng.*, vol. 128, pp. 107–120, 2018, doi: 10.1016/j.applthermaleng.2017.08.118.

[14] M. Darzi, D. Johnson, C. Ulishney, and N. Clark, "Low pressure direct injection strategies effect on a small SI natural gas two-stroke engine's energy distribution and emissions," *Appl. Energy*, vol. 230, no. May, pp. 1585–1602, 2018, doi: 10.1016/j.apenergy.2018.09.091.

[15] S. Bai-Gang, T. Hua-Yu, and L. Fu-Shui, "The distinctive characteristics of combustion duration in hydrogen internal combustion engine," *Int. J. Hydrogen Energy*, vol. 39, no. 26, pp. 14472–14478, 2014, doi: 10.1016/j.ijhydene.2014.04.013.

[16] H. Bayraktar and O. Durgun, "Development of an empirical correlation for combustion durations in spark ignition engines," *Energy Convers. Manag.*, vol. 45, no. 9–10, pp. 1419–1431, 2004, doi: 10.1016/j.enconman.2003.09.010.

[17] A. E. Dhole, R. B. Yarasu, and D. B. Lata, "Investigations on the combustion duration and ignition delay period of a dual fuel diesel engine with hydrogen and producer gas as secondary fuels," *Appl. Therm. Eng.*, vol. 107, pp. 524–532, 2016, doi: 10.1016/j.applthermaleng.2016.06.151.

[18] C. Zhang, A. Zhou, Y. Shen, Y. Li, and Q. Shi, "Effects of combustion duration characteristic on the brake thermal efficiency and NOx emission of a turbocharged diesel engine fueled with diesel-LNG dual-fuel," *Appl. Therm. Eng.*, vol. 127, pp. 312–318, 2017, doi: 10.1016/j.applthermaleng.2017.08.034.

[19] D. B. Lata, A. Misra, and S. Medhekar, "Investigations on the combustion parameters of a dual fuel diesel engine with hydrogen and LPG as secondary fuels," *Int. J.*

Hydrogen Energy, vol. 36, no. 21, pp. 13808–13819, 2011, doi: 10.1016/j.ijhydene.2011.07.142.

[20] J. Wang, Z. Huang, J. Zheng, and H. Miao, "Effect of partially premixed and hydrogen addition on natural gas direct-injection lean combustion," *Int. J. Hydrogen Energy*, vol. 34, no. 22, pp. 9239–9247, 2009, doi: 10.1016/j.ijhydene.2009.09.018.

[21] H. A. K. S. Al-Janabi and M. A. R. S. Al-Baghdadi, "Prediction study of the effect of hydrogen blending on the performance and pollutants emission of a four stroke spark ignition engine," *Int. J. Hydrogen Energy*, vol. 24, no. 4, pp. 363–375, 1999, doi: 10.1016/S0360-3199(98)00040-8.

[22] M. M. Roy, E. Tomita, N. Kawahara, Y. Harada, and A. Sakane, "Performance and emissions of a supercharged dual-fuel engine fueled by hydrogen-rich coke oven gas," *Int. J. Hydrogen Energy*, vol. 34, no. 23, pp. 9628–9638, 2009, doi: 10.1016/j.ijhydene.2009.09.016.

[23] M. M. Roy, E. Tomita, N. Kawahara, Y. Harada, and A. Sakane, "Comparison of performance and emissions of a supercharged dual-fuel engine fueled by hydrogen and hydrogen-containing gaseous fuels," *Int. J. Hydrogen Energy*, vol. 36, no. 12, pp. 7339–7352, 2011, doi: 10.1016/j.ijhydene.2011.03.070.

[24] C. Liew *et al.*, "An experimental investigation of the combustion process of a heavy-duty diesel engine enriched with H2," *Int. J. Hydrogen Energy*, vol. 35, no. 20, pp. 11357–11365, 2010, doi: 10.1016/j.ijhydene.2010.06.023.

[25] F. Ma, Y. Wang, J. Wang, S. Ding, Y. Wang, and S. Zhao, "Effects of combustion phasing, combustion duration, and their cyclic variations on spark-ignition (SI) engine efficiency," *Energy and Fuels*, vol. 22, no. 5, pp. 3022–3028, 2008, doi: 10.1021/ef8003027.

[26] S. Yousufuddin, "Experimental study on combustion duration and performance characteristics of a hydrogen-ethanol dual fueled engine," *Int. J. Automot. Eng. Technol.*, vol. 5, no. 3, pp. 85–101, 2016, doi: 10.18245/ijaet.287175.

[27] J. A. A. Yamin, H. N. Gupta, and B. B. Bansal, "THE EFFECT OF COMBUSTION DURATION ON THE PERFORMANCE AND EMISSION CHARACTERISTICS OF PROPANE-FUELED 4-Stroke S. I. ENGINES," *Emirates J. Eng. Res.*, vol. 8, no. 1, pp. 1–14, 2003, [Online]. Available: https://eng.uaeu.ac.ae/en/research/journal/issues/v8/pdf_iss1_8/1.pdf.

[28] A. Manmadhachary, M. Santosh Kumar, and Y. Ravi Kumar, "Design&manufacturing

of spiral intake manifold to improve Volument efficiency of injection diesel engine byAM process," *Mater. Today Proc.*, vol. 4, no. 2, pp. 1084–1090, 2017, doi: 10.1016/j.matpr.2017.01.123.

[29] M. H. Yang, "Payback period investigation of the organic Rankine cycle with mixed working fluids to recover waste heat from the exhaust gas of a large marine diesel engine," *Energy Convers. Manag.*, vol. 162, no. 142, pp. 189–202, 2018, doi: 10.1016/j.enconman.2018.02.032.

[30] M. Nazoktabar, S. A. Jazayeri, M. Parsa, D. D. Ganji, and K. Arshtabar, "Controlling the optimal combustion phasing in an HCCI engine based on load demand and minimum emissions," *Energy*, vol. 182, pp. 82–92, 2019, doi: 10.1016/j.energy.2019.06.012.

[31] Z. Lee and S. Park, "Particulate and gaseous emissions from a direct-injection spark ignition engine fueled with bioethanol and gasoline blends at ultra-high injection pressure," *Renew. Energy*, vol. 149, pp. 80–90, 2020, doi: 10.1016/j.renene.2019.12.050.

[32] S. Tsuboi, S. Miyokawa, M. Matsuda, T. Yokomori, and N. Iida, "Influence of spark discharge characteristics on ignition and combustion process and the lean operation limit in a spark ignition engine," *Appl. Energy*, vol. 250, no. January, pp. 617–632, 2019, doi: 10.1016/j.apenergy.2019.05.036.

[33] A. T. Nguyen, M. Dambrine, J. Lauber, and M. Sugeno, *Feedback linearization-based control approach for air system of a turbocharged SI engine: Toward a fuel-optimal strategy*, vol. 19, no. 3. IFAC, 2014.

[34] Mcgraw-Hill, *No Title*. [1] Heywood, J. B. Internal combustion engine fundamentals. New York, 1988.

[35] B. Fasolo, A. M. Doisy, A. Dupont, and F. Lavoisier, "Combustion system optimization of a new 2 liter diesel engine for EURO IV," *SAE Tech. Pap.*, no. 724, 2005, doi: 10.4271/2005-01-0652.

[36] J. Kermani *et al.*, "An experimental investigation of the effect of bore-to-stroke ratio on a diesel engine," *SAE Tech. Pap.*, vol. 6, 2013, doi: 10.4271/2013-24-0065.

[37] F. Payri, P. Olmeda, J. Martín, and R. Carreño, "Experimental analysis of the global energy balance in a di diesel engine," *Appl. Therm. Eng.*, vol. 89, no. x, pp. 545–557, 2015, doi: 10.1016/j.applthermaleng.2015.06.005.

[38] F. Payri, P. Olmeda, J. Martin, and R. Carreño, "A New Tool to Perform Global

Energy Balances in DI Diesel Engines," *SAE Int. J. Engines*, vol. 7, no. 1, pp. 43–59, 2014, doi: 10.4271/2014-01-0665.

[39] Z. S. Filipi and D. N. Assanis, "The effect of the stroke-to-bore ratio on combustion, heat transfer and efficiency of a homogeneous charge spark ignition engine of given displacement," *Int. J. Engine Res.*, vol. 1, no. 2, pp. 191–208, 2000, doi: 10.1243/1468087001545137.

[40] P. C. Miles and Ö. Andersson, "A review of design considerations for light-duty diesel combustion systems," *Int. J. Engine Res.*, vol. 17, no. 1, pp. 6–15, 2016, doi: 10.1177/1468087415604754.

[41] J. Benajes, R. Novella, J. M. Pastor, A. Hernández-López, and T. Duverger, "A computational analysis of the impact of bore-to-stroke ratio on emissions and efficiency of a HSDI engine," *Appl. Energy*, vol. 205, no. August, pp. 903–910, 2017, doi: 10.1016/j.apenergy.2017.08.023.

[42] B. Dogru, R. Lot, and K. K. J. Ranga Dinesh, "Valve timing optimisation of a spark ignition engine with skip cycle strategy," *Energy Convers. Manag.*, vol. 173, no. May, pp. 95–112, 2018, doi: 10.1016/j.enconman.2018.07.064.

[43] K. C. Nayak and P. P. Date, "Manufacturing of light automobile engine piston head using sheet metal," *Procedia Manuf.*, vol. 15, pp. 940–948, 2018, doi: 10.1016/j.promfg.2018.07.402.

[44] M. Cerdoun, S. Khalfallah, A. Beniaiche, and C. Carcasci, "Investigations on the heat transfer within intake and exhaust valves at various engine speeds," *Int. J. Heat Mass Transf.*, vol. 147, p. 119005, 2020, doi: 10.1016/j.ijheatmasstransfer.2019.119005.

[45] T. Wang, X. Jia, X. Li, S. Ren, and X. Peng, "Thermal-structural coupled analysis and improvement of the diaphragm compressor cylinder head for a hydrogen refueling station," *Int. J. Hydrogen Energy*, vol. 45, no. 1, pp. 809–821, 2020, doi: 10.1016/j.ijhydene.2019.10.199.

[46] G. Wang, W. Yu, X. Li, and R. Yang, "Influence of fuel injection and intake port on combustion characteristics of controllable intake swirl diesel engine," *Fuel*, vol. 262, no. August 2019, p. 116548, 2020, doi: 10.1016/j.fuel.2019.116548.

[47] Z. Guo *et al.*, "Numerical optimization of intake and exhaust structure and experimental verification on single-screw expander for small-scale ORC applications," *Energy*, vol. 199, p. 117478, 2020, doi: 10.1016/j.energy.2020.117478.

[48] C. Cinar, A. Uyumaz, H. Solmaz, and T. Topgul, "Effects of valve lift on the

combustion and emissions of a HCCI gasoline engine," *Energy Convers. Manag.*, vol. 94, no. x, pp. 159–168, 2015, doi: 10.1016/j.enconman.2015.01.072.

[49] Y. Zhang, H. Zhao, H. Xie, and B. Q. He, "Variable-valve-actuation-enabled high-efficiency gasoline engine," *Proc. Inst. Mech. Eng. Part D J. Automob. Eng.*, vol. 224, no. 8, pp. 1081–1095, 2010, doi: 10.1243/09544070JAUTO1436.

[50] K. J. A.-K. Osama H. Ghazal, Yousef S. Najjar, "Effect of Varying Inlet Valve Throat Diameter at Different IVO, IVC, and OVERLAP Angles on SI Engine Performance," *Proc. World Congr. Eng.*, vol. 3, 2011.

[51] M. Raghu and P. S. Mehta, "Influence of intake port design on diesel engine air motion characteristics," *Indian J. Eng. Mater. Sci.*, vol. 6, no. 2, pp. 53–58, 1999.

[52] A. Yasar, B. Sahin, H. Akilli, and K. Aydin, "Effect of inlet port on the flow in the cylinder of an internal combustion engine," *Proc. Inst. Mech. Eng. Part C J. Mech. Eng. Sci.*, vol. 220, no. 1, pp. 73–82, 2006, doi: 10.1243/095440605X32129.

[53] T. Y. K. and S. H. LEE, "Combustion and Emission Characteristics of Wood Pyrolysis Oil-Butanol Blended Fuels in a Di Diesel Engine," *Int. J. ...*, vol. 13, no. 2, pp. 293–300, 2012, doi: 10.1007/s12239.

[54] V. M. Latheesh, P. Parthasarathy, V. Baskaran, and S. Karthikeyan, "Design and CFD analysis of intake port and exhaust port for a 4 valve cylinder head engine," *IOP Conf. Ser. Mater. Sci. Eng.*, vol. 310, no. 1, 2018, doi: 10.1088/1757-899X/310/1/012122.

[55] S. K. Sabale and S. B. Sanap, "Design and Analysis of Intake Port of Diesel Engine for Target Value of Swirl," *Am. J. Mech. Eng.*, vol. 1, no. 5, pp. 138–142, 2013, doi: 10.12691/ajme-1-5-6.

[56] S. Suhaimi, R. Mamat, and N. R. Abdullah, "Investigation of the effects of inlet system configuration on the airflow characteristics," *IOP Conf. Ser. Mater. Sci. Eng.*, vol. 50, no. 1, 2013, doi: 10.1088/1757-899X/50/1/012009.

[57] A. Cairns, H. Zhao, A. Todd, and P. Aleiferis, "A study of mechanical variable valve operation with gasoline-alcohol fuels in a spark ignition engine," *Fuel*, vol. 106, pp. 802–813, 2013, doi: 10.1016/j.fuel.2012.10.041.

[58] S. Park and S. Song, "Model-based multi-objective Pareto optimization of the BSFC and NOx emission of a dual-fuel engine using a variable valve strategy," *J. Nat. Gas Sci. Eng.*, vol. 39, no. x, pp. 161–172, 2017, doi: 10.1016/j.jngse.2017.01.032.

[59] R. J. Middleton, L. K. M. Olesky, G. A. Lavoie, M. S. Wooldridge, D. N. Assanis, and J. B. Martz, "The effect of spark timing and negative valve overlap on Spark Assisted

Compression Ignition combustion heat release rate," *Proc. Combust. Inst.*, vol. 35, no. 3, pp. 3117–3124, 2015, doi: 10.1016/j.proci.2014.08.021.

[60] S. Szwaja *et al.*, "Influence of exhaust residuals on combustion phases, exhaust toxic emission and fuel consumption from a natural gas fueled spark-ignition engine," *Energy Convers. Manag.*, vol. 165, no. March, pp. 440–446, 2018, doi: 10.1016/j.enconman.2018.03.075.

[61] J. Yang, K. Sata, J. Kako, A. Ohata, and T. Shen, *Statistical model and control of residual gas mass in gasoline engines*, vol. 7, no. PART 1. IFAC, 2013.

[62] K. Sata, J. Kako, J. Yang, A. Ohata, and T. Shen, *Effect of transient residual gas fraction for gasoline engines*, vol. 7, no. PART 1. IFAC, 2013.

[63] C. Guardiola, V. Triantopoulos, P. Bares, S. Bohac, and A. Stefanopoulou, "Simultaneous Estimation of Intake and Residual Mass Using In-Cylinder Pressure in an Engine with Negative Valve Overlap," *IFAC-PapersOnLine*, vol. 49, no. 11, pp. 461–468, 2016, doi: 10.1016/j.ifacol.2016.08.068.

[64] L. M. Olesky, J. B. Martz, G. A. Lavoie, J. Vavra, D. N. Assanis, and A. Babajimopoulos, "The effects of spark timing, unburned gas temperature, and negative valve overlap on the rates of stoichiometric spark assisted compression ignition combustion," *Appl. Energy*, vol. 105, pp. 407–417, 2013, doi: 10.1016/j.apenergy.2013.01.038.

[65] H. Xie, L. Li, T. Chen, W. Yu, X. Wang, and H. Zhao, "Study on spark assisted compression ignition (SACI) combustion with positive valve overlap at medium-high load," *Appl. Energy*, vol. 101, pp. 622–633, 2013, doi: 10.1016/j.apenergy.2012.07.015.

[66] C. Park, S. Lee, G. Lim, Y. Choi, and C. Kim, "Full load performance and emission characteristics of hydrogen-compressed natural gas engines with valve overlap changes," *Fuel*, vol. 123, pp. 101–106, 2014, doi: 10.1016/j.fuel.2014.01.041.

[67] J. Hunicz, "An experimental study of negative valve overlap injection effects and their impact on combustion in a gasoline HCCI engine," *Fuel*, vol. 117, no. PART A, pp. 236–250, 2014, doi: 10.1016/j.fuel.2013.09.079.

[68] D. Agarwal, S. K. Singh, and A. K. Agarwal, "Effect of Exhaust Gas Recirculation (EGR) on performance, emissions, deposits and durability of a constant speed compression ignition engine," *Appl. Energy*, vol. 88, no. 8, pp. 2900–2907, 2011, doi: 10.1016/j.apenergy.2011.01.066.

[69] L. Liu, Z. Li, S. Liu, and B. Shen, “Effect of exhaust gases of Exhaust Gas Recirculation (EGR) coupling lean-burn gasoline engine on NOx purification of Lean NOx trap (LNT),” *Mech. Syst. Signal Process.*, vol. 87, pp. 195–213, 2017, doi: 10.1016/j.ymssp.2015.12.029.

[70] U. Asad and M. Zheng, “Exhaust gas recirculation for advanced diesel combustion cycles,” *Appl. Energy*, vol. 123, pp. 242–252, 2014, doi: 10.1016/j.apenergy.2014.02.073.

[71] J. Thangaraja and C. Kannan, “Effect of exhaust gas recirculation on advanced diesel combustion and alternate fuels - A review,” *Appl. Energy*, vol. 180, pp. 169–184, 2016, doi: 10.1016/j.apenergy.2016.07.096.

[72] B. Rohani and C. Bae, “Effect of exhaust gas recirculation (EGR) and multiple injections on diesel soot nano-structure and reactivity,” *Appl. Therm. Eng.*, vol. 116, pp. 160–169, 2017, doi: 10.1016/j.applthermaleng.2016.11.116.

[73] M. H. M. Yasin, R. Mamat, A. F. Yusop, P. Paruka, T. Yusaf, and G. Najafi, “Effects of Exhaust Gas Recirculation (EGR) on a Diesel Engine fuelled with Palm-biodiesel,” *Energy Procedia*, vol. 75, pp. 30–36, 2015, doi: 10.1016/j.egypro.2015.07.131.

[74] G. Fontana and E. Galloni, “Variable valve timing for fuel economy improvement in a small spark-ignition engine,” *Appl. Energy*, vol. 86, no. 1, pp. 96–105, 2009, doi: 10.1016/j.apenergy.2008.04.009.

[75] A. F. M. Mahrous, A. Potrzebowski, M. L. Wyszynski, H. M. Xu, A. Tsolakis, and P. Luszcz, “A modelling study into the effects of variable valve timing on the gas exchange process and performance of a 4-valve DI homogeneous charge compression ignition (HCCI) engine,” *Energy Convers. Manag.*, vol. 50, no. 2, pp. 393–398, 2009, doi: 10.1016/j.enconman.2008.09.018.

[76] K. Xu, H. Xie, M. Wan, T. Chen, and H. Zhao, “Effect of Valve Timing and Residual Gas Dilution on Flame Development Characteristics in a Spark Ignition Engine,” *SAE Int. J. Engines*, vol. 7, no. 1, pp. 488–499, 2014, doi: 10.4271/2014-01-1205.

[77] V. Velmurugan, S. M. Aathif Akmal, V. Paramasivam, and S. Thanikaikarasan, “Prediction of vibration and exhaust gas emission characteristics using palm oil with nano particle diesel fuel,” *Mater. Today Proc.*, vol. 21, no. xxxx, pp. 800–805, 2020, doi: 10.1016/j.matpr.2019.07.248.

[78] S. Binnig, S. Fuchs, C. A. Robles Collantes, and H. R. Volpp, “Exhaust gas condensate – formation, characterization and influence on platinum measuring

electrodes in diesel vehicles," *Sensors Actuators, B Chem.*, vol. 242, no. x, pp. 1251–1258, 2017, doi: 10.1016/j.snb.2016.09.082.

[79] T. D. M. Lanzanova, M. Dalla Nora, M. E. S. Martins, P. R. M. Machado, V. B. Pedrozo, and H. Zhao, "The effects of residual gas trapping on part load performance and emissions of a spark ignition direct injection engine fuelled with wet ethanol," *Appl. Energy*, vol. 253, no. July, p. 113508, 2019, doi: 10.1016/j.apenergy.2019.113508.

[80] R. B. R. da Costa *et al.*, "Combustion, performance and emission analysis of a natural gas-hydrous ethanol dual-fuel spark ignition engine with internal exhaust gas recirculation," *Energy Convers. Manag.*, vol. 195, no. February, pp. 1187–1198, 2019, doi: 10.1016/j.enconman.2019.05.094.

[81] L. Zhou, J. Hua, F. Liu, F. Liu, D. Feng, and H. Wei, "Effect of internal exhaust gas recirculation on the combustion characteristics of gasoline compression ignition engine under low to idle conditions," *Energy*, vol. 164, pp. 306–315, 2018, doi: 10.1016/j.energy.2018.08.109.

[82] M. Melaika, A. Rimkus, and T. Vipartas, "Air Restrictor and Turbocharger Influence for the Formula Student Engine Performance," *Procedia Eng.*, vol. 187, pp. 402–407, 2017, doi: 10.1016/j.proeng.2017.04.392.

[83] S. Falfari, G. M. Bianchi, G. Cazzoli, C. Forte, and S. Negro, "Basics on Water Injection Process for Gasoline Engines," *Energy Procedia*, vol. 148, no. Ati, pp. 50–57, 2018, doi: 10.1016/j.egypro.2018.08.018.

[84] J. A. Pagán Rubio, F. Vera-García, J. Hernandez Grau, J. Muñoz Cámara, and D. Albaladejo Hernandez, "Marine diesel engine failure simulator based on thermodynamic model," *Appl. Therm. Eng.*, vol. 144, no. March, pp. 982–995, 2018, doi: 10.1016/j.applthermaleng.2018.08.096.

[85] Z. Petranović, M. Sjerić, I. Taritaš, M. Vujanović, and D. Kozarac, "Study of advanced engine operating strategies on a turbocharged diesel engine by using coupled numerical approaches," *Energy Convers. Manag.*, vol. 171, no. May, pp. 1–11, 2018, doi: 10.1016/j.enconman.2018.05.085.

[86] A. E. Teo, M. S. Chiong, M. Yang, A. Romagnoli, R. F. Martinez-Botas, and S. Rajoo, "Performance evaluation of low-pressure turbine, turbo-compounding and air-Brayton cycle as engine waste heat recovery method," *Energy*, vol. 166, pp. 895–907, 2019, doi: 10.1016/j.energy.2018.10.035.

[87] A. Praptijanto, A. Muharam, A. Nur, and Y. Putrasari, “Effect of ethanol percentage for diesel engine performance using virtual engine simulation tool,” *Energy Procedia*, vol. 68, pp. 345–354, 2015, doi: 10.1016/j.egypro.2015.03.265.

[88] H. G. Pattas K., “Stickoxidbildung bei der ottomotorischen Verbrennung,” *MTZ*, vol. 12, pp. 397–404, 1973.

[89] G. Onorati A., Ferrari G., D’Errico, “1D Unsteady Flows with Chemical Reactions in the Exhaust Duct-System of S.I. Engines: Predictions and Experiments,” *SAE*, vol. 01, no. 0939, 2001.

PUBLICATIONS AND CONFERENCES

A. List of Publications

1. **Nguyen Xuan Khoa**, Ocktaeck Lim, "The effects of combustion duration on residual gas, effective release energy, engine power and engine emissions characteristics of the motorcycle engine", ***Applied Energy, Elsevier***, Volume 248, pp 54-63, 2019. https://doi.org/10.1016/j.apenergy.2019.04.075
2. **Nguyen Xuan Khoa**, Quach Nhu Y, Ocktaeck Lim, "Estimation of parameters affected in internal exhaust residual gases recirculation and the influence of exhaust residual gas on performance and emission of a spark ignition engine", ***Applied Energy, Elsevier***, Volume 278, pp 54-63, 2020. https://doi.org/10.1016/j.apenergy.2020.115699
3. **Nguyen Xuan Khoa**, Ocktaeck Lim, "Effective release energy, residual gas, and engine emission characteristics of a V-twin engine with various exhaust valve closing timings", ***Journal of Mechanical Science and Technology, Springer***, Volume 34, pp 477-488, 2020. http://doi.org/10.1007/s12206-019-1245-6
4. **Nguyen Xuan Khoa**, Ocktaeck Lim," Comparative Study of the Effective Release Energy, Residual Gas Fraction, and Emission Characteristics with Various Valve Port Diameter-Bore Ratios (VPD/B) of a Four-Stroke Spark Ignition Engine", ***Energies-MDPI***, Volume 13, 2020. https://doi:10.3390/en13061330
5. **Nguyen Xuan Khoa**, Ocktaeck Lim,"The effects of bore-stroke ratio on effective release energy, residual gas, peak pressure rise and combustion duration of a V-twin engine", ***Journal of Mechanical Science and Technology, Springer***, Volume 34(6)2020. http://doi.org/10.1007/s12206-020-0539-z
6. **Nguyen Xuan Khoa**, Ock Taeck Lim, "The effects of combustion duration on residual gas, effective release energy and engine power of motorcycle engine at full load", ***Energy Procedia, Elsevier***, Volume 158, pp 1835-1841, 2019. https://doi.org/10.1016/j.egypro.2019.01.429
7. **Nguyen Xuan Khoa**, Ock Taeck Lim,"The investigation into the effects of inlet port diameter-stroke ratio on effective release energy and residual gas of small SI- engine", ***Energy Proceedings***, Volume 4, pp 20, 2020. http://www.energy-proceedings.org/category/icae2019v4/page/20/
8. **Nguyen Xuan Khoa**, Ocktaeck Lim, "Comparative study on the influence of combustion duration on performance and emission characteristics of a spark ignition engine fueled with pure methanol and ethanol", *Applied Energy, Elsevier* preparing to submit (Status date 2020-09-20).
9. **Nguyen Xuan Khoa**, Ocktaeck Lim, "External exhaust gas recirculation and internal exhaust gas recirculation in internal combustion engine: A review", *Applied Energy, Elsevier*, preparing to submit (Status date 2020- 9-20).

B. List of Conferences

International Conferences

1. **Nguyen Xuan Khoa** and Octaeck Lim, International Conference of Applied Energy (ICAE) 2018, Hong-Kong, 2018.
2. **Nguyen Xuan Khoa** and Ocktaeck Lim, 1st International conference on meterialm Machines and Methods for Sustainable deverlopment (MMMS), Da Nang, Viet Nam, 2018.
3. **Nguyen Xuan Khoa** and Ocktaeck Lim, International Conference on Advanced Automotive Technology (ICAT) 2018, July 5-7, 2018, Gwangju, Korea.
4. **Nguyen Xuan Khoa** and Ocktaeck Lim, International Conference on Advanced Automotive Technology (ICAT) 2019, June 20-22, 2019, Gwangju, Korea
5. **Nguyen Xuan Khoa** and Ocktaeck Lim, International Conference on Applied Energy 2019, Aug 12-15, 2019, Västerås, Sweden.
6. **Nguyen Xuan Khoa** and Ocktaeck Lim, SpliTech2020 – 5th International Conference on Smart and Sustainable Technologies. Bol and Split, Croatia, September 23 – 26, 2020
7. Nguyen Xuan Khoa and Ocktaeck Lim, International Conference on Applied Energy 2020, November 29, 2020, Bangkok, Thailand.

Domestic Conferences

1. **Nguyen Xuan Khoa,** Ocktaeck Lim, KSAE, Annual Spring conference. Bexco, Busan. 2018
2. **Nguyen Xuan Khoa,** Ocktaeck Lim, KSAE, KSAE 2018 Conference Chapter Busan, Changwon and Ulsan, Changwon, Korea, 2018.
3. **Nguyen Xuan Khoa,** Ocktaeck Lim, KSAE 2019 Annual Conference and Exhibition, Ramada Plaza Jeju Hotel, Jeju, Korea, 2019.
4. **Nguyen Xuan Khoa,** Ocktaeck Lim, KSAE 2019 Annual Autumn Conference and Exhibition, HiCo hotel, Gyonggju, Korea, 2019.

APPENDIX

Engine simulation model

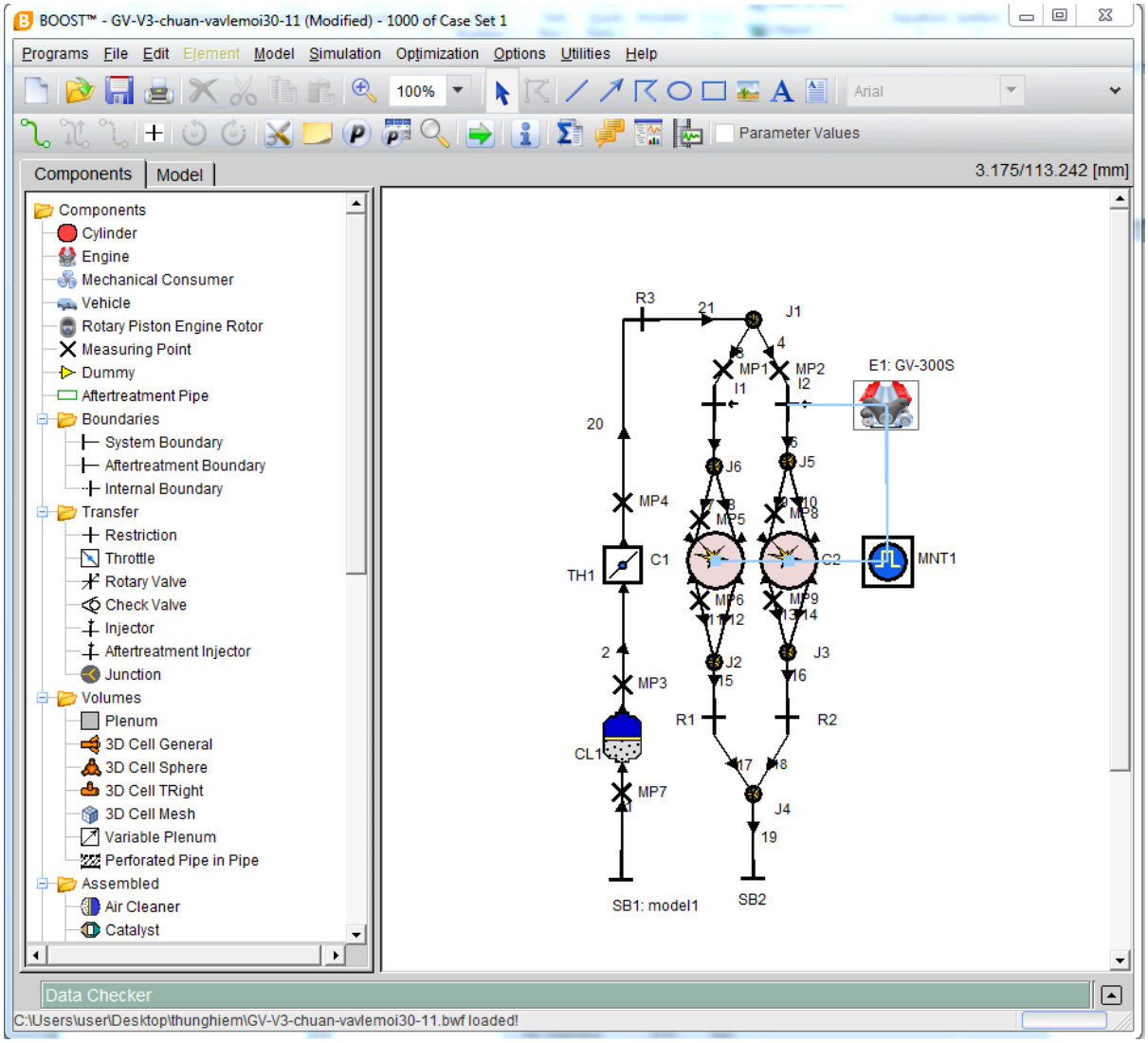

System boundary definition

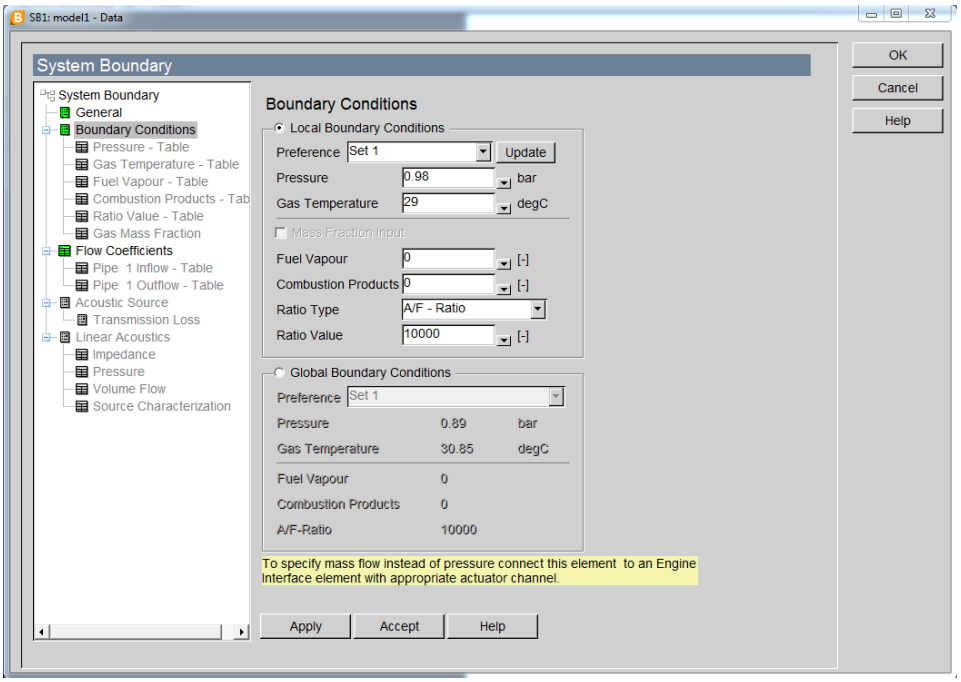

System pipe definition

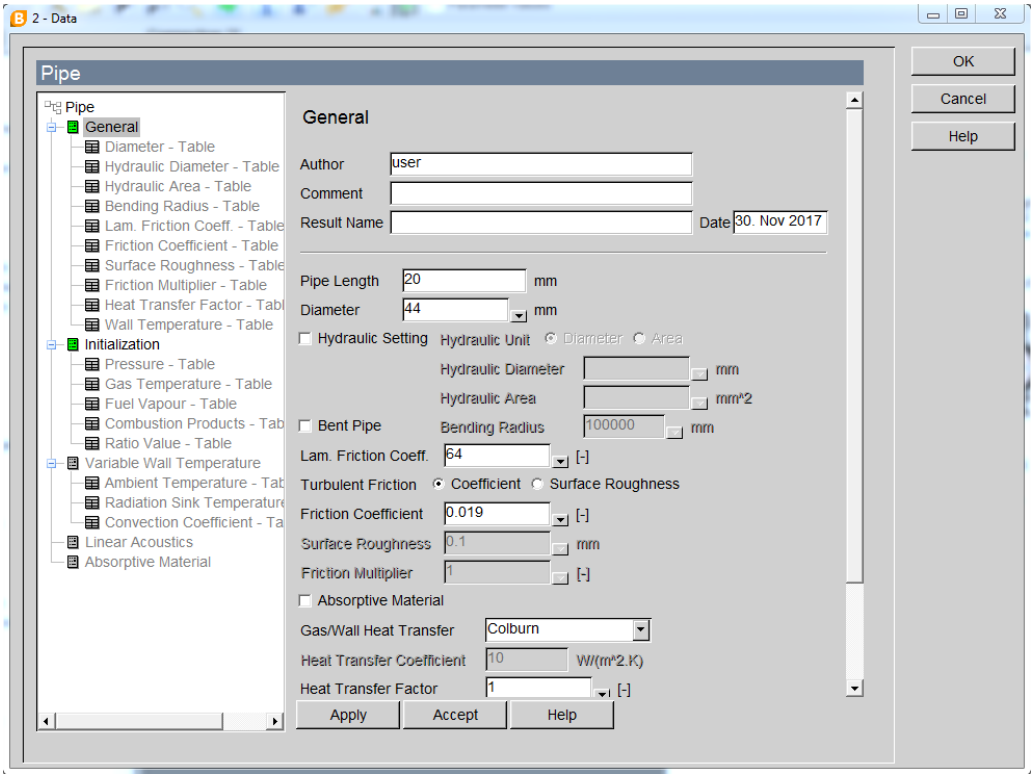

Air Cleaner definition

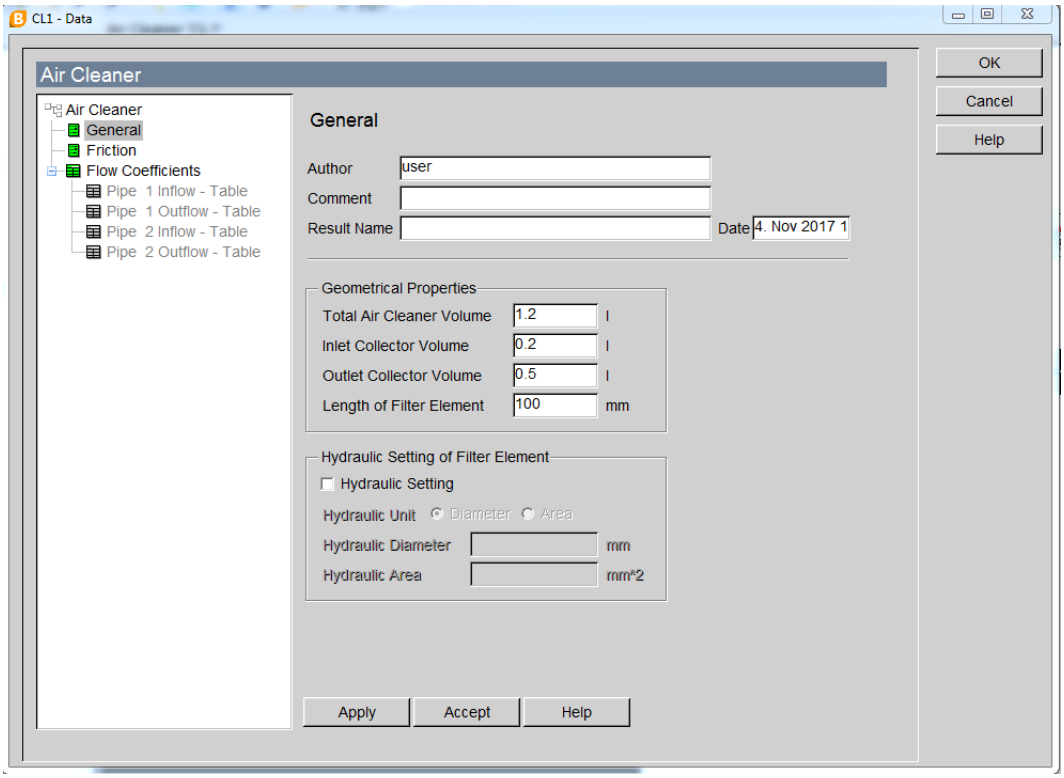

Throttle definition

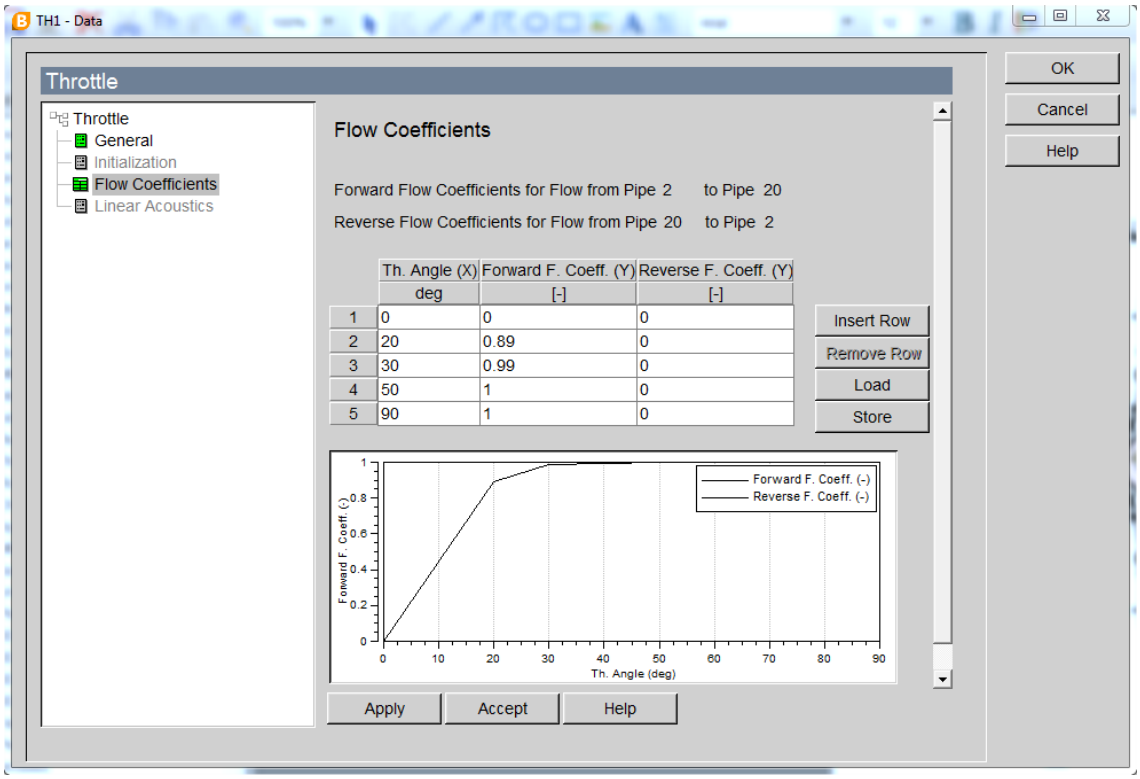

Injector definition

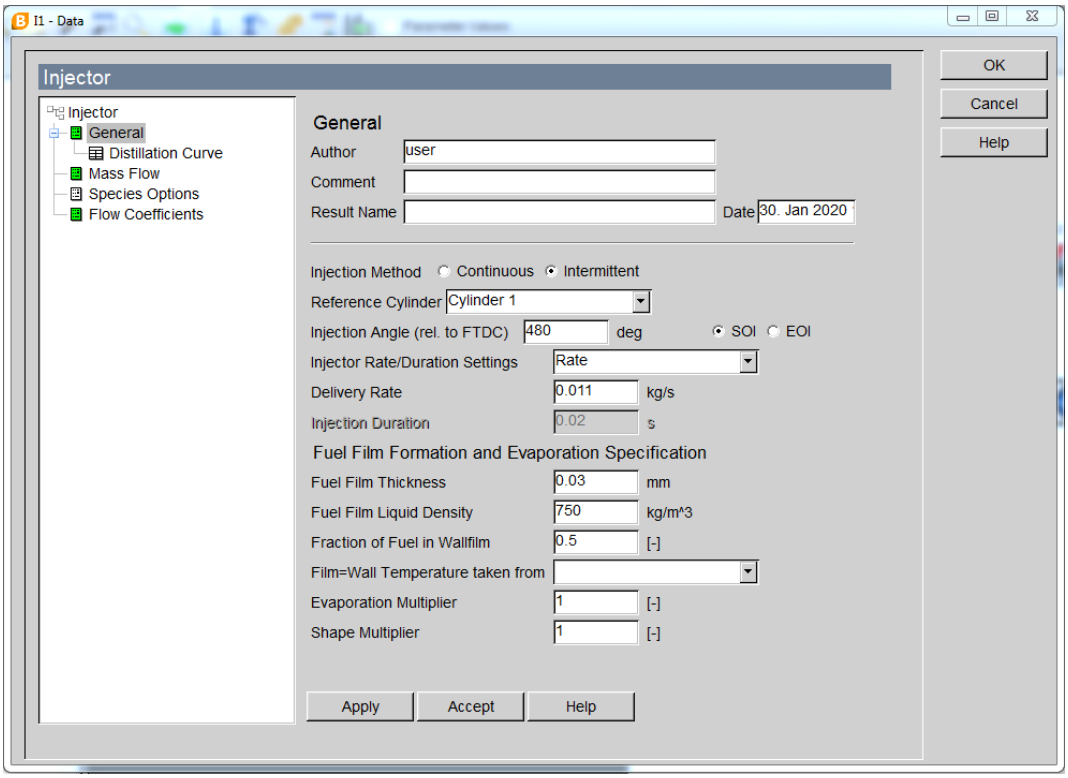

Cylinder definition

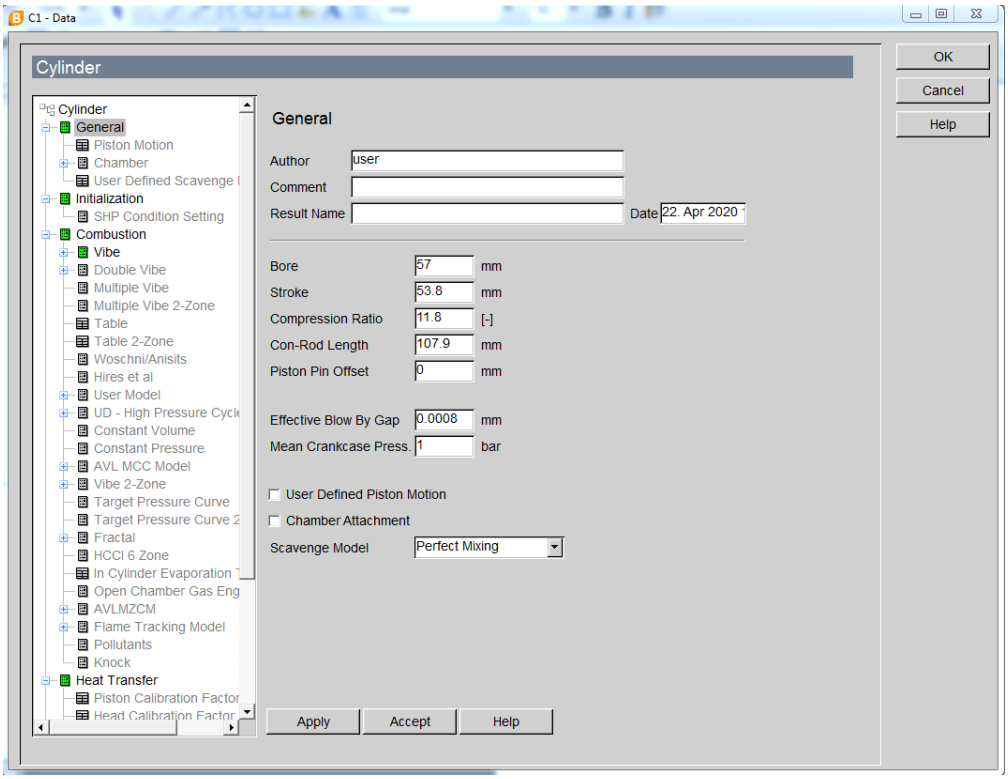

Cylinder heat release characteristics definition

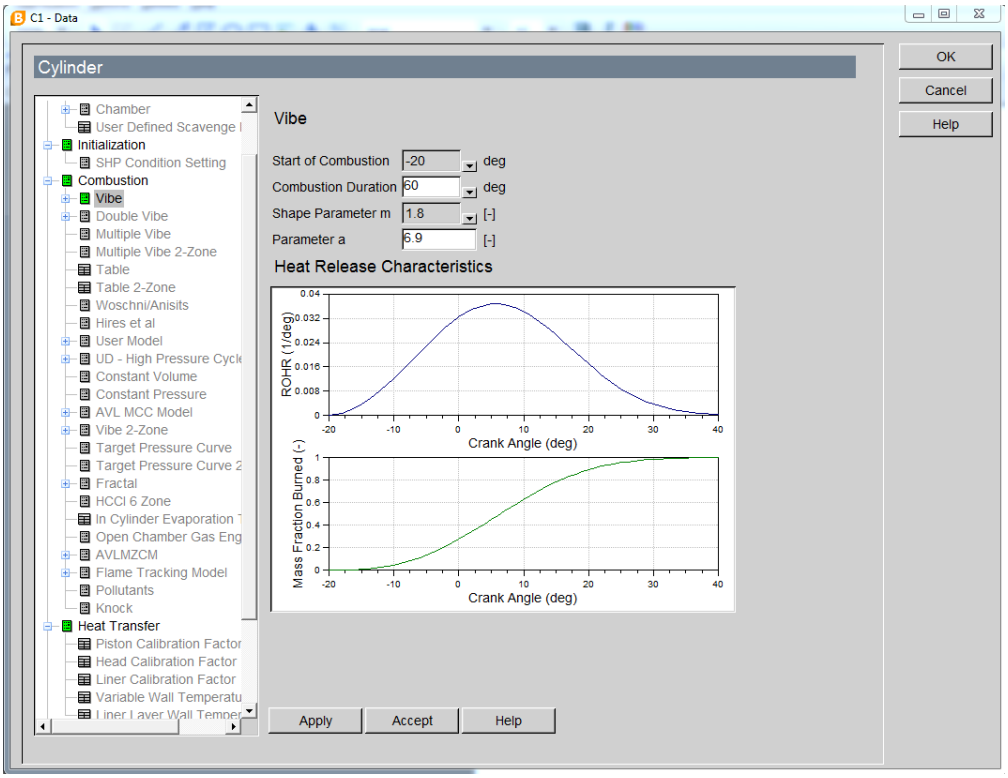

Cylinder heat transfer definition

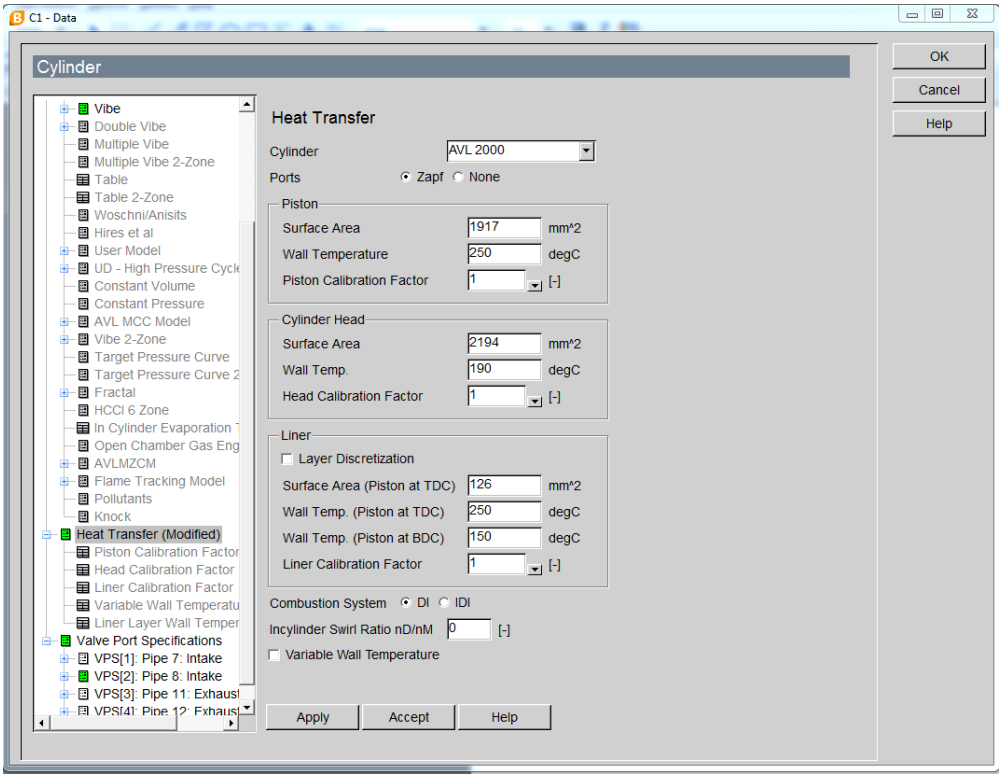

Cylinder heat transfer models

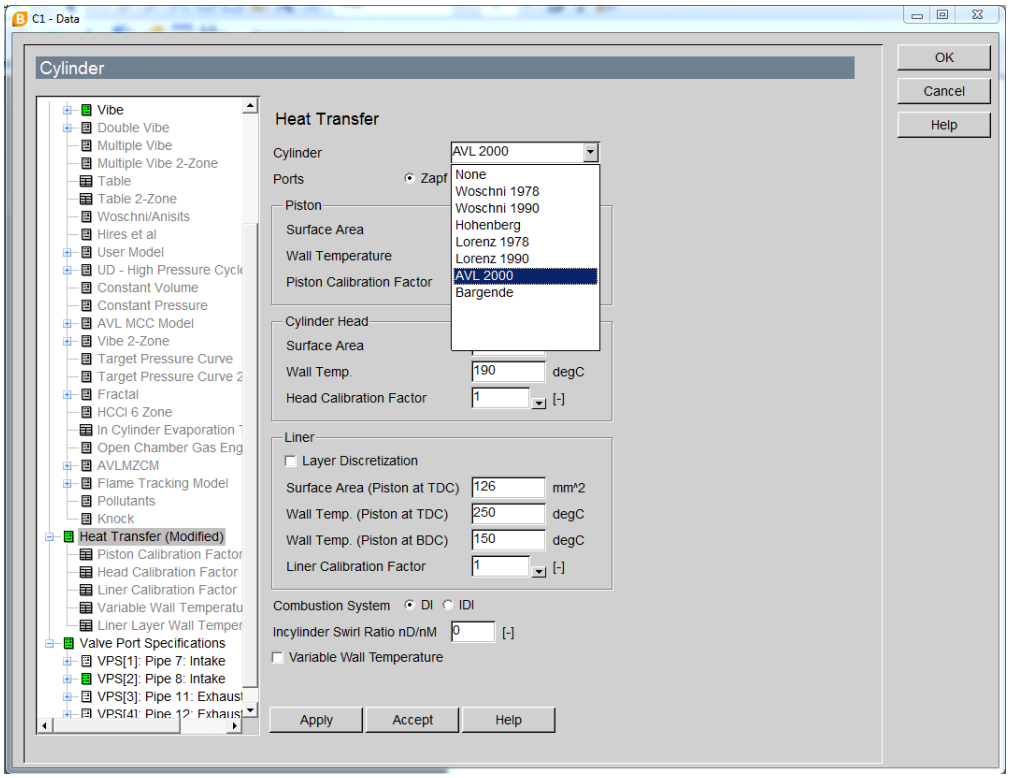

Intake valve lift definition

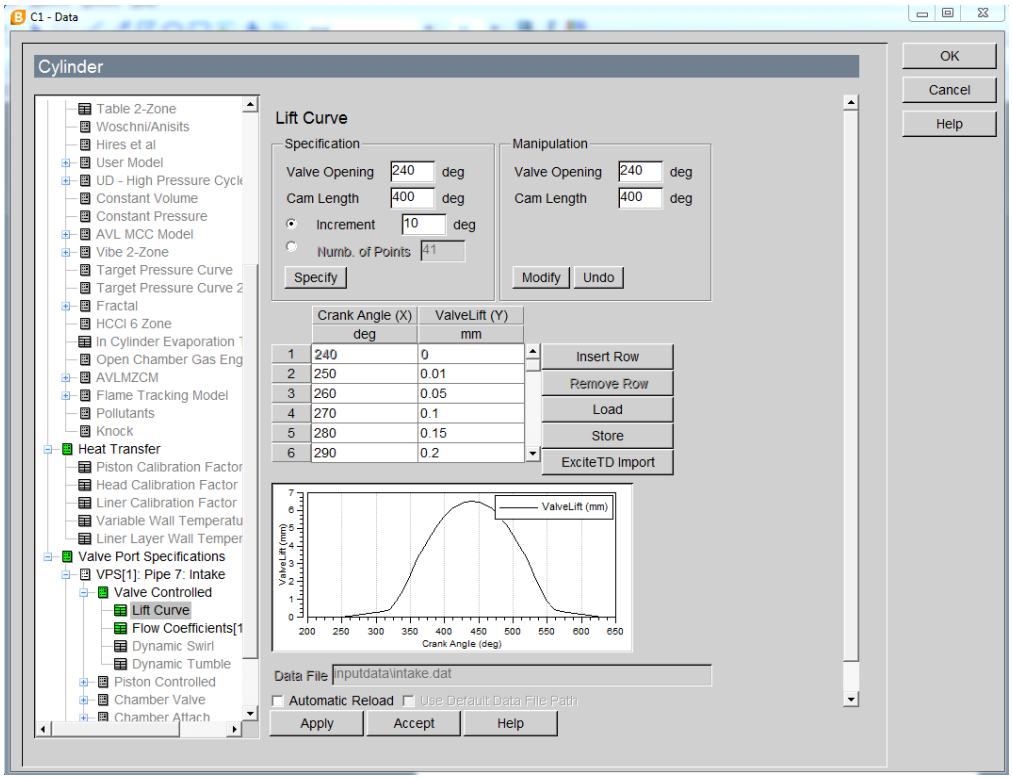

Exhaust valve lift definition

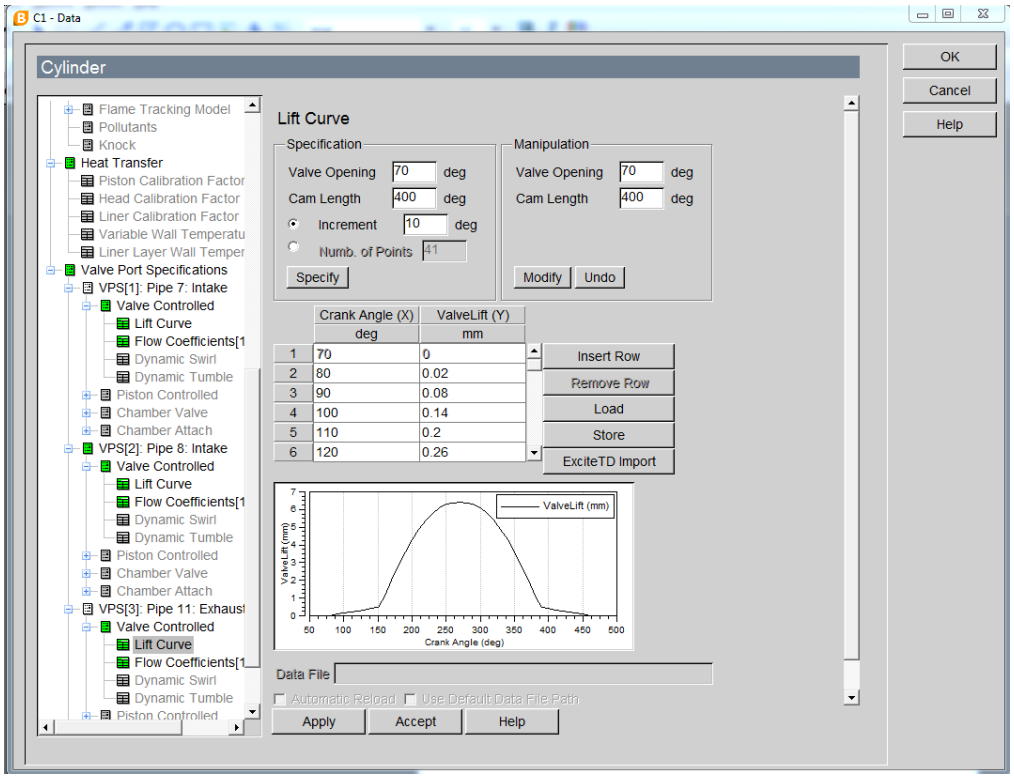

Pipe system restriction definition

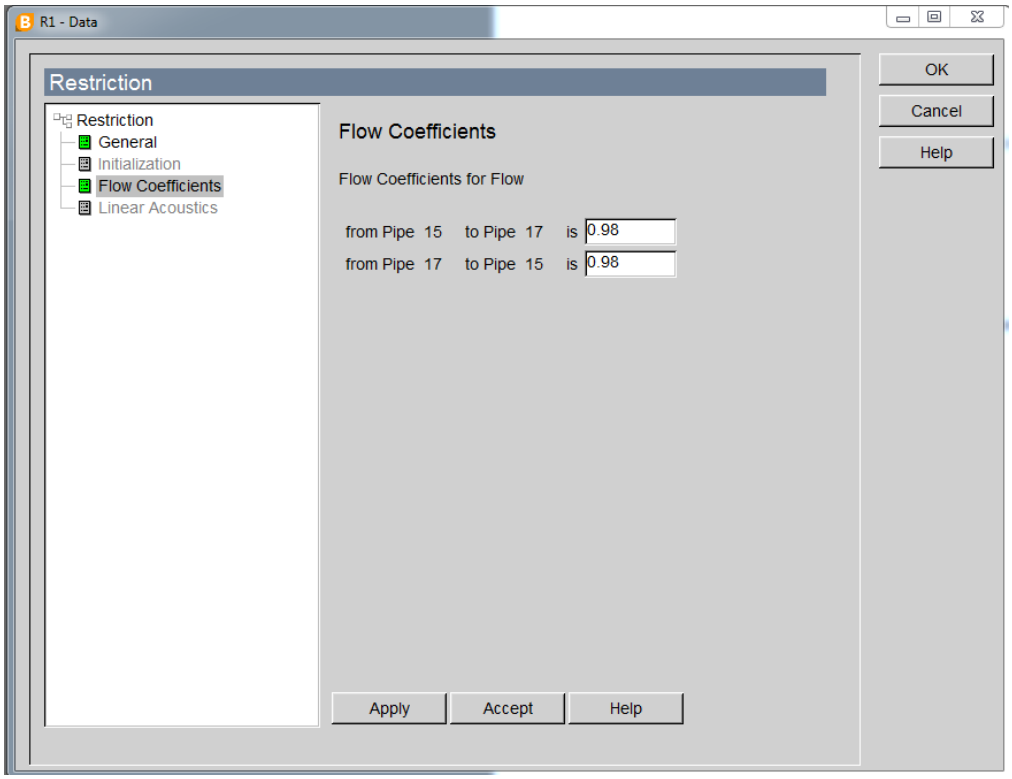

Engine general definition

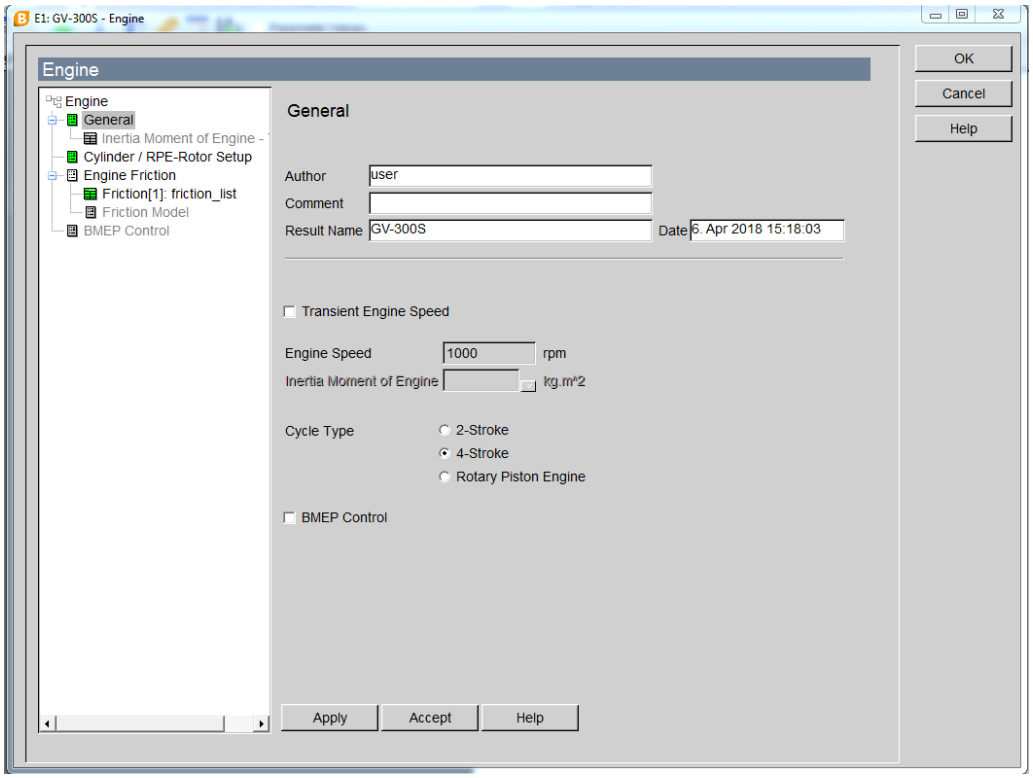

Monitor and sensor channels

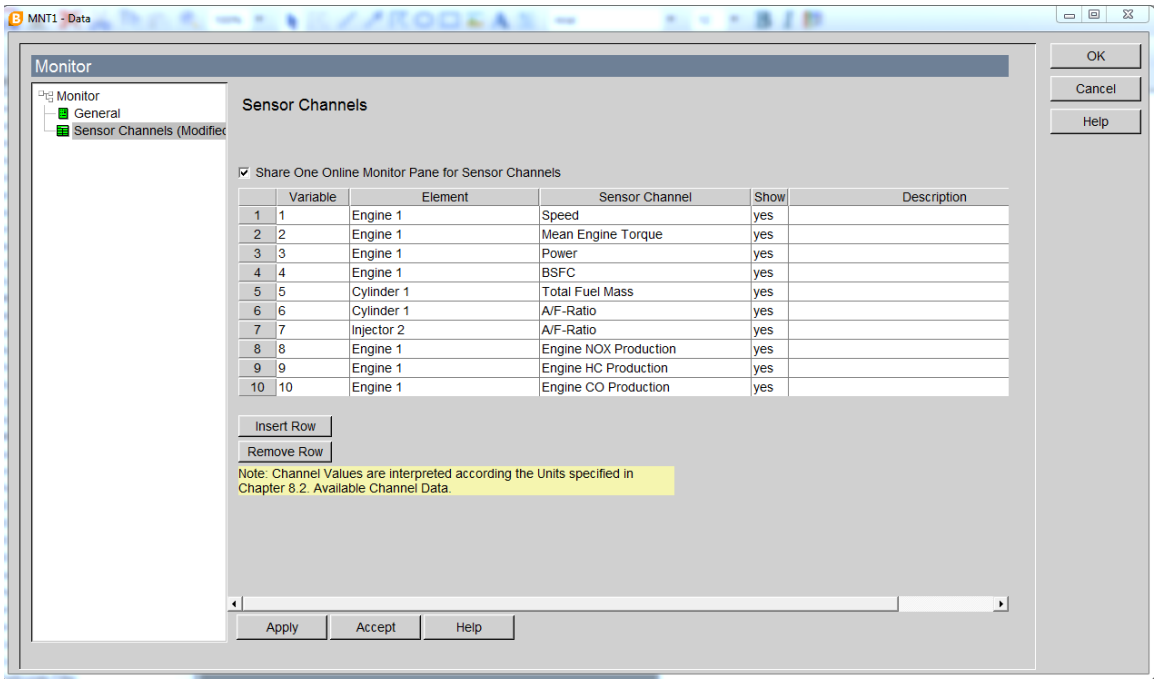

Simulation control/Global setup

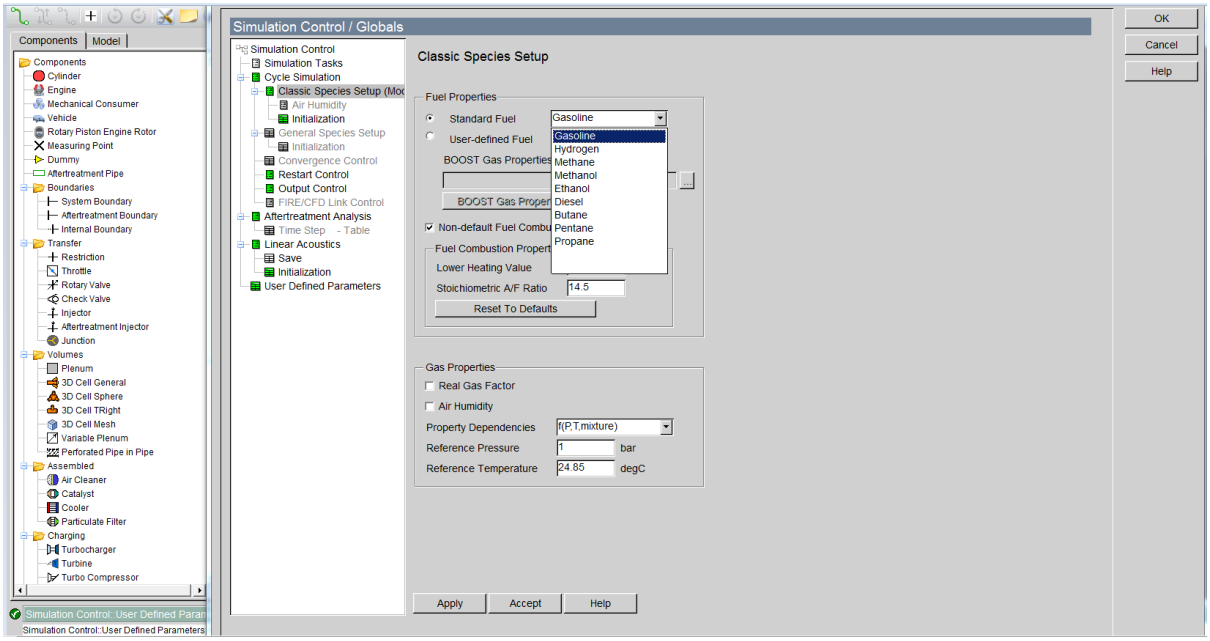

Junction component definition

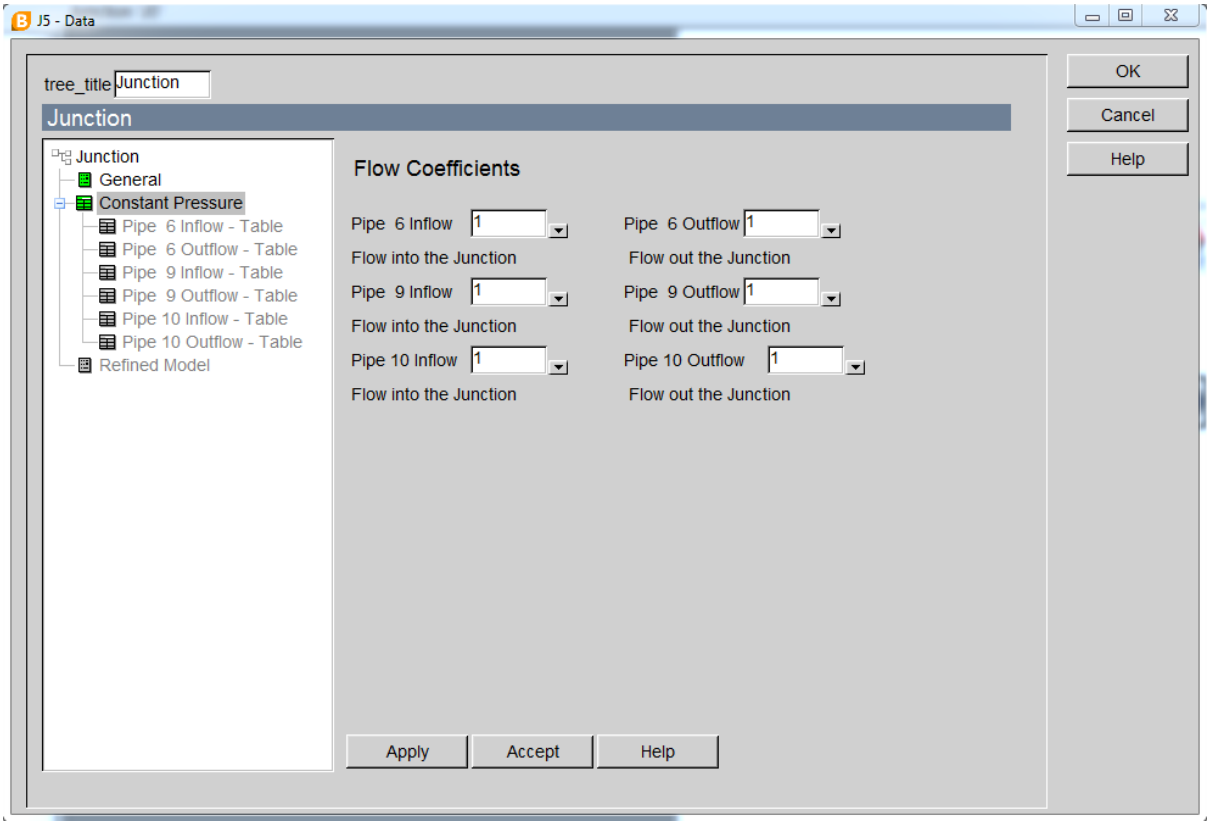

Output data summary

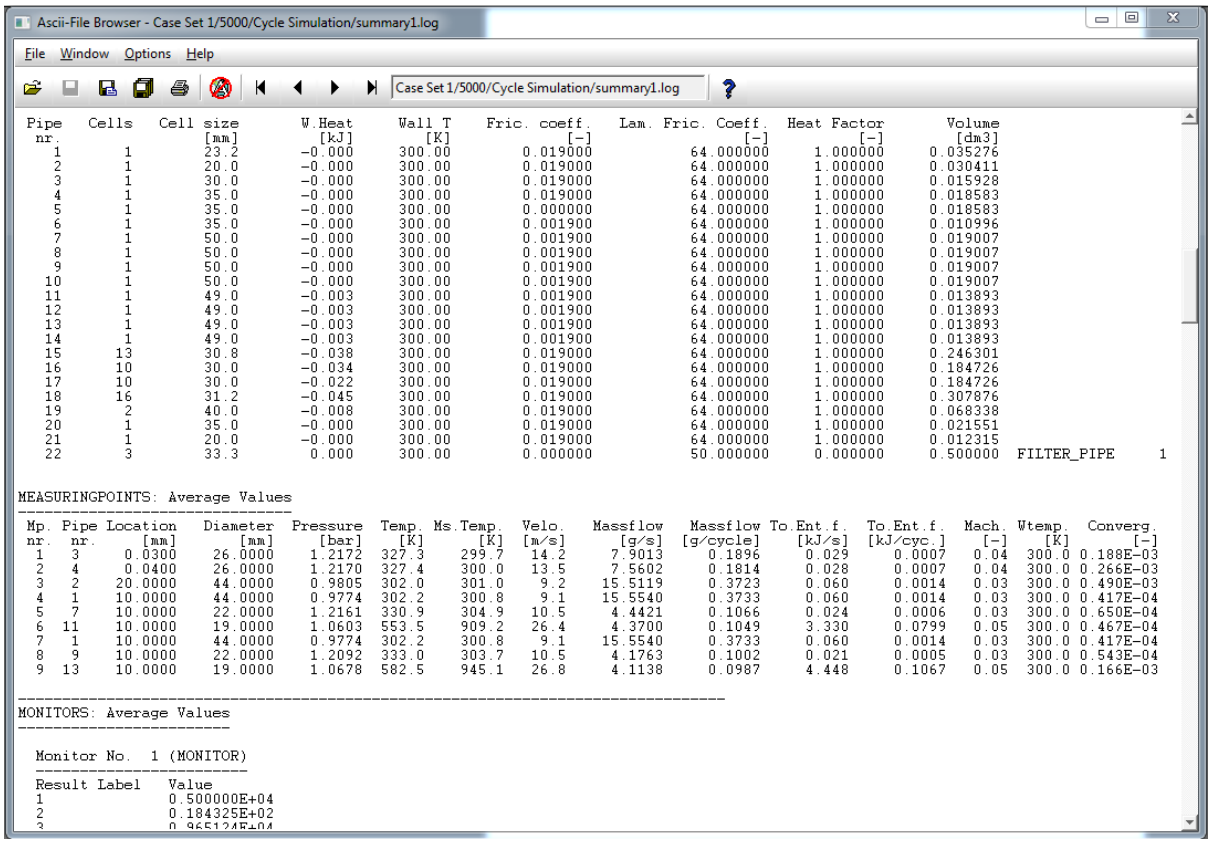


```
 Pipe   Cells   Cell size       W.Heat     Wall T    Fric. coeff.    Lam. Fric. Coeff.   Heat Factor        Volume
  nr.             [mm]          [kJ]        [K]          [-]              [-]              [-]           [dm3]
    1       1       23.2        -0.000      300.00       0.019000         64.000000        1.000000      0.035276
    2       1       20.0        -0.000      300.00       0.019000         64.000000        1.000000      0.030411
    3       1       30.0        -0.000      300.00       0.019000         64.000000        1.000000      0.015928
    4       1       35.0        -0.000      300.00       0.019000         64.000000        1.000000      0.018583
    5       1       35.0        -0.000      300.00       0.000000         64.000000        1.000000      0.018583
    6       1       35.0        -0.000      300.00       0.001900         64.000000        1.000000      0.010996
    7       1       50.0        -0.000      300.00       0.001900         64.000000        1.000000      0.019007
    8       1       50.0        -0.000      300.00       0.001900         64.000000        1.000000      0.019007
    9       1       50.0        -0.000      300.00       0.001900         64.000000        1.000000      0.019007
   10       1       50.0        -0.000      300.00       0.001900         64.000000        1.000000      0.019007
   11       1       49.0        -0.003      300.00       0.001900         64.000000        1.000000      0.013893
   12       1       49.0        -0.003      300.00       0.001900         64.000000        1.000000      0.013893
   13       1       49.0        -0.003      300.00       0.001900         64.000000        1.000000      0.013893
   14       1       49.0        -0.003      300.00       0.001900         64.000000        1.000000      0.013893
   15      13       30.8        -0.038      300.00       0.019000         64.000000        1.000000      0.246301
   16      10       30.0        -0.034      300.00       0.019000         64.000000        1.000000      0.184726
   17      10       30.0        -0.022      300.00       0.019000         64.000000        1.000000      0.184726
   18      16       31.2        -0.045      300.00       0.019000         64.000000        1.000000      0.307876
   19       2       40.0        -0.008      300.00       0.019000         64.000000        1.000000      0.068338
   20       1       35.0        -0.000      300.00       0.019000         64.000000        1.000000      0.021551
   21       1       20.0        -0.000      300.00       0.019000         64.000000        1.000000      0.012315
   22       3       33.3         0.000      300.00       0.000000         50.000000        0.000000      0.500000  FILTER_PIPE     1


MEASURINGPOINTS: Average Values
-------------------------------
 Mp. Pipe Location    Diameter  Pressure  Temp. Ms.Temp.  Velo.    Massflow   Massflow To.Ent.f.  To.Ent.f.  Mach. Wtemp.   Converg.
 nr.  nr.     [mm]        [mm]     [bar]    [K]     [K]   [m/s]      [g/s]  [g/cycle]    [kJ/s]  [kJ/cyc.]    [-]    [K]        [-]
  1    3     0.0300     26.0000    1.2172  327.3   299.7   14.2     7.9013     0.1896     0.029     0.0007   0.04  300.0 0.188E-03
  2    4     0.0400     26.0000    1.2170  327.4   300.0   13.5     7.5602     0.1814     0.028     0.0007   0.04  300.0 0.266E-03
  3    2    20.0000     44.0000    0.9805  302.0   301.0    9.2    15.5119     0.3723     0.060     0.0014   0.03  300.0 0.490E-03
  4    1    10.0000     44.0000    0.9774  302.2   300.8    9.1    15.5540     0.3733     0.060     0.0014   0.03  300.0 0.417E-04
  5    7    10.0000     22.0000    1.2161  330.9   304.9   10.5     4.4421     0.1066     0.024     0.0006   0.03  300.0 0.650E-04
  6   11    10.0000     19.0000    1.0603  553.5   909.2   26.4     4.3700     0.1049     3.330     0.0799   0.05  300.0 0.467E-04
  7    1    10.0000     44.0000    0.9774  302.2   300.8    9.1    15.5540     0.3733     0.060     0.0014   0.03  300.0 0.417E-04
  8    9    10.0000     22.0000    1.2092  333.0   303.7   10.5     4.1763     0.1002     0.021     0.0005   0.03  300.0 0.543E-04
  9   13    10.0000     19.0000    1.0678  582.5   945.1   26.8     4.1138     0.0987     4.448     0.1067   0.05  300.0 0.166E-03

--------------------------------------------------------------------------------
MONITORS: Average Values
------------------------

  Monitor No.  1 (MONITOR)
  --------------------------
  Result Label   Value
  1              0.500000E+04
  2              0.184325E+02
  3              0.965124E+04
```

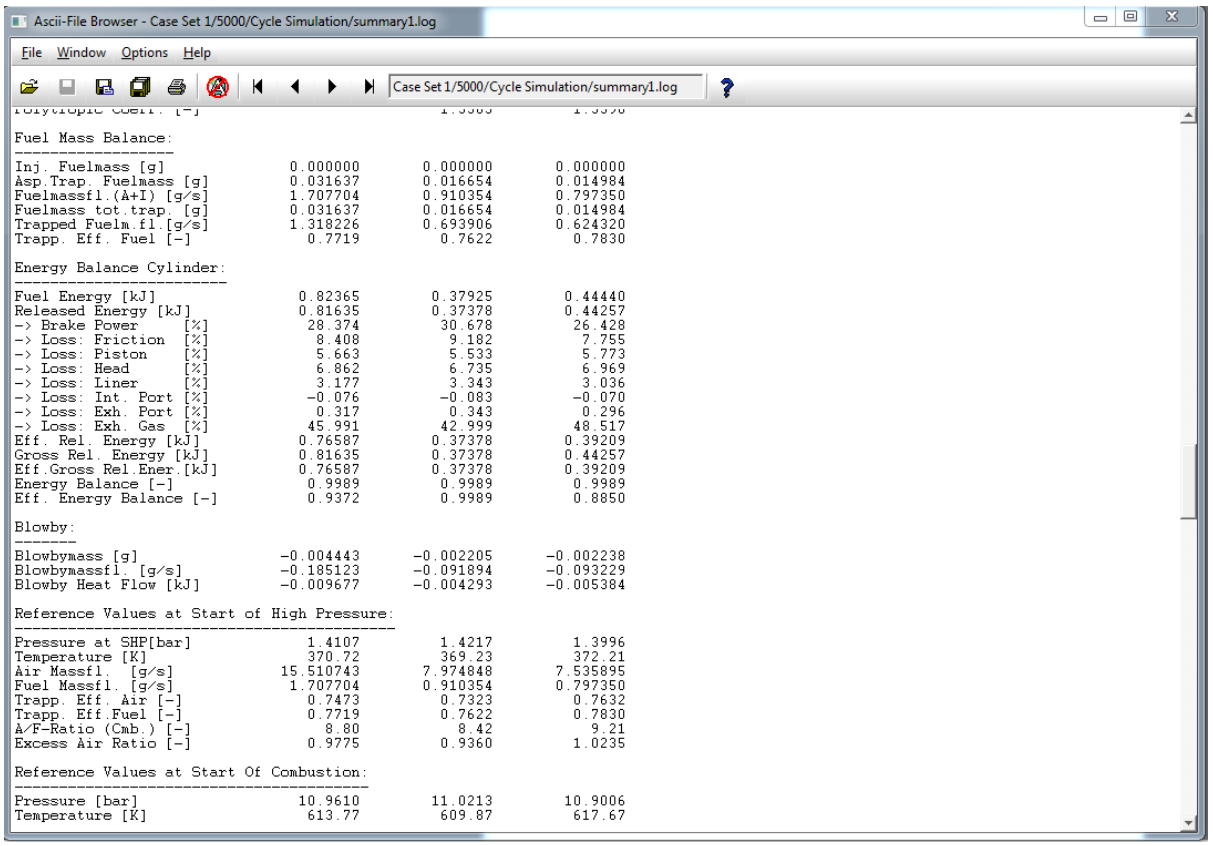


```
Polytropic Coeff. [-]                                1.3503          1.3570

Fuel Mass Balance:
------------------
Inj. Fuelmass [g]              0.000000        0.000000        0.000000
Asp.Trap. Fuelmass [g]         0.031637        0.016654        0.014984
Fuelmassfl.(A+I) [g/s]         1.707704        0.910354        0.797350
Fuelmass tot.trap. [g]         0.031637        0.016654        0.014984
Trapped Fuelm.fl.[g/s]         1.318226        0.693906        0.624320
Trapp. Eff. Fuel [-]             0.7719          0.7622          0.7830

Energy Balance Cylinder:
------------------------
Fuel Energy [kJ]                0.82365         0.37925         0.44440
Released Energy [kJ]            0.81635         0.37378         0.44257
-> Brake Power     [%]           28.374          30.678          26.428
-> Loss: Friction  [%]            8.408           9.182           7.755
-> Loss: Piston    [%]            5.663           5.533           5.773
-> Loss: Head      [%]            6.862           6.735           6.969
-> Loss: Liner     [%]            3.177           3.343           3.036
-> Loss: Int. Port [%]           -0.076          -0.083          -0.070
-> Loss: Exh. Port [%]            0.317           0.343           0.296
-> Loss: Exh. Gas  [%]           45.991          42.999          48.517
Eff. Rel. Energy [kJ]           0.76587         0.37378         0.39209
Gross Rel. Energy [kJ]          0.81635         0.37378         0.44257
Eff.Gross Rel.Ener.[kJ]         0.76587         0.37378         0.39209
Energy Balance [-]               0.9989          0.9989          0.9989
Eff. Energy Balance [-]          0.9372          0.9989          0.8850

Blowby:
-------
Blowbymass [g]                 -0.004443       -0.002205       -0.002238
Blowbymassfl. [g/s]            -0.185123       -0.091894       -0.093229
Blowby Heat Flow [kJ]          -0.009677       -0.004293       -0.005384

Reference Values at Start of High Pressure:
-------------------------------------------
Pressure at SHP[bar]             1.4107          1.4217          1.3996
Temperature [K]                  370.72          369.23          372.21
Air Massfl.  [g/s]             15.510743        7.974848        7.535895
Fuel Massfl. [g/s]              1.707704        0.910354        0.797350
Trapp. Eff. Air [-]              0.7473          0.7323          0.7632
Trapp. Eff.Fuel [-]              0.7719          0.7622          0.7830
A/F-Ratio (Cmb.) [-]               8.80            8.42            9.21
Excess Air Ratio [-]             0.9775          0.9360          1.0235

Reference Values at Start Of Combustion:
----------------------------------------
Pressure [bar]                  10.9610         11.0213         10.9006
Temperature [K]                  613.77          609.87          617.67
```

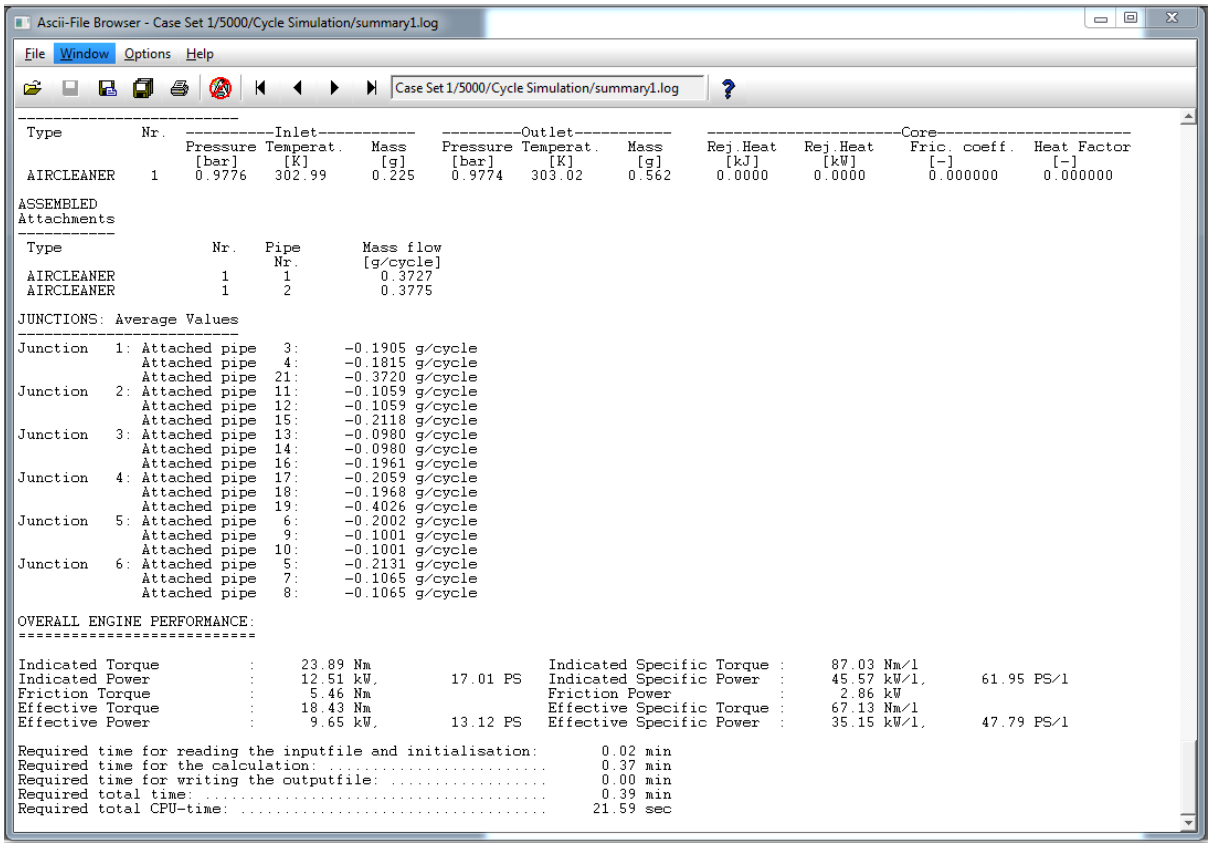


```
-------------------------
 Type          Nr.  ----------Inlet----------   ---------Outlet----------    ----------------------Core----------------------
                       Pressure Temperat.   Mass    Pressure Temperat.   Mass     Rej.Heat    Rej.Heat    Fric. coeff.   Heat Factor
                          [bar]     [K]      [g]       [bar]     [K]      [g]       [kJ]        [kW]          [-]            [-]
 AIRCLEANER     1     0.9776   302.99     0.225      0.9774   303.02    0.562     0.0000      0.0000      0.000000       0.000000

ASSEMBLED
Attachments
-----------
 Type                 Nr.    Pipe       Mass flow
                             Nr.        [g/cycle]
 AIRCLEANER            1      1          0.3727
 AIRCLEANER            1      2          0.3775

JUNCTIONS: Average Values
-------------------------
Junction   1: Attached pipe   3:     -0.1905 g/cycle
              Attached pipe   4:     -0.1815 g/cycle
              Attached pipe  21:     -0.3720 g/cycle
Junction   2: Attached pipe  11:     -0.1059 g/cycle
              Attached pipe  12:     -0.1059 g/cycle
              Attached pipe  15:     -0.2118 g/cycle
Junction   3: Attached pipe  13:     -0.0980 g/cycle
              Attached pipe  14:     -0.0980 g/cycle
              Attached pipe  16:     -0.1961 g/cycle
Junction   4: Attached pipe  17:     -0.2059 g/cycle
              Attached pipe  18:     -0.1968 g/cycle
              Attached pipe  19:     -0.4026 g/cycle
Junction   5: Attached pipe   6:     -0.2002 g/cycle
              Attached pipe   9:     -0.1001 g/cycle
              Attached pipe  10:     -0.1001 g/cycle
Junction   6: Attached pipe   5:     -0.2131 g/cycle
              Attached pipe   7:     -0.1065 g/cycle
              Attached pipe   8:     -0.1065 g/cycle

OVERALL ENGINE PERFORMANCE:
===========================

Indicated Torque          :     23.89 Nm                    Indicated Specific Torque :     87.03 Nm/l
Indicated Power           :     12.51 kW,       17.01 PS    Indicated Specific Power  :     45.57 kW/l,      61.95 PS/l
Friction Torque           :      5.46 Nm                    Friction Power            :      2.86 kW
Effective Torque          :     18.43 Nm                    Effective Specific Torque :     67.13 Nm/l
Effective Power           :      9.65 kW,       13.12 PS    Effective Specific Power  :     35.15 kW/l,      47.79 PS/l

Required time for reading the inputfile and initialisation:       0.02 min
Required time for the calculation: ..........                     0.37 min
Required time for writing the outputfile: ...........             0.00 min
Required total time: ........................................     0.39 min
Required total CPU-time: ....................................    21.59 sec
```

Knock function definition

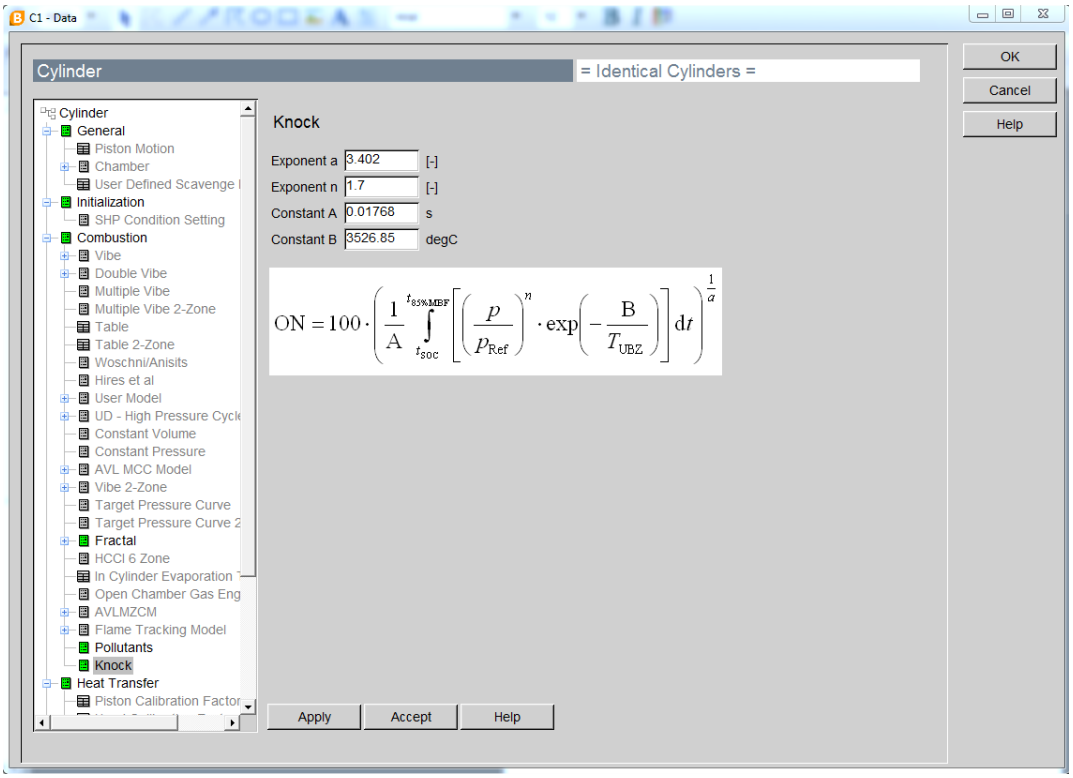

Exhaust emission formation definition

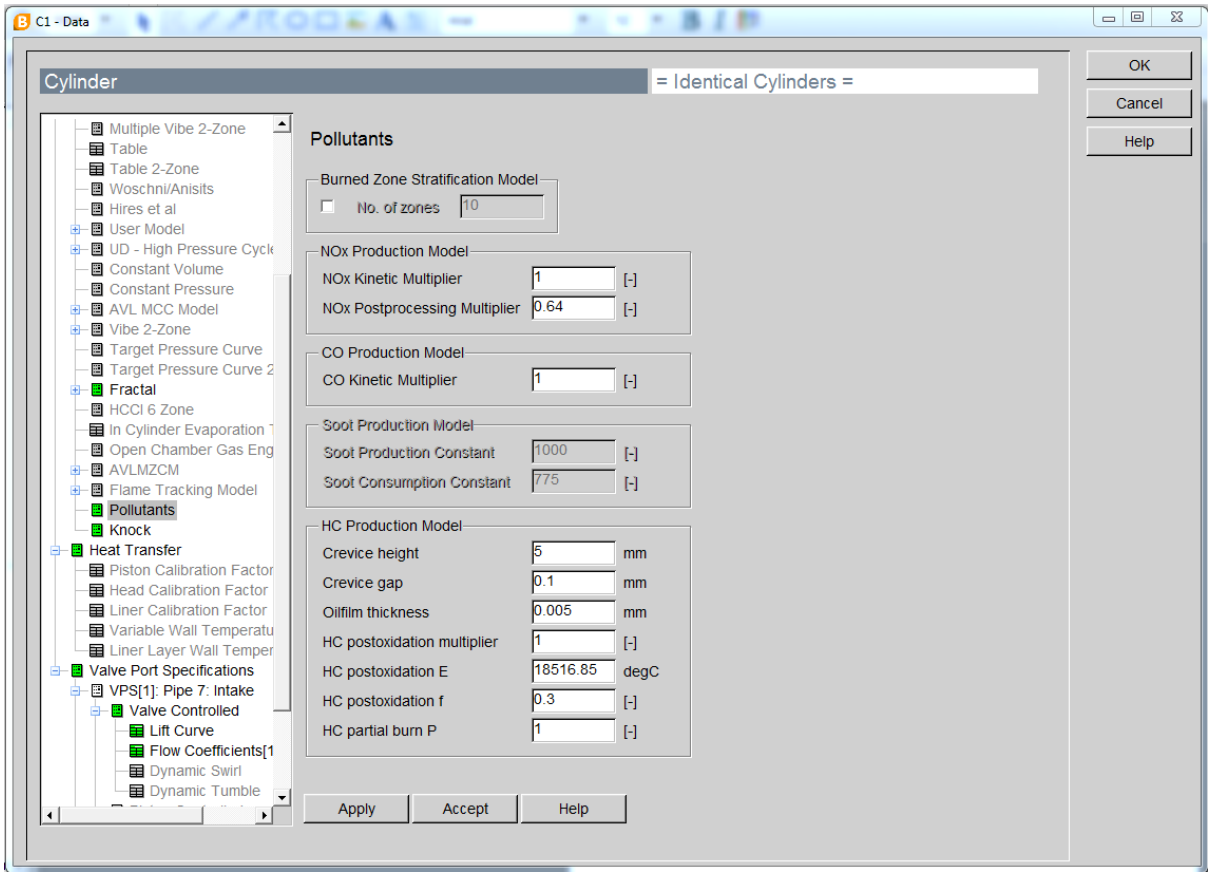

Simulation status

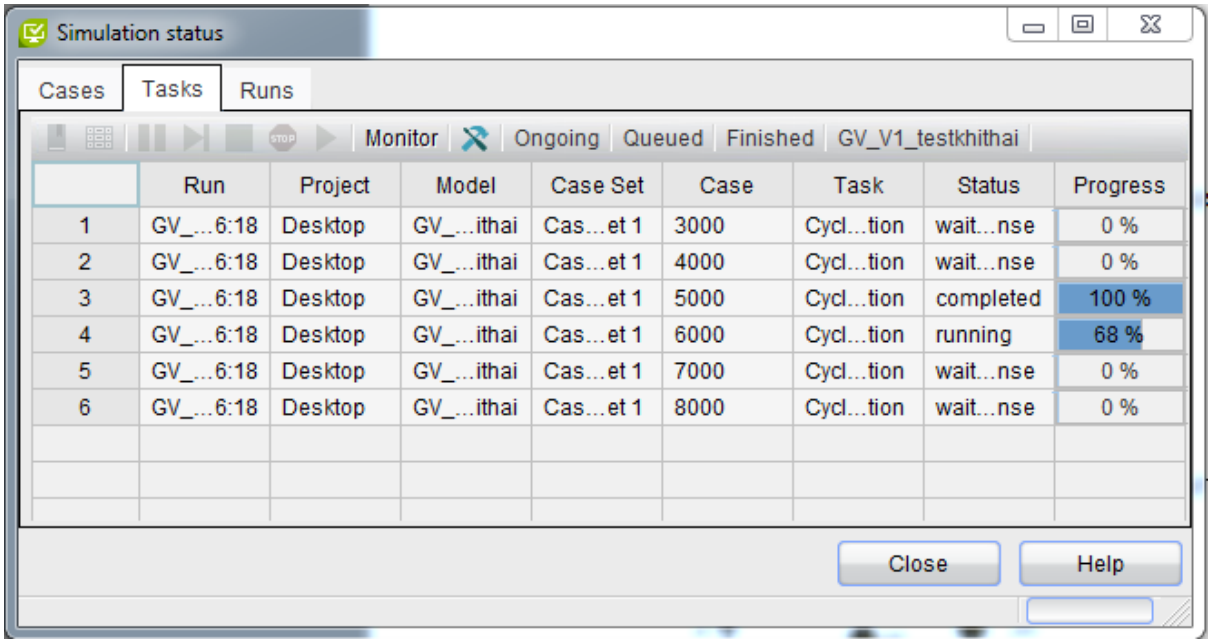

Simulation output results screen